UC Santa Barbara
UC Santa Barbara Electronic Theses and Dissertations

Title

Silica body building: Taxon-specific measures of diatom silica production and silicon stress in the California current

Permalink

Author

McNair, Heather

Publication Date

2017

Peer reviewed|Thesis/dissertation

UNIVERSITY OF CALIFORNIA

Santa Barbara

Silica body building: Taxon-specific measures of diatom silica production and silicon stress

in the California current

A dissertation submitted in partial satisfaction of the

requirements for the degree Doctor of Philosophy

in Marine Science

by

Heather Marie McNair

Committee in charge:

Professor Mark A. Brzezinski, Co-Chair

Professor Jeffrey W. Krause, Co-Chair, University of South Alabama

Professor Craig Carlson

Professor Debora Iglesias-Rodriguez

January 2018

The dissertation of Heather Marie McNair is approved.

_____

Craig Carlson

_____

Debora Iglesias-Rodriguez

_____

Jeffrey Krause, Committee Co-Chair

_____

Mark Brzezinski, Committee Co-Chair

December 2017

Silica body building: Taxon-specific measures of diatom silica production and silicon stress

in the California current

ACKNOWLEDGEMENTS

CURRICULUM VITAE OF HEATHER MARIE MCNAIR

EDUCATION

Ph.D. candidate, Interdepartmental Program in Marine Science   (expected) Dec 2017
University of California Santa Barbara, Santa Barbara, CA
Advisor: Dr. Mark Brzezinski and Dr. Jeffery Krause

B.A. Marine Science and **B.S.** Environmental Science   2006-2010
University of California Berkeley, Berkeley, CA

RESEARCH EXPERIENCE

Ph.D. Thesis Research   2012-Present
University of California Santa Barbara, Santa Barbara, CA

Graduate Research Assistant   2012-Present
University of California Santa Barbara, Santa Barbara, CA

Research Assistant/Intern   June-December, 2011
Dauphin Island Sea Lab, Dauphin Island, AL

Research Intern   June 2009-August 2010
Tahoe Environmental Research Center, Incline Village, NV

Research Cruises

Chief Scientist: Rebecca Robinson   McMurdo Station, Antarctica to Christchurch, NZ
R/VIB Nathanial B. Palmer   Jan 20-Mar 6, 2017

Chief Scientist: Kimberlee Thamatrakoln   Newport, OR to Port Hueneme, CA
R/V Oceanus   April 19-May 2, 2015

Chief Scientist: Ken Bruland   San Diego to San Diego, CA
R/V Melville   July 4-21, 2014

Chief Scientist: Jeffrey Krause   Moss Landing to Moss Landing, CA
R/V Point Sur   June 27-July 5, 2013

PUBLICATIONS

McNair, H.M., Brzezinski, M.A., Till, C.P., Krause, J.W. *Taxon-specific contribution to silica production in natural diatom assemblages.* (Accepted). Limnology and Oceanography.

Cohen, N.R., Ellis, K.A., Lampe, R.H., **McNair, H.M.,** Twining, B.S., Maldonado, M.T., Brzezinski, M.A., Kuzminov, F.I., Thamatrakoln, K., Till, C.P., Bruland, K.W., Sunda, W.G., Bargu, S., Marchetti, A. (Accepted). *Diatom transcriptional and physiological responses to changes in iron bioavailability across ocean provinces.* Frontiers in Marine Science. DOI: 10.3389/fmars.2017.00360.

Jones, J.M., Sweet, J., Brzezinski, M.A., **McNair, H.M.,** Passow, U. (2016) *Evaluating Carbonate System Algorithms in a Nearshore System: Does Total Alkalinity Matter?* PLoS ONE 11(11): e0165191. DOI: 10.6084/m9.figshare.4213338.

McNair, H. M., Brzezinski, M. A. and Krause, J.W. (2015) *Quantifying diatom silicification with the fluorescent dye, PDMPO.* Limnology and Oceanography: Methods, 13: 587-599, doi:10.1002/lom3.10049

PRESENTATIONS
Invited Speaker

"Applications of confocal microscopy and Imaris", Microscopy Workshop**,** Neuroscience Research Institute, UC Santa Barbara, 2015

"Dyeing Diatoms," Department seminar series, Dauphin Island Sea Lab, 2014

Conferences

McNair, H.M, Brzezinski, M.A., Krause J.W., Parker, C., Brown, M., Coale, T., and Bruland, K. *Pumping iron and silica bodybuilding*, oral presentation, Ocean Science Meeting, New Orleans, 2016 (talk)

McNair, H.M, Brzezinski, M.A. and Krause J.W. *Genus-specific contributions to diatom community silica production,* Silicamics, Brest, France 2015 (poster)

McNair, H.M, Brzezinski, M.A. and Krause J.W. *Peering into a 'black box' measurement-resolving group-specific silicon production rates in a natural diatom assemblage,* Molecular Life of Diatoms, Seattle 2015 (poster)

McNair, H.M, Brzezinski, M.A. and Krause J.W. *Who does what? Partitioning silica production among diatom groups in field assemblages,* Ocean Science Meeting, Honolulu 2014 (poster)

AWARDS AND HONORS
Funding

Coastal Fund of Associated Students, Major Funding Award   2015
- Funding awarded for confocal microscopy time and stipend for an undergraduate intern. Coastal Fund awards projects that focus on preservation and protection of the Santa Barbara shoreline.

Fellowships

Research Accelerator Award   2016
- Awarded to a student with an environmental focus thesis to be used for field and lab expenses.

Nejet Ezal Memorial Scholarship   2014
- Awarded to a graduate student in Marine Sciences based on an essay prompt "The Walkabout-the Voyage is Itself a Mystery"

Recognition

Outstanding Teaching Assistant, Nominated   2013
- Nominated by students and faculty for contributions to the teaching and learning process of UC Santa Barbara

TEACHING AND MENTORING
University Teaching Experience

Ecology Evolution and Marine Biology 142C: Processes in Oceans   2016
Teaching Assistant, Profs. Uta Passow and Debora Iglesias-Rodriguez

Guest Lecture, "Phytoplankton," Introduction to Oceans, Prof. Anna James   2016

Ecology Evolution and Marine Biology 142BL: Methods in Aquatic Ecology 2013-2015
Teaching Assistant, Prof. Sally MacIntyre

Mentoring Experience

Diana Gutierrez, undergraduate/post bachelor lab assistant   2015- 2017
Brett Russel, undergraduate intern   December-June 2015
San Marcos High School, reference/mentor for phytoplankton science project   2014
Cooke Bridges Program, University of California Santa Barbara   2013

ABSTRACT

Silica body building: Taxon-specific measures of diatom silica production and silicon stress in the California current

by

Heather Marie McNair

Ornately detailed frustules of silica encase the cells of one of the most productive primary producers in the world. Diatoms are responsible for roughly 20% of global primary production. They are unique among phytoplankton in their requirement of silicon for growth. Low concentrations of silicon in the surface ocean limit diatom silica production and possibly growth across ocean regions. The immense morphological and physiological diversity among diatoms suggests that community composition could be influenced by silicon availability and likewise difference in community compositions could affect the biogeochemical role of diatoms. However, until recently the ability to resolve relationships between community composition and silicon concentration was absent because methods to quantify differences in silica production and growth rate among co-occurring diatom taxa did not exist.

The first part of this dissertation (Chapter 2) describes the development of a new method to quantify single-cell silica production rates in mixed diatom assemblages. The method leverages the co-deposition of the fluorescent tracer, PDMPO (2-(4-pyridyl)-5-((4-(2-dimethylaminoethylaminocarbamoyl)methoxy)phenyl)oxazole) with newly deposited

biogenic silica to measure single cell silica production rates using confocal microscopy. This method was used to quantify taxon-specific silica production and growth rates in the California upwelling zone for the remaining dissertation chapters.

Chapter three explores the contribution of co-occurring taxa to community silica production and examines the physiological attributes of the most influential diatom taxa. Over short time scales (~1 d) the most productive taxa in the community were the ones with the largest combined frustule surface area. This lead to a disproportionate fraction of community production occurring in large diatoms. Over longer timescales (3-10 d) the influence of growth rate increases so that over the course of the bloom a taxon with substantial cell size and high growth rate will be the largest contributor to silica production. These results offer a novel perspective into the mechanics of the influence of community composition in silicon cycling.

Chapter four begins to tease apart the role of resource limitation in these communities by examining the hierarchical physiologic response of taxa to silicon limitation. Co-occurring taxa, experiencing the same environment, showed a large range of silicon limitation. However, the physiological response to limitation was generally conserved among taxa. Taxa that were silicon limited preferentially decreased the silica content of their frustule and to a lesser extent decreased the rate of production of new frustule with little alteration to growth rate. The short-term relative contribution of individual taxa to community silica production or the relative abundance of taxa was not altered by silicon limitation. The combined results from this dissertation highlight some of the mechanistic ways that diatoms influence biogeochemical cycling, with community

composition dictating downstream nutrient availability and nutrient induced physiologic

changes affecting the fate of diatom bound nutrients.

Table of Contents

LIST OF FIGURES

LIST OF TABLES

Chapter 1 Introduction

Diatoms have a ubiquitous global distribution (Finlay 2002; Malviya et al. 2016). They are one of the most ecologically diverse organisms in the ocean, having found niches in high and low nutrient environments, in the benthos, under sea ice, and as free-floating plankton. As plankton, diatom abundance ranges from hundreds of cells per liter in the oligotrophic, oceanic gyres (e.g. Scharek et al. 1999) to millions of cells per liter in high-nutrient, coastal upwelling zones (e.g McNair et al. in press). Diatoms are highly productive, over the course of a year oceanic diatoms will produce about 20% of total global primary production (Nelson et al. 1995) which is as much organic carbon as all the terrestrial rainforests combined (Field et al. 1998).

High productivity and global distribution make diatoms an integral part of aquatic food webs and biogeochemical cycles. Diatoms form the base of the most productive oceanic food webs (Mann 1993). Their relatively large cell size decreases the number of trophic transfers by bypassing small grazers and results in a more efficient transfer of energy to higher consumers than food webs built upon smaller phytoplankton (e.g. Pomeroy 1974). The higher order consumers of these food webs are often economically important fishes the stocks of which have been linked to diatom production (Finney et al. 2002). Large cell size and the silica, mineral-ballasted, cell walls (called frustules) of diatoms make them influential organisms in the biological pump (e.g. Alldredge and Silver 1988; Buesseler 1998) that transfers carbon from the atmosphere and surface ocean to the deep ocean. Additionally, the use of silicon for frustule construction ties diatoms to the global silicon cycle.

The distribution and concentration of silicon in the ocean varies with time and depth and reflects a balance between lithogenic inputs, biologic uptake and sedimentation. Silicic acid ($Si(OH)_4$) is the primary dissolved form of silicon in the oceans. Three primary mechanisms add silicic acid to the ocean: the majority, ~82% comes from chemical weathering of silicate rocks and subsequent transfer to the ocean by rivers, 8% from dissolution of small lithogenic particles from aeolian transport, and 10% from the weathering of submarine basalt (Tréguer and De La Rocha 2013). Prior to the proliferation of silicifying organisms the oceans were nearly saturated (~1 mM) with silicon (Holland 1984). In the contemporary ocean silicic acid concentrations have decreased, mainly through the evolution of biological uptake, such that the average is 70 µM (Tréguer et al. 1995) but can range from < 1 µM in the surface to 160 µM in the deep ocean (Broecker and Peng 1982).

Silicic acid is used by a number of organisms, such as sponges and radiolarian, however diatoms are the primary biological drivers of the oceanic silicon cycle (Nelson et al. 1995). Diatoms take-up silicic acid then deposit it as polymerized, amorphous silica (SiO_2), in their frustule. Without silicic acid diatom growth halts (Paasche 1973a) making silicic acid an essential nutrient for diatoms. Diatoms use 30-40 times the amount of silicic acid that enters the ocean per year (Nelson et al. 1995). In the current ocean, the residence time of silicic acid is about 15,000 years which gives the approximation that a single atom of Si will cycle through diatoms 39 times before deposition on the sea floor (Tréguer et al. 1995). Diatom productivity in the surface ocean depletes silicic acid levels to concentrations that begin to limit silica production (e.g. Brzezinski et al. 2008; Krause et al. 2012) and growth rate (e.g. Dugdale et al. 1995).

The inseparable relationship between diatoms and silicon has become a defining factor in global marine ecosystem models. In these models diatom growth and abundance can be limited by silicon availability in addition to nitrogen and iron (e.g. Moore et al. 2002; Follows et al. 2007). The generated outcomes of the models generally reflect observed diatom abundance and distribution and thus suggests that, in regions of the ocean, silicon availability plays a fundamental role in diatom ecology. However, our current understanding the direct influence of silicon in shaping diatom communities and in turn, of community composition in affecting the cycle of silicon, largely stems from laboratory experiments.

The silicified frustule of a diatom cell is made-up of distinct parts: two valves that are linked by a number of thin structures called girdle bands (Fig. 1). Together, a valve and the linked girdle bands form a theca, which is half of the frustule. As the cell grows, it elongates by creating new girdle bands. After the cell has undergone mitosis and is ready to divide, two new valves are formed and the mother cell is split into two daughter cells (Fig. 1). The rate of frustule production is not constant and thus silicic acid uptake and deposition are restricted to portions of the cell cycle where the cell is elongating or dividing (Brzezinski et al. 1990). The external concentration of silicic acid can affect the rate of silica production and growth of the diatom such that as silicic acid decreases a diatom cell will create thinner frustule then decrease its growth rate (Paasche 1975; Brzezinski et al. 1990).
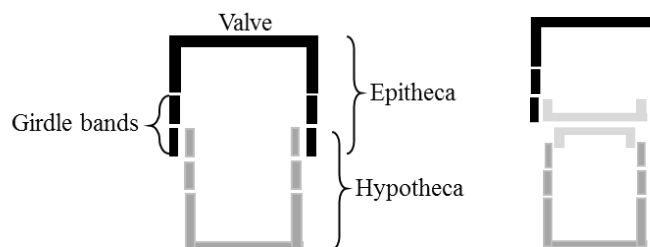
Figure 1-1: A diatom cell is composed of two halves, an upper and lower theca, that consist of a valve and girdle bands. The cell elongates with growth and just before division creates two new valves. The resulting two new daughter cells each contain half of the mother cell.

3

Silicon metabolism can be approximated using the Michaelis-Menten enzyme kinetic model for silica production and the Monod equation for growth.

$$V = \frac{V_m * [Si(OH)_4]}{K_s + [Si(OH)_4]}$$

$$\mu = \frac{\mu_m * [Si(OH)_4]}{K_\mu + [Si(OH)_4]}$$

Where the specific silica production rate (V) for a given concentration of silicic acid ($[Si(OH)_4]$) is a function of the maximum rate of silica production (V_m) and the half-saturation constant (K_s) which is the silicic acid concentration where the rate of silica production if half of the maximum rate. Similarly, the growth rate (μ) for a given concentration of silicic acid ($[Si(OH)_4]$) is a function of the maximum growth rate (μ_m) and the half-saturation constant (K_μ). Both equations are hyperbolic and reflect an asymptotic increase towards maximum with increasing silicic acid availability. The shapes of the curves are governed by the constants (V_m, μ_m, K_s and K_μ) which reflect the specific physiology of the cell. Half saturation constants for silica production and growth range over an order of magnitude and maximum silica production and growth rates range over a factor of five (Martin-Jézéquel et al. 2000).

The range of these kinetic constants reflects the immense diversity across diatom species. This interspecific variability suggests that within a natural diatom community, where taxa have variable physiological capabilities, there would be a range of realized growth rates and silica production rates among co-occurring taxa. The composition of a silicon-limited diatom community at equilibrium reflects the physiologic capabilities of species; the dominant species being the one with the highest growth rate for the given silicic acid concentration (Tilman 1977a). Diatom community composition, in turn, affects the

4

community silica production rate. Shifts in community composition towards more or less productive species can potentially alter the ecological function of diatoms.

Evidence suggests that nutrient use and export potential can significantly change with diatom community composition (Krause et al. 2010; Baines et al. 2010; Durkin et al. 2012; Assmy et al. 2013). Diatoms are one of the most diverse groups of oceanic organisms (Kooistra et al. 2007; Malviya et al. 2016). Cell size ranges from ~5 µm to 2 mm (Hoppenrath et al. 2007) and the silica content of diatom cells, which generally scales with cell size (Conley et al. 1989; Menden-Deuer and Lessard 2000), spans as many orders of magnitude (Brzezinski 1985). This wide range of diversity causes differences in community composition to affect rates of nutrient consumption (Krause et al. 2010), the efficiency of particulate organic and inorganic matter export (Baines et al. 2010; Durkin et al. 2012; Assmy et al. 2013), and biomass available to consumers (Finney et al. 2002; Assmy et al. 2013). While a species' impact in a community is related to its abundance, a number of studies have suggested that cell abundance alone may not accurately predict the influence a species has on biogeochemical cycles (Villareal et al. 1993; Goldman 1993; Durkin et al. 2012).

While there is strong evidence suggesting that community composition plays an important role in the biogeochemical function of diatoms and that silicon availability should differentially affect diatom growth and production, methodological limitations have restricted the measure of taxa-specific dynamics in natural communities. Previous studies have qualitatively partitioned silica production among species in natural communities (e.g. Durkin et al. 2013; Znachor et al. 2015), however, a quantitative method to measure taxon-specific silica production rates and growth rates in communities of mixed species was

lacking. Our current understanding of the interplay between silicon and diatoms largely comes from laboratory experiments with single diatom species (e.g.Guillard et al. 1973; Paasche 1980; Tantanasarit et al. 2013) and *in situ* experiments that measure diatom dynamic through the response of the community as a whole (e.g. Nelson and Brzezinski 1990; Brzezinski et al. 2003; Krause et al. 2015).

The goal of this dissertation was to develop a new method for quantifying single-cell silica production in mixed diatom assemblages and then used that method to examine the role of community composition in silica production as well as the effect of silicic acid concentration on cell physiology. Chapter two details the development and testing of the quantitative method for measuring cell-specific silica production rates using the fluorescent tracer, PDMPO (2-(4-pyridyl)-5-((4-(2-dimethylaminoethylaminocarbamoyl)methoxy)phenyl)oxazole), which is co-deposited with silica in newly formed frustule. Chapter three quantifies taxon-specific contributions to silica production in naturally occurring diatom communities within the California upwelling zone and examines the physiological attributes of the most influential taxa. Chapter four examines the effect of silicon limitation on those communities by looking at taxa-specific physiologic alterations with silicon availability and the resulting changes in contribution to silica production and community composition.

Chapter 2 Quantifying diatom silicification with the fluorescent dye, PDMPO

Abstract

Diatoms require silicic acid to construct ornately detailed cell walls called frustules. The growth and geographic distribution of diatoms is often controlled by the availability of silicic acid. Analytical methods exist to assess diatom community biogenic silica ($bSiO_2$) production, but partitioning production among taxa has been largely qualitative. We present a method for the quantitative analysis of taxa-specific silica production through labeling diatoms with the fluorescent dye PDMPO [2-(4-pyridyl)-5-((4-(2-dimethylaminoethylaminocarbamoyl)methoxy)phenyl)oxazole]. To make PDMPO a quantitative tool: diatom frustules were solubilized to assess the total diatom community incorporation by quantitation of PDMPO fluorescence using a fluorometer, and laser confocal microscopy was used to quantify the fluorescence of PDMPO in single diatom cells. We created a fluorescence standard to intercalibrate the raw fluorescence signals of the fluorometer and microscope and to determine the fluorescence per mole of PDMPO. PDMPO incorporation was converted to silica production using diatom $bSiO_2$:PDMPO incorporation ratios which varied systematically with silicic acid concentration. Above 3 µM $Si(OH)_4$, $bSiO_2$:PDMPO was constant and PDMPO incorporation was converted to silica production using a mole ratio of 2,916 as determined from cultures. Below 3 µM, the ratio was a linear function of [Si(OH)4] ($bSiO_2$:PDMPO $= 912.6$ x [$Si(OH)_4$]), as determined using data from two oceanographic cruises. Field evaluation of the method showed that total community PDMPO incorporation generally agreed to within 30% of radioisotope-

determined silica production. This PDMPO method has the potential to be a powerful tool for understanding physiology, silicification and resource competition among diatom taxa.

Introduction

Diatoms are one of the most ecologically diverse and successful organisms in the ocean; they account for 20 – 40% of total oceanic primary production (Nelson et al. 1995), play a fundamental role in a number of global biogeochemical cycles and serve as the base of many productive aquatic food webs (Mann 1993). High productivity, large cell size and mineral-ballasted cell walls make diatoms an important vector for carbon export from the surface ocean (Alldredge and Silver 1988; Buesseler 1998). Diatoms are unique among phytoplankton due to an obligate need for silicon to produce cell walls of polymerized silica known as frustules. Diatom growth and productivity can therefore be strongly influenced by the availability of silicic acid, i.e. dissolved silica (Brzezinski 1992). Despite silicon being the second most abundant element in Earth's crust, diatom consumption of silicic acid depletes concentrations in the surface-ocean to levels where diatom Si uptake (Brzezinski et al. 2008; Krause et al. 2012) and growth rate (Dugdale et al. 1995) can become Si limited.

Silicic acid availability can alter the relative abundance of diatoms within phytoplankton assemblages (Tilman 1982). Such composition shifts can drive changes in the efficiency of the biological pump where size and growth of phytoplankton are linked to sinking and export from the surface ocean (Martin et al. 1991; Harrison 2000). The large cell size of diatoms, relative to smaller phytoplankton, results in the more efficient transfer of energy to top trophic levels, supporting larger macrozooplankton biomass than smaller phytoplankton taxa (e.g. Pomeroy 1974). Understanding the distribution of diatom silica

production and how silicic acid concentration affects diatom community structure is key to understanding and modeling energy flow through aquatic food webs.

Currently, the analytical methods to measure rates of Si use by diatoms in natural communities include measuring net changes in silicic acid (Pondaven et al. 2000) and biogenic silica ($bSiO_2$) (Brzezinski and Nelson 1989; Krause et al. 2010) over time, or determination of gross rates of $bSiO_2$ production using silicon isotope tracers (Goering et al. 1973; Nelson et al. 1976; Brzezinski et al. 1997). To better understand the influence of silicic acid availability on natural diatom assemblages, knowledge of interspecies variability in silicic acid uptake and species-specific contributions to $bSiO_2$ production is required. Previous work suggests that Si limitation can shift diatom species composition, where low Si environments select for lightly silicified species with lower Si requirements (Dortch et al. 2001). Diatom community composition, dictated by nutrient availability and grazing pressure, can play a substantial role in community silicification (Assmy et al. 2013). The elemental stoichiometry of diatoms can differ depending on nutrient availability and can cause a preferential drawdown of one macronutrient over another (Brzezinski et al. 2002). Nutrient availability may also alter the degree of diatom silicification: frustule thinning occurring in low silicic acid conditions (Brzezinski et al. 2011a) and thickening in low iron conditions (Hutchins and Bruland 1998).

A number of attempts have been made to partition total biogenic silica biomass or total silica production among the different diatom groups present within natural diatom assemblages. Blain et al. (1997) used numerical abundance and surface area to estimate the contribution of different species to total biogenic silica production in the equatorial Pacific. This method assumed a constant $bSiO_2$ per unit surface area for estimating the $bSiO_2$

production for all species, and assumed that all cells were active and growing at the same rate. However, frustule thickness can vary at least five-fold among species grown in nutrient replete conditions (Paasche 1980) and three-fold for cells of the same species under nutrient stress (Brzezinski et al. 1990). Identification of actively silicifying cells was addressed by Shipe and Brzezinski (1999) who used autoradiography with the radioisotope ^{32}Si to visualize newly formed frustules in *Rhizosolenia* mats from the North Pacific subtropical gyre. With the autoradiograph, the fraction of active cells and the doubling time of species could be measured in the mixed assemblages of the mats. Difficulties with this method are the cost of ^{32}Si (~$1200 per µCi) and the considerable lag time between taking and analyzing a sample due to the need for ^{32}Si to reach equilibrium and the months of exposure to create the autoradiograph. An alternative probe was needed, something that would label newly deposited silica, was inexpensive, and quicker to visualize. Brzezinski and Conley (1994) found that the fluorescent dye, Rhodamine 123, was incorporated into newly deposited silica when present in growth media and could trace silica deposition in diatom cultures with negligible toxic effects. However, the low fluorescent yield, low incorporation ratio of the dye with $bSiO_2$, and emission overlap of Rhodamine 123 with chlorophyll made the dye difficult to use. More recently, a different fluorescent dye, 2-(4-pyridyl)-5-((4-(2-dimethylaminoethylaminocarbamoyl)methoxy)phenyl)oxazole (PDMPO) has proved more useful for tracking newly deposited biogenic silica in frustules (Shimizu et al. 2001).

PDMPO was first synthesized by Diwu et al. (1999) as a pH indicator for acidic cellular organelles. Shimizu et al. (2001) found that like Rhodamine 123, PDMPO was incorporated into the silica deposition vesicle (SDV) and ultimately into newly formed diatom frustules, and that the fluorescence intensity increased when the dye was in the

presence of silicic acid. LeBlanc and Hutchins (2005) developed a method to make PDMPO

a useful tool for identification of cells actively depositing $bSiO_2$ within a natural assemblage.

One of the key findings from LeBlanc and Hutchins's (2005) work was evidence that

PDMPO was incorporated in a nearly constant ratio with biogenic silica. Thus, quantitative

silicification rates of the total diatom community can be measured by applying the

$bSiO_2$:PDMPO ratio to the amount of PDMPO incorporated (LeBlanc and Hutchins 2005).

However, determination of silica production in single cells by PDMPO incorporation was

still qualitative (Leblanc and Hutchins 2005). Znachor and Nedoma (2008) developed a

method to image and measure single cell PDMPO fluorescence to look at relative

differences in diatom species silicification, but estimates of the absolute amount of Si

incorporation were not reported. Since these studies, PDMPO has been employed in a

number of diatom ecology studies (e.g. Durkin et al. 2012, 2013; Saxton et al. 2012;

Znachor et al. 2013), but none have used PDMPO as a quantitative tool for allocating Si

incorporation among diatoms in a natural assemblage.

Several challenges must be overcome to fully realize PDMPO as a quantitative tool

for studying $bSiO_2$ production in natural diatom assemblages. To measure the total

community silicification with PMDPO by fluorometry, diatom silica must be solubilized

without degrading the incorporated dye. Dissolving the labeled frustules eliminated the need

to quantify how many cells are in the excitation and emission views of the fluorometer and it

avoids complications due to heterogeneous particle distribution. Using PDMPO to measure

silica production at the single cell level requires quantification of single cell fluorescence

and accurate calibration of the relationship between incorporated PDMPO and the amount of

new silica polymerized. Because cells are solubilized for fluorometry but visualized intact

using microscopy, intercalibration between instruments requires a fluorescence standard which can be used in both measurement states. In this paper we describe improvements to the PDMPO method that take PDMPO labeling from a qualitative assessment to a quantitative measurement of newly deposited silica in both natural diatom assemblages and in individual diatom cells.

Materials and Procedures

Fluorescent dye

The fluorescent dye, PDMPO, LysoSensor Yellow/Blue DND-160, was used to label newly deposited diatom frustules. Vials of 1 mM PDMPO stocks (50 µL volume in dimethylsulfoxide) were purchased from Molecular Probes and stored in the dark at -20° C until use. PDMPO has an excitation maximum within UV wavelengths (357 – 377 nm) and has dual emission maxima, 417 – 483 nm and 490 – 530 nm in the pH range of 5.0 – 7.0 (Diwu et al. 1999). However, in acidic conditions, or in the presence of hydrated amorphous silica, the dual emission peaks collapse into a single peak at 534 nm (Shimizu et al. 2001).

Labeling protocol

A vial of PDMPO was thawed and centrifuged to consolidate the dye into a single droplet and facilitate quantitative transfer to experimental samples. Previous work found that incubations with the manufacture's recommended 1 µM concentration decreased growth rates in longer incubations (48 and 96 hours), but this apparent toxicity could be overcome by decreasing the dye concentration to 0.125 µM, which still provided adequate and consistent labeling (LeBlanc and Hutchins 2005). The protocol, described here, results in a final PDMPO concentration of 0.157 µM in seawater samples (48 µL PDMPO in 306 mL

sweater). This concentration produced well-labeled cells and did not affect growth rate in 8 species tested (t-test, p=0.36, 10 experiments total among 8 species).

Laboratory cultures were incubated for 24 hours and field samples were incubated for 4 – 24 hours, depending on the goals of each experiment. Cultures were incubated at 50 μE m^{-2} s^{-1} under cool fluorescent light (14/10 h light dark cycle) at 16° C. In field samples, PDMPO was added to 250 mL polycarbonate bottles (brim volume 306 mL). The bottles were then placed in light bags with various combinations of mesh screening to mimic the light intensity at the depths of sample collection and incubated in deckboard incubators cooled by flowing surface seawater. After incubation, a 100 mL aliquot of the labeled sample was removed from the bottle and reserved for measurement of single cell PDMPO incorporation; the rest of the sample was used to determine total community PDMPO incorporation. All culture samples and most natural phytoplankton samples were incubated with a paired replicate sample that did not contain PDMPO in order to quantify background fluorescence for the total community incorporation measurements. An additional separate 100 mL sample was collected at the beginning of the incubations and fixed with 4 mL of Bouin's solution for cell identification and enumeration.

Total community PDMPO incorporation

To quantify total community PDMPO incorporation unbound PDMPO was removed from the sample and the diatoms were dissolved for fluorometric analysis as follows. Samples were filtered onto polycarbonate filters (1.2 μm pore, 25 mm diameter). The cells and filter were transferred to a 15 mL polypropylene conical centrifuge tube, covered in 10 mL of 100% methanol (American Chemical Society grade) and placed in the dark at 4° C for 24 hours to remove unbound PDMPO and to eliminate photopigments. This methanol

extraction was tested on diatom cultures and largely eliminated the unbound PDMPO

(Figure 1) and most of the photopigments, thereby lowering the background fluorescence

and increasing measurement sensitivity. After extraction, the filter was compressed to the

bottom of the tube with a Teflon rod and centrifuged (10 min, 1230 x g) to pellet the cells.

The methanol supernatant was aspirated to 1 mL, ensuring all cells remained in the sample.

Test tube, filter and remaining methanol were dried, uncapped, in a warm (<60° C) vacuum

oven until the methanol evaporated, leaving the sample dry. The effect of drying on PDMPO

fluorescence was evaluated by comparing known quantities of PDMPO in 1 mL of methanol

that were either dried at room temperature or at 60° C. There was no statistically significant

difference between the fluorescence of the samples dried at the two temperatures ($p=0.31$, t-

test, $n=10$).
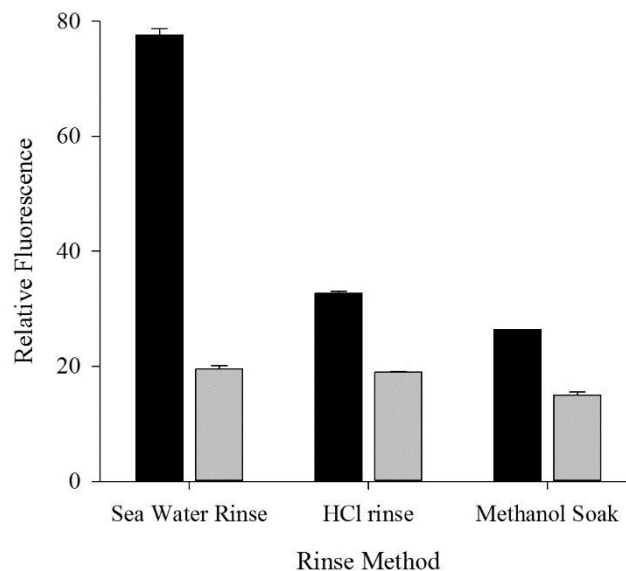
Figure 2-1: Comparison of rinse methods (0.2 µm filtered sea water, 10% HCL, and 100% Methanol) to eliminate unbound PDMPO. The black bars represent fluorescence in *T. weissflogii* and the gray bars represent fluorescence of *C. socialis*.

Frustule-bound PDMPO in the dried samples was solubilized and quantified

fluorometrically. When dry, 0.2 mL of 0.5M HF was added to the crushed filter and cells

14

and all contents were mixed with a Teflon rod to remove air bubbles from the filter to allow

contact between cells and the HF. After a 1-hr digestion, the samples were neutralized with

2.8 mL of saturated boric acid (~1 M). The fluorescence of the solution was quantified using

a Trilogy Laboratory Fluorometer (Turner designs) with the crude oil snap-in module (Light

Emitting Diode (Center Wavelength) 365 nm, excitation 350/80 nm, emission 410 – 600

nm). Raw fluorescence was converted to PDMPO concentration using a standard curve of

known concentrations of PDMPO in the same chemical matrix (HF/boric acid). Hot NaOH

digestion was found to degrade the fluorescence of the dye (Figure 2) and therefore,

dissolution with HF is recommended over dissolution with sodium hydroxide in a hot water

bath (95°C) as is used in determining biogenic silica concentration (Paasche 1973b). No

degradation of dye fluorescence was observed with the HF dissolution. Once boric acid is

added, the fluorescence is stable for at least one month (data not shown).
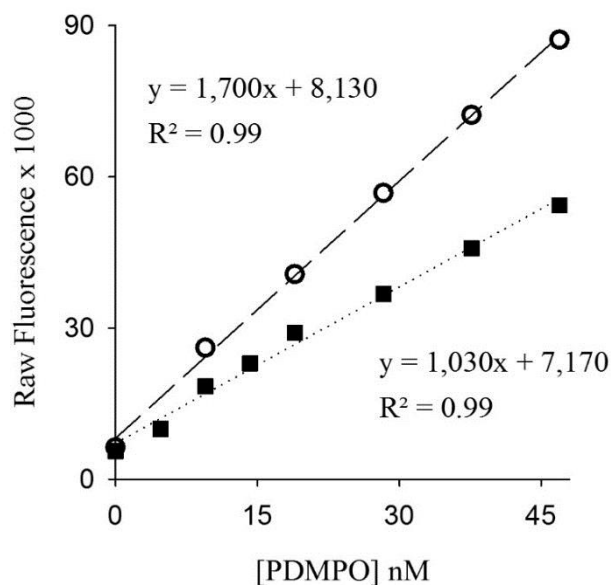
Figure 2-2: Standard curves of PDMPO in 0.2 N NaOH. Open circles represent standards that were not heated. Squares represent the fluorescence of the same standards after one hour at 98°C.

Paired seawater blanks without PDMPO were processed the same way as the labeled samples and allowed for correction of signal from autofluorescence. Blanks from field samples scaled with chlorophyll concentration (R^2=0.39). For field samples where we did not have a paired blank, a linear regression was derived from the relationship between PDMPO and Chl a was used to estimate the blank for the sample (Equation 1).

$$\textit{Blank} \text{ [PDMPO]} = 0.005 \text{ x [total Chl]} + 0.04 \tag{1}$$

where Blank [PDMPO] is the equivalent concentration of PDMPO of the blank in nM units and [total Chl] is the total chlorophyll concentration (μg L^{-1}) in the seawater as measured by fluorometry (Smith et al. 1981). The uncertainty in estimated blank values (~0.1 nM PDMPO) is 10 – 50 times smaller than the typical sample reading.

Single cell PDMPO incorporation

Quantitative assessment of single-cell PDMPO incorporation requires accurate measurement of the quantity of dye incorporated into the frustule of a cell. Cells were mounted on slides and imaged using laser confocal microscopy to quantify the fluorescence from PDMPO within single diatom cells. Excitation of the dye with a laser offered more consistent energy than a mercury lamp and the precise depth imaging of the confocal microscope offered finely-resolved three-dimensional fluorescence reconstruction. The raw fluorescence signal collected from the confocal was converted to an absolute amount of PDMPO incorporated using a fluorescence standard (see below).

Following experimental incubations the seawater subsample for microscopy was immediately centrifuged for ten minutes (1230 x g) and the supernatant removed. As with the total community incorporation measurement, unbound PDMPO and most photopigments were removed by the addition of 10 mL of methanol and storage for at least 24-hrs in the

16

dark at 4° C. Samples can be stored in this state for up to 2 years (the longest period tested).

Slides were prepared by resuspending an aliquot (20,000 to 40,000 cells based on

enumeration from an independent Bouin's preserved sample) of the methanol and cell

mixture in 10 mL of 0.2 μm filtered seawater and then filtering the suspension under low-

vacuum (<13 kPa) onto a polycarbonate filter (1.2 μm, 25 mm). The filtered was placed,

sample-side down, on a drop of deionized distilled water (>18 MΩ) on a polylysine-coated

glass slide. Flash freeze spray was applied to the opposite side of the slide from the sample.

The filter was then quickly peeled back and removed using forceps, leaving the cells on the

slide without the filter (Franck 2002). After the slide dried at room temperature in the dark, a

cover slip was applied with ProLong gold antifade (Life Technologies). The coverslip was

sealed to the slide with clear nail polish and stored in the dark at 4° C.

Cells were imaged using an Olympus Fluoview 1000 Spectral Confocal microscope

at the Neuroscience Research Institute at University of California Santa Barbara and using a

Nikon A1 Confocal Microscope at the University of South Alabama. Some photopigments

that fluoresce in the same excitation/emission settings as PDMPO remained in cells after

extraction in methanol (Figure 3, top panel). That interference was removed by imaging in

two wavelength channels (Figure 3, middle panel), one configured to best match the

wavelength excitation/emission for PDMPO and the other employing a longer wavelength

excitation/emission combination configured for photopigments. The PDMPO channel was

excited with a 405 nm diode laser and emissions measured from 450 – 550 nm.

Photopigments were excited with a 559 nm diode-pumped laser and emissions measured

from 618 – 718 nm. Images were acquired in sequence, first exciting with the 405 nm laser

then the 559 nm. Cell fluorescence was imaged in three dimensions using an optimized z-

step, which is half the axial resolution of the objective: 420 nm on the Olympus confocal

and 250 nm on the Nikon confocal.
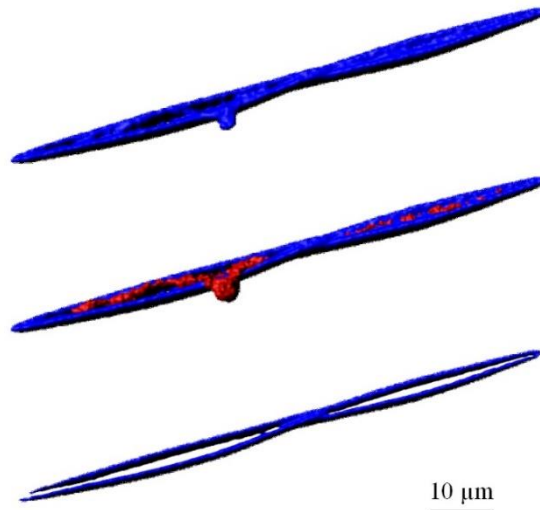
Figure 2-3: False-color images of Pseudo nitzschia sp. cells labeled with PDMPO. Top view is the total fluorescence of a chain of two cells in the PDMPO channel. The middle view is the PDMPO channel, emission from 450 – 550 nm (blue) overlaid with the longer wavelength 618 – 718 nm photopigment channel (red). Bottom view is the corrected PDMPO fluorescenceFigure 3. False-color images of Pseudo nitzschia sp. cells labeled with PDMPO. Top view is the total fluorescence of a chain of two cells in the PDMPO channel. The middle view is the PDMPO channel, emission from 450 – 550 nm (blue) overlaid with the longer wavelength 618 – 718 nm photopigment channel (red). Bottom view is the corrected PDMPO fluorescence.

Images were analyzed using Imaris 7.6.5 software (Bitplane). Total cellular

fluorescence was calculated using the surface function in Imaris. A surface was created

around voxels above a threshold fluorescence, essentially creating a three dimensional

volume with ~420 nm or ~250 nm depth resolution. Voxels that fluoresced in the long

wavelength channel were located and removed from the short wavelength image to create a

surface that represented only PDMPO fluorescence (Figure 3, bottom panel; see Assessment

section). Total PDMPO fluorescence was calculated by summing fluorescence intensity

values of all voxels within the photopigment-corrected volume.

Fluorescence standard

Standardized fluorescence (RFU $_{confocal}$) values for individual cells from the confocal microscope were converted to the standardized fluorescence of the fluorometer (RFU $_{fluorometer}$) and then to absolute amounts of PDMPO (moles). This required determination of the RFU $_{confocal}$: RFU $_{fluorometer}$ ratio which was accomplished using a fluorescence standard of uniformly labelled *Thalassiosira weissflogii* (CCMP 1051). Alternative fluorescence standards proved insufficient. Fluorescent beads were applicable to the microscope, but were not an appropriate for the fluorometer because the volume illuminated in the cuvette on the fluorometer was unknown and beads can clump or sink (albeit slowly), these factors hampered calculation of fluorescence yields of a single bead on the fluorometer. Solutions of PDMPO could be analyzed on the fluorometer but proved problematic on the microscope. A labelled diatom met the requirements for a standard that could be analyzed on both the fluorometer and on the confocal microscope to intercalibrate the two instruments.

The identity of the diatom used to construct the standard is immaterial. Most important is that the number of cells analyzed is known and that the cells are uniformly labelled with PDMPO. This allows the average cellular fluorescence for individual cells determined by the microscope to be compared directly to the average cellular fluorescence determined by fluorometry (RFU$_{fluorometer}$ ÷ number of cells dissolved). The quotient of the cellular fluorescence from the two instruments yields the RFU $_{confocal}$: RFU $_{fluorometer}$ which quantifies the difference in the fluorescence representing a fixed mass of PDMPO for the two approaches.

The fluorescence standard was prepared by growing *T. weissflogii* in batch culture, in f/2 media with 300 µM silicic acid. *T. weissflogii* was an ideal species for the standard

because it does not form chains, making individual cell measurements easier, and it is easy to grow. The high concentration of silicic acid avoided cell limitation of Si uptake by low silicic acid which can lower cellular silicon content (see Martin-Jézéquel et al. 2000). This resulted in even labeling (standard error of individual cell fluorescence on the confocal was 5% of the average) of the frustules as PDMPO was incorporated over multiple generations under Si-replete growth conditions (Brzezinski and Conley 1994). The experimental culture was first acclimated in media without PDMPO (three doublings), then a subsample was transferred to media containing 0.148 µM PDMPO with high-silicic acid. The culture was harvested after five doublings, when 96% of the cells had fully labeled frustules and processed as described above.

Fluorescence normalization on the confocal microscope

Fluorescence intensity varied significantly among diatom taxa, and within diatom taxa, consistent with the results of Durkin et al. (2012, 2013). This made it necessary to adjust the photomultiplier voltage on the Olympus confocal and the gain on the Nikon confocal to ensure measureable PDMPO fluorescence signal without saturating the detector. Readings taken at different voltages were normalized to 650 V on the Olympus confocal and a gain of 4 on the Nikon confocal, as these were the most frequent settings employed when measuring samples. The relationship of fluorescence as a function of voltage or gain was obtained by measuring uniformly labeled cells of *T. weissflogii* that also served as the fluorescence standard described above, at settings that spanned the range of values used to image all cells. This produced an exponential relationship ($R^2=0.92$) between voltage and PDMPO fluorescence on the Olympus confocal and a linear relationship ($R^2=0.81$) between voltage and PDMPO fluorescence on the Nikon confocal.

Measurements of single cell PDMPO incorporation on the two different microscopes produced very similar estimates of total PDMPO incorporation, within the variation of the sample. Data from the Olympus microscope at University of California Santa Barbara was compared with the Nikon microscope at University of South Alabama by imaging the *T. weissflogii* standard on each instrument in addition to one sample from a recent cruise. The *T. weissflogii* standard was used to convert the cruise sample from measured RFU to moles of PDMPO yielding a value of 0.22 ± 0.22 (SD) nmol PDMPO cell^{-1} for the Olympus confocal and 0.25 ± 0.12 (SD) nmol PDMPO cell^{-1} for the Nikon.

bSiO$_2$:PDMPO incorporation ratio

The methods described above detail how to quantitatively measure total PDMPO incorporation by a diatom culture, a natural diatom assemblage or a single diatom cell. PDMPO incorporation can be converted to Si production using knowledge of the bSiO$_2$:PDMPO ratio in diatoms provided this ratio is reasonably consistent among diatom taxa. Work by LeBlanc and Hutchins (2005) with two cultured species support this assumption; the standard error of the bSiO$_2$:PDMPO ratio was 24% of the mean. The present method expands on their work to further examine the central tendency and variability of the ratio using the protocols described above. Culture experiments were conducted with actively growing cells (growth rates from 0.2 to 0.8 day^{-1}) to measure change in biogenic silica and the incorporation of PDMPO over 24 hours (Table 1). Culture species were a combination of isolates established from the California coast and cultures purchased from the National Center for Marine Algae and Microbiota (East Boothbay, Maine USA).

21

Table 2-1: Diatom cultures used to determine mol:mol ratio of Si deposited to PDMPO incorporated. (SC77 was isolated by Holly Bowers)

Thalassiosira weissflogii (CCMP 1051, isolated 5/13/1985)
Chaetoceros socialis (CCMP 172)
Odontella aurita (CCMP 595)
Corethron hystrix (CCMP 308)
Pseudo-nitzschia multiseries (SC77, Huntington Beach)
Isolated from California coast July 2012
Chaetoceros socialis (Avila Beach)
Melosira varians (Santa Cruz)
Chaetoceros didymus (Monterey Bay)

Cultures were incubated in pairs, one control (blank) without added PDMPO and one with added PDMPO, at ~16° C for 24 hours (light/dark cycle of 14/10). Biogenic silica concentration was measured at the beginning and end of each experiment using a NaOH digestion in teflon tubes (Krause et al. 2009) and colorimetric ammonium molybdate method (e.g. Brzezinski and Nelson 1995). PDMPO incorporation was measured using the fluorometer in parallel as described above. The mole ratio of the increase in biogenic silica to the incorporation of PDMPO ($bSiO_2$:PDMPO) for eight species had a median value of 2,916 ± 708 (SE), n=8. This incorporation ratio was similar to what LeBlanc and Hutchins (2005) found in their culture experiments where the average ratio was 2,800 ± 780, despite the differences in measurement protocols. We use and report the median value instead of the mean for the culture data because the frequency distribution of the data skew towards higher values which biases the average.

A summary of the major steps of the method described above are presented in Figure 4.

Cell-specific silicification determination using PDMPO

Label Cells
- [PDMPO] 0.157 μM
- Blank [PDMPO] 0 μM

Total community production
- Blank and labeled samples

Single cell production
- Labeled sample only

Methanol leach
- Filter sample onto 25 mm filter
- Transfer filter and cells to 10 mL of 100% methanol for 24 hours at 4°C

Methanol leach
- Concentrate cells by centrifugation, remove seawater supernatant
- Add 10 mL of 100% methanol, wait 24 hours or longer at 4°C

Frustule solubilization
- Pelletize filter
- Centrifuge and remove supernatant
- Dry in vacuum oven < 60°C
- Add 0.2 mL 0.5 M HF, digest 1 hour
- Add 2.8 mL of saturated boric acid

Slide preparation
- Resuspend cells in filtered sea water
- Filter onto 25 mm filter
- Freeze transfer to slide

Cellular fluorescence measurement
- Using a confocal microscope, image ~ 20 cells per diatom taxa

[PDMPO] measurement
- Read samples on a fluorometer (filter settings: excitation 350/80 nm, emission 410 – 600 nm)
- Convert $RFU_{fluorometer}$ to [PDMPO] using PDMPO standard curve in HF/boric acid matrix.

Flourescence conversion
- Use $RFU_{confocal}$: $RFU_{fluorometer}$ of *T. weisfloggi* standard to convert $RFU_{confocal}$ to $RFU_{fluorometer}$
- Calculate [PDMPO] from standard curve.

Convert PDMPO incorporation to $bSiO_2$ production
- >3 μM [Si(OH)$_4$], $bSiO_2$:PDMPO ratio of 2,900
- <3 μM [Si(OH)$_4$], $bSiO_2$:PDMPO = 912.6 x [Si(OH)$_4$]

Figure 2-4: Flow chart for quantitative use of PDMPO for measuring diatom silicification. Not shown is the separate sample required for enumeration of diatom abundance and assemblage structure.

Assessment

Field assessment of the $bSiO_2$: PDMPO incorporation ratio

Field measurements of biogenic silica production and PDMPO incorporation were used to verify the applicability of the laboratory-derived $bSiO_2$:PDMPO ratio during two scientific cruises. Sampling occurred during the "Dye labeling of diatoms" (DYEatom)

23

cruise from June 27 to July 5, 2013 aboard the *R/V* Point Sur off the California coast between Monterey Bay and offshore of Bodega Bay and on the Iron Bruland (IrnBru) cruise from July 4 to July 21, 2014 aboard the *R/V* Melville off the west coast of the United states between San Diego, California and Southern Oregon. Total community PDMPO incorporation was compared with total community silica production measured with the radioisotope ^{32}Si. All incubation volumes (306 mL) were consistent between the two methods, PDMPO and ^{32}Si, and across samples. Silica production samples were spiked with (262.8 Bq) of high-specific activity ^{32}Si (15,567 Bq μg^{-1} Si). At the end of each incubation, samples were filtered through 1.2 μm polycarbonate filters and ^{32}Si incorporation determined as in Krause et al. (2011). Total community PDMPO incorporation was measured following the protocol described above using the same seawater samples and type of filters as used to measure ^{32}Si incorporation.
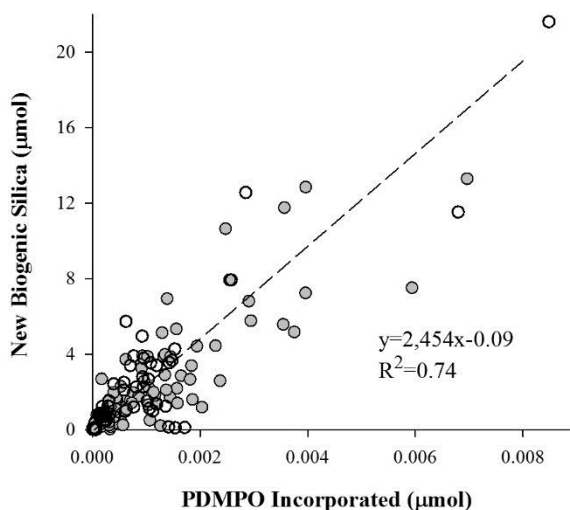
Figure 2-5: Field assessment of the bSiO$_2$: PDMPO incorporation mole in a Model II regression between PDMPO incorporation and new biogenic silica production measured from ^{32}Si from two different cruises. Closed gray circles are data points from the DYEatom cruise, open circles are data from IrnBru cruise.

The bSiO$_2$:PDMPO mole ratio from the cruise samples was calculated as the slope of the regression of ^{32}Si incorporation rates and PDMPO incorporation rates using a Model II,

reduced major axis regression (Bohonak 2004). The resulting average $bSiO_2$:PDMPO mole

ratio was $2,454 \pm 89$ (SE) (n = 201, R^2=0.74) with a 95% confidence interval (2,279 to

2,629) (Figure 5). Previous work suggested that the $bSiO_2$:PDMPO incorporation ratio may

depend on the concentration of silicic acid in the environment (Durkin et al. 2013). We

observed that the ratio did not show a significant trend with silicic acid concentrations over

3 µM (R^2=0.01) (Figure 6a); however, below 3 µM the ratio decreased linearly with respect

to the concentration of silicic acid (R^2=0.64) (Figure 6b). Changes in the $bSiO_2$:PDMPO

incorporation ratio with respect to silicic acid concentration have been seen in other studies

as well (Jennifer Long, personal communications). It is recommended that the

$bSiO_2$:PDMPO mole ratio be calculated from the regression as 912.6 x $[Si(OH)_4]$ when

ambient silicic acid concentrations are below 3µM. Note that the regression is forced

through the origin based on the assumption that silica production and PDMPO incorporation

cease at a $[Si(OH)_4]$ of zero.

a.

b.
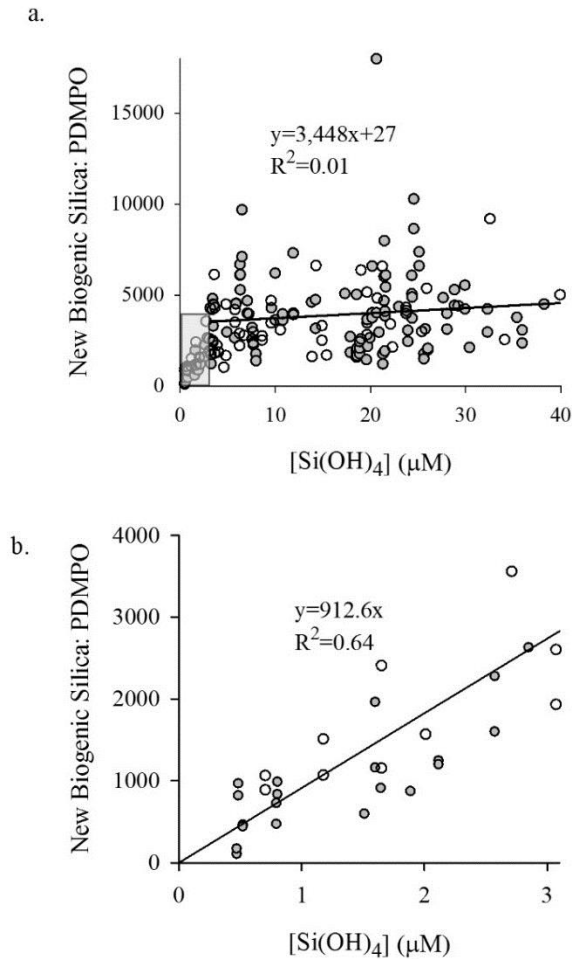
Figure 2-6: bSiO$_2$:PDMPO mole ratio from field samples plotted across the range of silicic acid concentrations observed on two cruises. Closed gray circles are data points from the DYEatom cruise, open circles are data from IrnBru cruise. (A) The regression line was fit to all data above 3 µM [Si(OH)$_4$]. (B) Enlarged plot of the boxed section from (A) fit with a linear regression forced through the origin.

Figure 7 shows the result of a second approach to finding the central tendency of the bSiO$_2$:PDMPO mole ratio from the cruise samples when [Si(OH)4] exceeds 3µM. The cubed root of the ratio was taken to normalize the data. The median of this transformed data corresponds to a bSiO$_2$:PDMPO mole ratio of 3,402. The slope of the regression and the median of the transformed data are within 15% and 17% respectively, of the ratio from the diatom cultures. Although there is significant variability in the bSiO$_2$:PDMPO incorporation ratio, the variance is such that using the median culture ratio to calculate silica production

26

from total community PDMPO incorporation for field samples where [Si(OH)$_4$] exceeds

3µM will yield production rates that are within 30% of rates determined using ^{32}Si. In cases

where ambient [Si(OH)$_4$] is < 3 µM using the recommended regression produces agreement

within 36%.
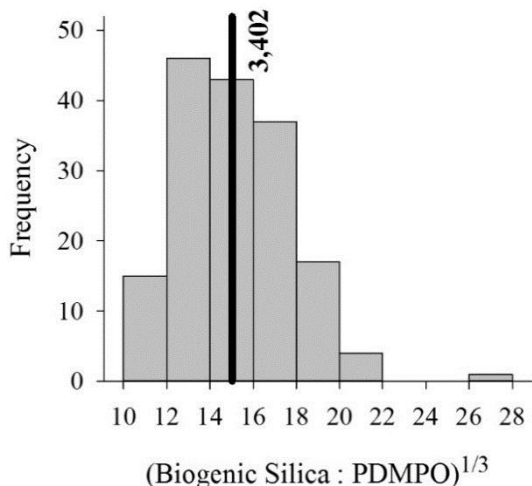
Figure 2-7: The normally transformed distribution of the ratio from field samples above 3 µM Si(OH)$_4$ from the two cruises. The solid line depicts the median 3,402.

Proof of concept in culture

Cultures of *Pseudo-nitzschia multiseries, Chaetoceros socialis* (CCMP 172) and

Chaetoceros didymus were used to test the agreement between total PDMPO incorporation

and single cell incorporation measurements. The three cultures were grown the same way as

the cultures for the incorporation ratio experiments: at ~16° C in polycarbonate bottles for

24 hours on a 14/10 hour light-dark cycle. Two measurements of the average amount of

PDMPO incorporated by a cell, one calculated as the quotient of the total PDMPO

incorporation and cell abundance, and the other from single cell fluorescence using

microscopy, show close agreement, with disparities ranging from 3 – 19% among the three

species (Table 2).

27

Table 2-2: Comparison between total community incorporation and single cell incorporation in culture. Range indicates standard deviation.

Species	Total incorporation (nmol PDMPO)	Average PDMPO incorporation from total incorporation (amol PDMPO cell^{-1})	Average PDMPO incorporation from microscopy (amol PDMPO cell^{-1})	Ratio Microscopy: Total
Pseudo-nitzschia multiseries	16.2 ± 0.27	153 ± 2.54	148 ± 131	97%
Chaetoceros socialis (CCMP 172)	10.2 ± 1.3	38.2 ± 4.8	31.0 ± 15.7	81%
Chaetoceros didymus	2.99 ± 0.32	81.6 ± 35.4	82.9 ± 25.1	99%

Proof of concept in field samples

Here we present the results from one sample from the DYEatom cruise as an example of a field application for PDMPO. This sample was collected from just below the surface with a Niskin rosette. Ambient silicic acid concentration was 5.7 µM; the incubation was performed with Si amendment to 23.8 µM [Si(OH)$_4$]. Initial biogenic silica concentration was 5.6 µM. Replicate samples were incubated under the same conditions with either additions of PDMPO, ^{32}Si, or a no-addition blank. A Bouin's preserved sample was not saved, thus to determine cell abundance and identify the diatom genera present, a subsample of the methanol preserved aliquot was counted in a 10 mL Utermöhl settling slide. *Pseduo-nitzschia spp.* dominated the diatom community, accounting for 82% of all diatom cells in the sample. *Chaetoceros spp.* made up 15% the community, while *Leptocylindrus danicus* accounted for 3%. Other genera were present in the assemblage but were numerically rare. Over the course of the incubation 0.68 nmol of PDMPO was incorporated, which yields a rate of silica production within 4% of that measured by ^{32}Si when using the culture bSiO$_2$:PDMPO mole ratio of 2,916.

28

PDMPO incorporation varied by a factor of three among diatom groups. The average cellular PDMPO content for *Pseduo-nitzschia spp.* in the sample was 1.9×10^{-7} nmol cell^{-1} (n=33 chains) with a standard deviation of 1.1×10^{-7} nmol. On average, a single cell of *Leptocylindrus danicus* incorporated only 42% as much PDMPO, $0.8 \times 10^{-7} \pm 0.7 \times 10^{-7}$ nmol cell^{-1} (SD, n=6 chains), as a cell of *Pseudo-nitzschia spp.* The numerically rare, *Thalassiosira spp.* incorporated slightly more PDMPO than *Pseudo-nitzschia spp,* $2.1 \times 10^{-7} \pm 0.4 \times 10^{-9}$ nmol cell^{-1} (SD, n=2 chains). The high standard deviations relative to the mean is expected as cells were not uniformly labeled with different cells depositing different parts of the frustule.

The total community PDMPO incorporation for the field experiment was compared to the total community incorporation extrapolated from cell counts and the PDMPO incorporation by the dominate diatom genera. Total community PDMPO incorporation reconstructed from single cell measurements is 9% greater than the total community estimate. Single cell incorporation suggests that 0.75 ± 0.44 nmol of PDMPO was incorporated by the numerically dominant diatoms (i.e. *Pseduo-nitzschia spp.*, *Chaetoceros spp.*, *Leptocylindrus danicus*) over the course of the incubation, while the totally community incorporation measured 0.68 nmol PDMPO. Using the mole to mole ratio from culture, 0.75 nM of PDMPO translates to 2.2 µmol Si L^{-1} of new bSiO$_2$, which is about 9% higher than the 2.0 µmol Si L^{-1} measured with ^{32}Si.

Discussion

The PDMPO method is unique in that it allows for quantitative, taxon-specific silica production measurements in natural diatom assemblages. Results from the DYEatom cruise highlight some of the unique abilities of the method where the role of individual diatom

genera within a mixed community can be examined using single-cell PDMPO incorporation. A genus' contribution to total PDMPO assimilation and thus total biogenic silica production, can be calculated using single cell incorporation and cell abundance data. *Pseudo-nitzschia spp.* accounted for 98% of the community PDMPO, which is a larger fraction of production than numerical abundance, 82%, would suggest. The *Thalassiosira spp.* also accounted for more of the community PDMPO, about 30% more than their numerical abundance. Conversely, *Leptocylindrus danicus* accounted for only 1% of the community PDMPO compared to its 3% numerical abundance. Such comparisons begin to reveal the contribution of individual taxa in a naturally diverse system informing how Si production is partitioned. This will enable experiments to examine species-specific responses to shifts in silicic acid concentration and how competition for Si may drive diatom species succession. Such understanding will inform selection of physiological parameters used in biological and biogeochemical chemical models especially those employing trait based or taxa specific approaches (Pokras and Mix 1985).

With previous PDMPO methods, community silicification could be measured quantitatively, but contribution of different diatom groups could only be inferred qualitatively. The present method overcame key analytical issues to make PDMPO fluorescence a quantitative measurement for both total community and single cell silicification. Dissolving frustules in hot NaOH (LeBlanc and Hutchins 2005) degraded the dye, so a dissolution method using low molarity HF at room temperature was devised. Accurate measurement of single-cell PDMPO fluorescence required eliminating the residual signal from photopigments by imaging with both a short and a long wavelength excitation. Converting the raw single cell fluorescence to PDMPO was accomplished using a novel

fluorescence standard material consisting of uniformly labelled diatoms. The fluorescence of the standard can be quantified on both a fluorometer and on a microscope allowing RFU from microscopy to be converted to the amount PDMPO incorporated. Interspecific variation in the $bSiO_2$:PDMPO mole ratio was further quantified and evaluated for converting PDMPO incorporation into biogenic silica production and found to be independent of [$Si(OH)_4$] above 3 μM with a median of 2,916 and coefficient of variation of about 20% consistent with past findings (LeBlanc and Hutchins 2005). The ratio appears to be a linear function of [$Si(OH)_4$] below 3μM.

PDMPO not only provides information on silica production among taxa, but the total PDMPO incorporation measurement is relatively simple to perform at sea, allowing silica production estimates to be obtained in near real time. This method is more economical, faster and less cumbersome than attempting near-real time measurements of silica production using the recent modifications to ^{32}Si methodology (Krause et al. 2011). The required equipment for the PDMPO method is simple and relatively inexpensive: a fluorometer capable of the correct excitation and emission wavelengths, a refrigerator for storing samples during pigment extraction, a small centrifuge, and a drying oven. Qualitative imaging of single cells can be accomplished at sea using a variety of epi-fluorescence microscopes equipped with the appropriate filters. We chose to use a laser confocal microscope and high depth resolution to increase the accuracy of the florescence measurements.

There are a number of uncertainties with the method. Perhaps the most important is the $bSiO_2$:PDMPO incorporation ratio. Using cultures, we found the median ratio was 2,916 with a variance of nearly 30%. The ratio was independent of the growth rate of the cultures

($R^2 = 0.01$) ruling our growth rate as a dominant source of variation. The ratio determined from the Model II regression of natural assemblages, which includes taxa not examined in culture, falls within the confidence interval for the culture-determined ratio and has a narrower confidence interval than the culture results. Our protocols produced an incorporation ratio that was similar to what LeBlanc and Hutchins (2005) found in their culture experiments ($2,800 \pm 780$) and in their field work ($3,045 \pm 230$). However, our field data suggests a linear decrease in the ratio when silicic acid concentration is below 3 µM. We recommend using the ratio determined from cultures, 2,916 to convert quantitative PDMPO incorporation to biogenic silica incorporation when silicic acid concentration is above 3 µM because confounding factors like detection limit, detrital matter, radiolarians and grazing were minor or eliminated in the laboratory experiments. When silicic acid concentration is below 3 µM, we recommend using the linear relationship: $bSiO_2$:PDMPO = 912.6 x [$Si(OH)_4$] determined from the field data.

The decrease in the $bSiO_2$:PDMPO incorporation ratio below 3 µM may be related to shifts in diatom silicon physiology at low substrate concentrations. PDMPO may label newly deposited silica by replacing some of the organic molecules occluded within the frustule potentially polyamines as seen with the fluorescent dye, NBD-N2 and NBD-N3 (Annenkov et al. 2010). Diatoms thin their frustules in order to maintain close to maximum growth rates in low Si water (Brzezinski et al. 1990, 2011a). A decrease in the $bSiO_2$:PDMPO incorporation ratio could occur if the concentration of organic molecules used to organize polymerization in the SDV remains fairly constant while silica content decreases. If this were true, the changing ratio could signify frustule thinning under Si stress. Such mechanistic explanations will remain speculative until the biochemistry of

silicification and the precise role of occluded organic molecules within diatom frustules are better understood.

Determining the average cellular PDMPO fluorescence for different diatom taxa is another source of uncertainty. Single cell fluorescence varied substantially among cells within the cultures imaged for the proof of concept section (see above). This does not represent measurement error, rather it is associated with the inherent variability in the Si content of the various structures being deposited by individual cells during the incubation in this largely asynchronous culture; such conditions would also be expected in a field diatom assemblages. This led to a standard deviation that was 90% of the average cellular PDMPO incorporation within the *P. multiseries* culture. The standard deviation in the fully labeled *T. weissflogii* culture was much lower, 30%. When the measurement goal is a mean incorporation rate we recommend imaging 20 cells or chains for the most abundant diatom taxa, which we find lowers the standard deviation to <100% of the mean. The number of cells that it is practical to image is dictated by the time and expense of searching for cells. As cells become rarer, it may be possible to only image 5-10 cells. Durkin et al. (2012) observed that PDMPO fluorescence of a relatively rare centric diatom (>40 µm) was three orders of magnitude higher than a small, abundant *Fragilariopsis sp.* within the same sample; therefore, these large rare cells could contribute substantially to total community PDMPO incorporation. Despite the high uncertainty associated with imaging fewer rare cells, we note that this variability contains useful biological information and can be exploited to examine cell synchrony, the timing and sequence of frustule development, and division rates (Shipe and Brzezinski 1999).

The PDMPO method is a fairly sensitive means of assessing total community silica production rates. The detection limit of the method was determined by the variability of the unlabeled blanks. Twice the standard deviation of the blank values corresponds to a detection limit of 0.07 µmol Si L^{-1} d^{-1}. Thus, total community silica production can easily be measured in productive coastal waters like Monterey Bay, where silica production ranges from $1 - 30$ µmol Si L^{-1} d^{-1} (Brzezinski et al. 1997) and the Southern Ocean where silica production ranges from $0.25 - 1$ µmol Si L^{-1} d^{-1} (Brzezinski et al. 2001). The method is currently less adept for measuring silica production in the open ocean. Silica production rates at Bermuda Atlantic Time-Series station in the Sargasso Sea average 0.06 µmol Si L^{-1} d^{-1} (Brzezinski and Nelson 1995) and those at the Hawaii Ocean Time series station ALOHA average 0.03 µmol Si L^{-1} d^{-1} (Brzezinski et al. 2011b) which are both at, or just below the detection limit of the current method. It is likely that sensitivity will scale linearly with sample size such that, increasing sample volumes from the current 306 mL to a liter or more would allow production measurements in oligotrophic waters albeit at a higher cost per sample (i.e. three-times as much dye required to get same labeling concentration). It is important to note that the greatest power of the PDMPO method is the ability to measure production by individual cells. Oligotrophic waters do not present an analytical challenge in this regard.

The sensitivity of the PDMPO may also be increased by adding an ionophoric antibiotic rinse in an attempt to remove PDMPO from other organisms within the samples such as dinoflagellates. Despite the methanol rinse we observed PDMPO labeling in non-diatom cells in some of our samples. Alvarado (2012) found that rinsing a sample with ionophoric antibiotics reduces the fluorescence of PDMPO in dinoflagellates by 70%

without significantly changing the fluorescence of the PDMPO bound in diatom frustules. Similarly, using the HF dissolution method we found rinsing with the same ionophores, monensin and nigercin (10 µM), reduced PDMPO fluorescence in a culture of *Pyrocystis fusiformis* incubated in f/2 media with 0.157 nM PDMPO for 24 hours to levels that were not significantly different than the blank (t-test, p=0.12, n=9). For future work, we suggest adding an ionophore rinse as an extra step in filtering the total community measurement as well in preparing the slides for single cell incorporation.

Comments and Recommendations

One of the key components of this method is the conversion of PDMPO to biogenic silica using the $bSiO_2$:PDMPO mole ratio. The cause of variability in this ratio within and among diatom species is not well understood. Future work might consider obtaining isolates of dominant species for culture experiments from assemblages being studied in the field to better contain the incorporation ratio specific to a study site. Or, if ^{32}Si is being used to measure silica production, a site specific ratio can be determined specific to each sampling location by comparing bulk PDMPO incorporation with ^{32}Si production.

PDMPO has the potential to be a powerful tool for understanding diatom physiology, controls on silica production, diatom resource competition and global Si cycling. Additionally, this method can be used to estimate kinetic parameters for Si production, i.e. K_s and V_{max}, for individual diatom taxa. PDMPO can be used to study directly the morphologic shifts such as frustule thinning (Brzezinski et al. 1990) or thickening in Fe limited water (Hutchins and Bruland 1995; Takeda 1998). Knowledge of the contribution of individual diatom taxon to overall community silica production rates will further refine

production models to increase our understanding of the biological and silica pumps in the

ocean.

Chapter 3 Taxon-specific contributions to silica production in natural diatom assemblages

Abstract

The metabolic activity and growth of phytoplankton taxa drives their ecological function and contribution to biogeochemical processes. We present the first quantitative, taxon-resolved silica production rates, growth rates, and silica content estimates for co-occurring diatoms along two cross-shelf transects off the California coast using the fluorescent tracer PDMPO (2-(4-pyridyl)-5-((4-(2-dimethylaminoethylaminocarbamoyl)methoxy)phenyl)oxazole), and confocal microscopy. Taxon contribution to total diatom community silica production was predominantly a function of the surface area of new frustule that each taxon created as opposed to cell abundance or frustule thickness. The influential role of surface area made large diatoms disproportionately important to community silica production over short time scales (<1 d). In some cases, large taxa that comprised only ~15% of numerical cell abundance accounted for over 50% of total community silica production. Over longer time scales relevant to bloom dynamics, the importance of surface area declines and growth rate becomes the dominant influence on contribution to production. The relative importance of surface area and growth rate in relation to silica production was modeled as the time needed for a smaller, faster-growing taxon to create more surface area than a larger, slower-growing taxon. Differences in growth rate between the taxa effected the model outcome more than differences in surface area. Shifts in relative silica production among taxa are time restricted by finite resources that limit the duration of a bloom. These patterns offer clues as to how

taxa respond to their environment and the consequences for both species succession and the potential diatom contribution to elemental cycling.

Introduction

Diatoms play a pivotal role in marine biogeochemistry performing up to one fifth of global primary production (Nelson et al. 1995) by quickly converting inorganic nutrients to biomass. The export of nutrients is especially efficient through diatoms because they are ballasted by a siliceous cell wall, or frustule, that increases the efficiency of carbon export compared to non-mineralized taxa (Buesseler 1998; Armstrong et al. 2001). Diatoms form frustules by actively taking-up silicic acid ($Si(OH)_4$) from the water column and subsequently polymerizing the silicon as hydrated amorphous silica, i.e. opal or biogenic silica ($bSiO_2$). Silica production is closely linked to the cell cycle (Brzezinski et al. 1990): the formation of new valves during cell division and the subsequent deposition of girdle bands enables diatoms to both divide and elongate while encased in a rigid housing. Without sufficient $Si(OH)_4$ diatom growth halts (Darley and Volcani 1969). High diatom productivity and efficient export of particulate silica results in the depletion of silicic acid in the surface-ocean to levels that can limit diatom silica production (Brzezinski et al. 2008; Krause et al. 2012) and potentially growth rate (Dugdale et al. 1995). Differences in silica production and growth rate not only affect the silicon cycle but can also affect the concentration, distribution and fate of other important biogeochemical elements like carbon (Smetacek 1999), nitrogen (Zimmerman et al. 1987), iron (Ingall et al. 2013), and the ratio of silicon to nitrogen (Brzezinski et al. 2002; Matsumoto et al. 2002).

Diatoms are widely recognized as an important functional group in many ocean food-web and biogeochemical models (Jin et al. 2006; Friedrichs et al. 2007) but evidence

also suggests that diatom community composition can significantly alter nutrient use and export potential (Krause et al. 2010; Baines et al. 2010; Durkin et al. 2012; Assmy et al. 2013). Diatoms are one of the most diverse groups of oceanic organisms (Kooistra et al. 2007; Malviya et al. 2016). Cell size ranges from ~5 µm to 2 mm (Hoppenrath et al. 2007) and the silica content of diatom cells, which generally scales with cell size (Conley et al. 1989; Menden-Deuer and Lessard 2000), spans as many orders of magnitude (Brzezinski 1985). Cellular silica content can also vary with cell morphology, which is an important factor when comparing differences in silicification—the amount of Si per unit area off the cell wall—between diatom species (Baines et al. 2010). This wide range of diversity causes differences in community composition to affect rates of nutrient consumption (Krause et al. 2010), the efficiency of particulate organic and inorganic matter export (Baines et al. 2010; Durkin et al. 2012), and biomass available to consumers (Finney et al. 2002). Recent efforts in the Southern Ocean found that thick-shelled, heavily-silicified diatoms were less susceptible to copepod grazing and sequestered more silicon relative to carbon than did thinner-shelled species (Assmy et al. 2013) highlighting a mechanism by which community composition can affect the magnitude of carbon export. A number of studies have suggested that cell abundance may not accurately predict the influence a species has on biogeochemical cycles (Villareal et al. 1993; Goldman 1993; Durkin et al. 2012), yet quantitative measures of taxa-specific silica production of co-occurring diatom taxa do not exist.

Diatom community composition is shaped in part through a diversity of adaptations among taxa to the environment. Diatom species employ disparate metabolic strategies to exploit different nutrient sources within the same environment (Alexander et al. 2015) and

culture studies reveal a range of affinities for a given nutrient (Timmermans et al. 2004; Meyerink et al. 2017). These diverse strategies theoretically allow species to either co-exist or promote species succession and dominance by a few superior competitors. High nutrient environments are often dominated by rapidly growing diatoms like *Chaetoceros* (e.g. Hutchins et al. 1998) that are able to quickly take advantage of abundant nutrients and divide up to three times a day (Myklestad 1977). Slower growing diatoms such as *Rhizosolenia,* employ strategies such as vertical migration (Villareal et al. 1996) and symbiosis (Venrick 1974) and contribute significantly to the silica production in oligotrophic environments (Shipe et al. 1999). Differences in growth rate will influence community composition, species succession, and the identity of diatoms that dominate silica production in a given area.

The ecological and biogeochemical function of a diatom can also be impacted by its physiological plasticity in silicification. Diatoms can alter silicification by changing frustule thickness (Paasche 1973b; Wilken et al. 2011), altering morphology (Marchetti and Harrison 2007; Marchetti and Cassar 2009), and by shifting the degree of condensation of opal (i.e. density of Si) produced in response to environmental stress (La Vars et al. 2013). Changes in silicification will alter a species' contribution to total silica production and influence susceptibility to grazing (Wilken et al. 2011), silica dissolution, and export (Assmy et al. 2013) which in turn can alter dissolved nutrient distributions (Brzezinski et al. 2002; Matsumoto et al. 2002). When silicic acid ($Si(OH)_4$) concentration becomes limiting, diatoms can decrease silicification, which decreases cellular silica quotas and allows them to maintain near maximal growth rates (Paasche 1973a; Brzezinski et al. 1990; Nelson and Dortch 1996). Silicification can also be affected indirectly by changes in growth rate

(Claquin et al. 2002). Generally, there is an inverse relationship between growth rate and silicification (Flynn and Martin-Jezequel 2000) that is hypothesized to result from temporal elongation of the silica precipitation stages of the cell cycle as division rates slow (Brzezinski 1992). Environmental conditions that indirectly affect silicification include light, temperature, macronutrient concentration (including N, P and Si) and trace metal availability (Martin-Jézéquel et al. 2000 and references therein). While it is likely that differences in cell physiology affect the cycling of silica, how the interplay between growth rate and silicification influences silica production rates of natural diatom assemblages remains unclear.

The recent development of a new method that uses the fluorescent dye, PDMPO (2-(4-pyridyl)-5-((4-(2-dimethylaminoethylaminocarbamoyl)methoxy)phenyl)oxazole) and confocal microscopy to quantify cell-specific silica production rates (McNair et al. 2015) has made it possible to assess silica production rates, silicification, and growth rates of co-occurring diatom taxa allowing evaluation of how taxonomic composition of diatom communities drives observed rates of total community silica production. Moreover, this method allows evaluation of how several cell attributes such as abundance, surface area, size, and growth rate, determine a species contribution to total community silica production. Previous studies have used PDMPO to qualitatively measure diatom silica production in both marine and freshwater systems (LeBlanc and Hutchins 2005; Znachor and Nedoma 2008; Durkin et al. 2012; Znachor et al. 2013) each with a different approach to quantifying PDMPO fluorescence (i.e. flow cytometry, confocal or epifluorescent microscopy with unique image analysis). Here, we apply the PDMPO method of McNair et al. (2015) along two transects off the California coast to diagnose and quantify the factors governing

individual species contribution to total diatom silica production. Our analysis is facilitated by the wide range of environmental conditions diatoms experience along the strong cross-shelf gradients in nutrient concentration, diatom biomass, and silica production in this coastal upwelling zone.

Methods

Environmental data

This study was conducted as part of the July 2014, IrnBru (MV1405) cruise aboard the R/V *Melville*. Data presented here were collected during two transects. The northern transect (Transect 9) was sampled from 20-21 July, 2014 and started near Cape Blanco (Oregon, United States) and the southern transect (Transect 2) was sampled from 7-8 July, 2014 and began near Point Arena (California, United States, Fig. 1). Each transect was designed to follow the trajectory of a cold plume of upwelled water as it was advected off shore. The northern transect extended ~100 km southwest away from shore and the southern transect extended ~200 km west, away from shore.
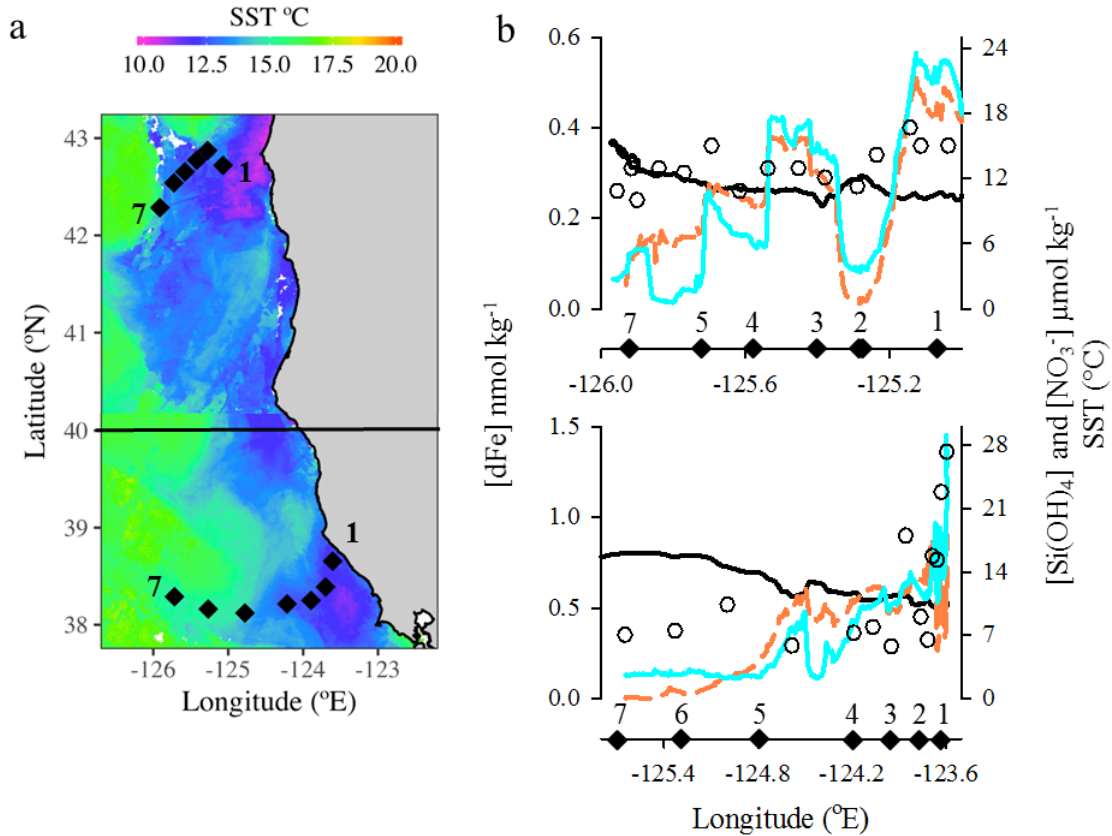
Figure 3-1: (a) California coast with stations of the northern and southern transect depicted as black diamonds superimposed over SST depicted as a color gradient, numbers correspond to stations which are sequentially labeled with 1 nearest to shore and 7 farthest offshore. SST from Aqua MODIS 8 day composite. Northern transect SST centered on July 20, 2014, southern transect SST composite centered on July 7, 2014 are separated by a black line. (b) The concentration of nitrate (orange dashed line), silicic acid (cyan line), dissolved iron (white circles) and sea surface temperature, SST (black line) across the northern (top) and southern (bottom) transects; stations are marked along the x-axis with a diamond and station number.

A suite of environmental measurements were taken at regular intervals along both transects. Sea surface temperature (SST) and salinity were recorded from the ship's flow-through seawater system. Water samples were collected in the upper 5 m using a towed trace metal clean surface pump, the GeoFish (Bruland et al. 2005). Water collected from the GeoFish was used for incubation experiments as well as for determination of trace metal and macronutrient concentrations. Nitrate, phosphate, and silicic acid were measured onboard using a Lachat flow injection analysis system (Parsons et al. 1984). All sample and reagent bottles for analysis of dissolved Fe (dFe) were rigorously cleaned in accordance with the

GEOTRACES cookbook (Cuttler et al. 2014). Dissolved iron concentrations for Transect 2 were measured using an offline preconcentration method followed by analysis with a Thermo Fisher Element XR inductively coupled plasma mass spectrometer (ICP-MS) according to Biller and Bruland (2012) as adapted by Parker et al. (2016) and dFe concentration for Transect 9 were measured using a shipboard flow injection analysis method with a catalytically enhanced adsorption signal as in Lohan et al. (2006) with adaptations described in Biller et al. (2013).

A variety of samples were taken to characterize the biology across the transects. Biogenic silica ($bSiO_2$) and $[Si(OH)_4]$ were measured using the colorimetric ammonium molybdate methods (Brzezinski and Nelson 1995; Krause et al. 2009). Diatom cell abundance and taxonomic identification was determined by preserving a 100 mL aliquot of water with 5 mL of Bouin's Solution in French square bottles. Cells were enumerated and identified by microcopy following the Utermöhl method (Utermohl 1958).

Silica production rates

Community *s*ilica production rates were measured radiometrically using ^{32}Si and diatom taxon-specific silica production rates, growth rates, and silicification were measured fluorometrically with PDMPO. Both production rates were measured in 24 h deck-board incubations. The 24 h incubation time ensured samples experienced equal length of light and dark despite differences in starting times. At roughly equal 2 h intervals along the transects, surface water was collected from the GeoFish and pooled into carboys, that had sat with 10% trace-metal-grade HCl at least three days, within a trace metal clean enclosure. The pooled water from the carboy was then used to fill three 250 mL polycarbonate bottles, that were acid cleaned with 10% trace-metal-grade HCl overnight, to the brim—one each for

^{32}Si, PDMPO, and a PDMPO blank which allows for subtraction of natural fluorescence in the sample that overlaps with PDMPO emission. Additional subsamples were used to determine bSiO$_2$, [Si(OH)$_4$], and diatom cell abundance and identification. The three sample bottles were spiked with either high-specific activity ^{32}Si (15,567 Bq µg^{-1} Si) or 48 µL of 1 mM PDMPO (LysoSensor Yellow/Blue DND-160, Molecular Probes) or nothing (PDMPO blank). 260.5 Bq of ^{32}Si was added to samples from the northern transect and 293 Bq of ^{32}Si was added to samples from the southern transect; we decided less isotope was needed for the northern transect upon reassessment after the southern transect.

Following the 24 h incubation, water samples were vacuum filtered through 25 mm, 1.2 µm polycarbonate filters. Community silica production rates were determined by measuring ^{32}Si incorporation using low-level beta detection as in Krause et al. (2011). Cell-specific silica production rates were determined by measuring PDMPO incorporation following McNair et al. (2015) but with an alteration to slide preparation. Instead of the freeze transfer method described in McNair et al. (2015), microscope slides for this study were prepared by resuspending an aliquot of the concentrated methanol sample (McNair et al. 2015) in deionized distilled water (~ 18MΩ) to dissolve some of the precipitated salts. The sample was centrifuged and the supernatant removed to concentrate the cells, the remaining 200 µL of concentrated sample was pipetted as a droplet onto a polylysine-coated, glass slide. After the water evaporated, a coverslip was applied with ProLong gold antifade (Life Technologies) and sealed with clear nail polish. Preparing the slides in this matter helped keep the more delicate parts (i.e. setae) of frustules intact whereas the freeze transfer method used previously damaged more fragile cells. Cells were imaged using the Olympus Fluoview 1000 Spectral Confocal microscope at the Neuroscience Research

Institute at the University of California, Santa Barbara as described in McNair et al. (2015). Confocal microscopy takes a series of images at discrete depth steps of 420 nm which are reassembled with image analysis to create a 3D reconstruction of a cell which allows us to measure the total fluorescence of a cell as well as the total surface area of frustule that has been labeled.

Image processing

Each cell image was analyzed for total fluorescence and the surface area labeled with PDMPO using Imaris 8.4.0 software (Bitplane) as in McNair et al. (2015). Cellular PDMPO was converted to $bSiO_2$ using a laboratory-created standard of fully labeled diatom cells of known (i.e. independently measured) silica content (McNair et al. 2015) allowing fluorescence to be quantitatively converted to Si incorporation. Measures of cellular silicification ($bSiO_2$ μm^{-2}) were derived by dividing the amount of silica produced by the surface area of the 3-dimensional frustules. Eleven taxa were included in the single-cell analysis. Taxa were chosen based on numerical abundance and presence at multiple stations.

The silica produced per taxonomic group was calculated as the product of the average silica produced by a single-cell of that taxon over the course of the incubation and the cell abundance of that taxon from the start of the incubation. A novel method was used to calculate single-cell silica production rates that employed patterns of PDMPO labeled frustule to trace daughter cells formed during the incubation back to a starting mother cell. Figure 2 illustrates the PDMPO labeling pattern expected for both solitary and chain forming cells, starting with a mother cell that is poised to divide and deposit a new valve. Division of the mother cell results in two daughter cells with one fully labeled valve each (D1). Both daughter cells then proceed to deposit girdle bands resulting in two half-labeled

cells at the end of one division. In the second division (D2), both daughter cells divide and produce girdle bands—in total, two of the four new daughters are fully labeled and the other two are half labeled (Fig. 2). A third division results in six fully labeled daughters and two half-labeled daughters (D3). Thus, the silica produced by a single-cell from the start of the incubation (mother cell) is the combined fluorescence of all the daughter cells.
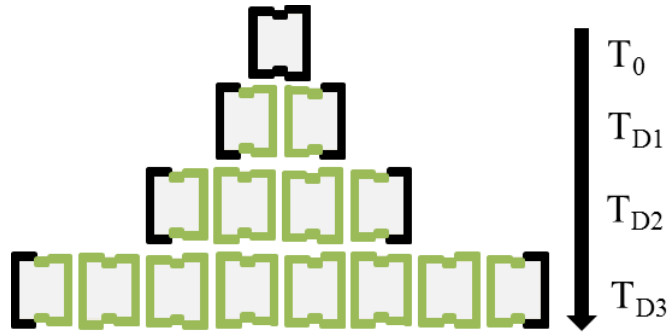
Figure 3-2: Pattern of florescent PDMPO label (green) as the cell goes through one, two and three divisions.

The fluorescent PDMPO pattern in every image of every cell collected with the confocal microscope was analyzed to calculate the average silica production of mother cells. For chain forming diatoms, the history of division is preserved in the labeling pattern of the chain—if a chain consists of two half-labeled cells, one division occurred and an entire cell's worth of silica is attributed to a single mother cell. Daughter cells physically separate in solitary forms necessitating a different approach. Because we are imaging a small, random, subsample of the cells from the total population we assume that in the case of solitary forms we never imaged two daughter cells from the same dividing mother cell. Thus, a half-labeled, solitary cell indicates that a mother cell divided and produced the fluorescent-labeled silica deposited in the observed daughter plus an equal amount of silica from the second daughter that was not imaged. Cells that were labeled entirely were assumed to originate from a mother cell that divided at least twice producing the equivalent of three entire cells worth of biogenic silica (Fig. 2). In our experiments, half-labeled cells of

47

solitary species were regularly encountered, while fully labeled cells were rare compared to an expectation of the 50% relative abundance expected if most cells had undergone two divisions. For slowly dividing cells, where only a portion of the girdles were labeled, the deposition rate is simply the amount of silica corresponding to the measured total cellular PDMPO fluorescence over the incubation. Total silica production by each taxon was calculated as the product of the abundance of the taxa at the beginning of the incubation and the average single-cell silica production rate for measured cells. Alternatively to this method, taxon-specific silica production rates could be calculated as the product of average the fluorescence per cell within a taxon then multiply by the abundance of the taxon at the end of the incubation, which would yield the same result as the method we employed. However, our cell counts were taken at the beginning, not the end, of the incubation and we find that the amount of detail gained from the method above makes the extra effort worth the result.

The frustule labeling pattern was also used to calculate cell growth rates using a method similar in concept to Shipe and Brzezinski (1999) and Brzezinski and Conley (1994) (Fig. 2). Using the logic above, rapidly growing, solitary cells were estimated to have undergone one (half-labeled cells) or two (fully-labeled cells) divisions corresponding to a growth rate of 0.69 d^{-1} and 1.39 d^{-1} respectively. For chain forming diatoms the number of labeled cells produced is more easily determined allowing growth rate to be calculated with the logistic growth equation where N is the number of cells at time t and N_0 is the number of cells at t_0:

$$\mu = \frac{\ln(\frac{N}{N_0})}{t} \tag{1}$$

For slowly dividing cells, the division rate was calculated from the fraction of total

cell surface area that was labeled. The total cell surface area for centrics was calculated as a

cylinder with diameter and depth measurements from microscopy images. The image

processing software, Imaris calculates the area of fluorescent label for any object in an

image; for all other taxa, total surface area measurements were taken from fully labeled cells

of a similar size within the taxa. This latter calculation implicitly assumes that silicification

occurs at a constant rate for all components of the frustule, which is only approximate given

the links between the formation of each component of the frustule and the cell cycle

(Brzezinski et al. 1990; Brzezinski 1992).

The surface area of a cell at the beginning of the incubation was back-calculated

from the surface area labeled with PDMPO and the calculated growth rate. First, the

exponential growth equation was defined in terms of surface area where SA_{int} is the surface

area of the cell at the beginning of the incubation, SA_{new} is the new frustule surface area

created over the course of the 24h incubation, μ is the daily growth rate and t is the time in

days:

$$(SA_{new} + SA_{int}) = SA_{int}e^{\mu t}$$

Solving for SA_{int} gives equation 2:

$$SA_{int} = \frac{SA_{new}}{(e^{\mu t}-1)} \tag{2}$$

The silica content of each individual cell was calculated by multiplying silicification (fmol

Si μm^2) by the surface area of the cell (μm^2).

Statistical analysis

All statistical analyses were conducted using JMP 12 software (SAS Institute Inc.).

Simple linear regressions rather than reduced major axis regressions were used to test the

effect of cell surface area, growth rate, and silicification on silica production rates because of the asymmetric relationship between variables (i.e. the X and Y variables were not interchangeable) (Smith 2009). The general multiplicative nature of allometric measurements often necessitates data to be log transformed (Kerkhoff and Enquist 2009) to ensure residuals are normally distributed. This was also the case for the regressions preformed here; surface area data and silica production rates were log transformed for ordinary least squares linear regressions. ANCOVA was used to test for differences in growth rate between the transects.

Results

Method comparison

The participation of multiple research groups in the IrnBru cruise created the opportunity to compare methods that measure the silica content of single diatom cells. Single-cells of *Chaetoceros* were analyzed for silica content using PDMPO and confocal microscopy (McNair et al. 2015) and using synchrotron x-ray fluorescence (SXRF) (Twining et al. 2011). SXRF cannot resolve the fine-scale setae so they were excluded from these comparison measurements. Because PDMPO and SXRF data were not analyzed from the same stations, the silica content of *Chaetoceros* were compared from two geographically close stations, situated at the edge of the continental shelf. The average silica content of 28 *Chaetoceros* cells from station 2 of the southern transect (38°23'20.40"N, 123°42'3.60"W, collected July 7, 2014) was determined by analyzing fully labeled *Chaetoceros* cells using Imaris software to isolate the fluorescence of the main body of each cell. The average silica content using the PDMPO method was 0.20 ± 0.07 (S.D.) pmol Si cell^{-1}. Using the SXRF

method, 13 cells of *Chaetoceros* had an average of 0.17 ± 0.05 (S.D.) pmol Si cell^{-1} (Twining, unpubl. data). The cells analyzed with SXRF were collected 29 km south and three days after the collection of cells for PDMPO (38° 9'11.23"N, 123°34'47.35"W, collected July 10, 2014). Despite the variation in silica content of *Chaetoceros* across the transects, the two methods find very similar results giving independent verification of the data produced through the PDMPO method.

Environmental setting and diatom community trends

The thirteen stations examined in this study sampled a range of environmental conditions. The transects roughly traced the trajectory of upwelled water by sampling through a plume of cold water as determined from daily SST satellite images (Fig. 1). The northern transect generally stayed within the upwelled plume except for station 2. Along the southern transect station 1 through 4 were in the upwelled plume, station 5 marked a transition to warmer more oligotrophic water seen at stations 6 and 7.

Nearshore, where deep water had most recently been upwelled to the sunlit surface, the water was cold and contained high concentrations of macronutrients (Fig. 1). Nitrate and silicic acid concentrations were higher nearshore on the northern transect than the southern transect (Table 1). Conversely, [dFe] was higher along the southern transect than the northern. Nutrient concentrations decreased away from shore and water temperature increased. Macronutrient concentrations were highly correlated: nitrate and phosphate ($r = 0.96$, $p < 0.001$), nitrate and silicic acid ($r = 0.84$, $p < 0.001$) and silicic acid and phosphate ($r = 0.85$, $p < 0.001$) although at some stations silicic acid depletion exceeded that of nitrate (Fig. 1) which is indicative of Fe stress (Hutchins and Bruland 1998).

Diatom assemblage composition of the eleven taxa included in the single-cell analysis varied between the two transects as well as between stations within a transect (Fig. 3a and c). Smaller diatoms such as *Fragilariopsis pseudonana c.f.,* small centrics, and *Nitzschia americana,* dominated the assemblages at station 1 and 7 in the northern transect and at stations 5 and 7 of the southern transect. Along the southern transect, the diatom assemblages at stations 1 through 4 were composed of >90% of *Chaetoceros spp.* Assemblage composition was more diverse across stations in the northern transect, with 3-4 diatom taxa contributing to most of the cell abundance, although *Chaetoceros spp.* were consistently 50-80% of the assemblages at stations 3 through 5. The large diatoms *Proboscia alata* and *Lauderia annulata* were observed at all stations along the northern transect except for station 1.
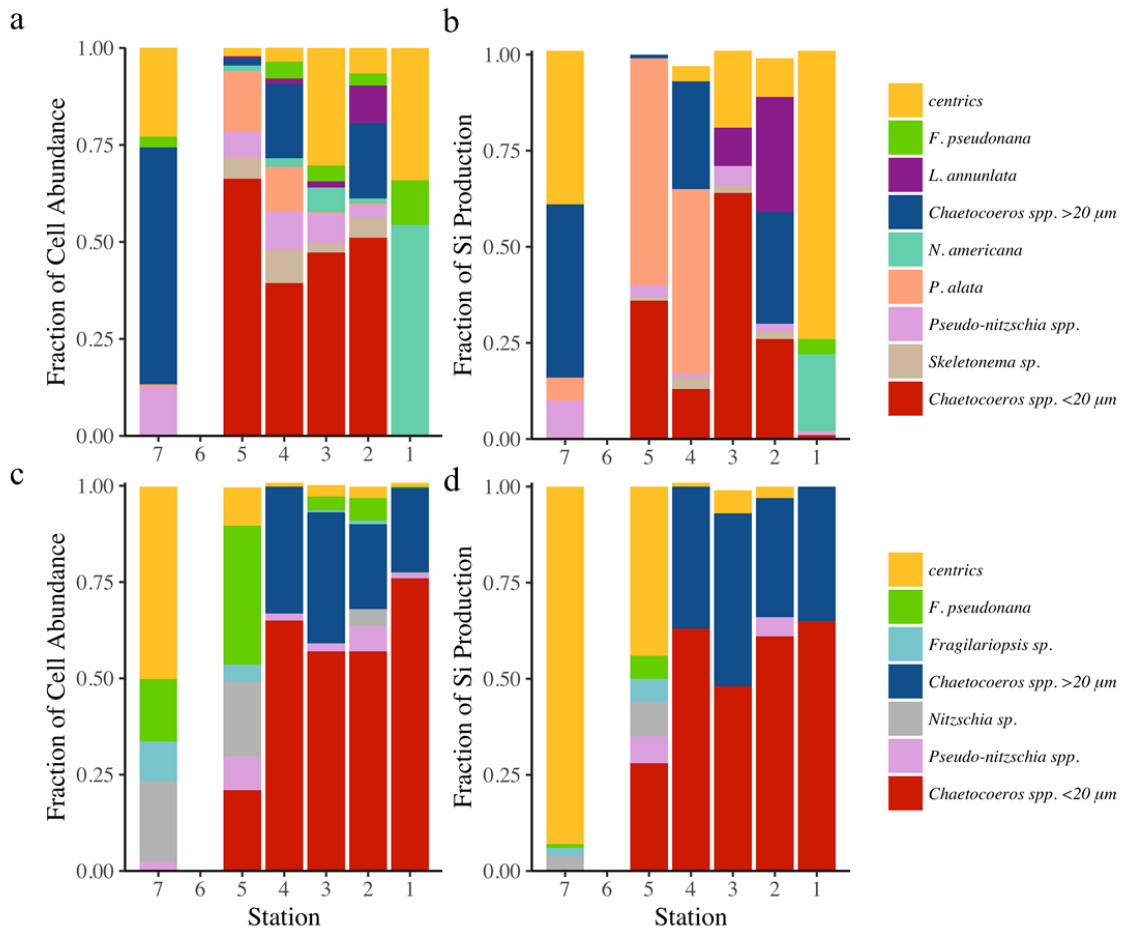
Figure 3-3: The fraction of cell abundance for taxa included in the single-cell analysis along the northern (a) and southern (c) transect. The fraction of silica produced by groups along the northern (b) and southern (d) transect. Note, cells from taxa not included in the single-cell analysis are not considered here.

The concentration of bSiO$_2$, a metric for diatom biomass, increased away from shore along the northern transect from 0.9 µmol L^{-1} at station 1 to 5.2 µmol L^{-1} at station 5, and decreased away from shore along the southern transect from 10.6 µmol L^{-1} at station 1 to 0.06 µmol L^{-1} at station 7 (Table 1). Diatom community silica production rates (ρ, µmol L^{-1} d^{-1}) as measured with ^{32}Si tracer, fluctuated across the transects and generally increased with increasing bSiO$_2$. Specific silica production rates (V_b, d^{-1}), the rate of silica produced normalized to the concentration of bSiO$_2$, were higher near shore in both transects. The highest specific silica production rate measured was 0.85 d^{-1} at station 1 of the northern

transect, followed closely by station 3 on the southern transect, 0.85 d^{-1}. The lowest specific

silica production rates were measured at station 5, 0.21 d^{-1}, on the northern transect and

station 6 and 7, 0.10 d^{-1}, on the southern transect.

Table 3-1: Overview of the environmental variables from both transects and diatom community silica production rates

Northern Transect

St.	T (°C)	Salinity	$[NO_3^-]$ ($\mu mol\,kg^{-1}$)	$[PO_4^{2-}]$ ($\mu mol\,kg^{-1}$)	$[Si(OH)_4]$ ($\mu mol\,kg^{-1}$)	[dFe] ($nmol\,kg^{-1}$)	Diatoms ($x10^3\,cells\,L^{-1}$)	$bSiO_2$ (μM)	Silica Production		
									ρ ($\mu mol\,Si\,L^{-1}\,d^{-1}$)	V_b (d^{-1})	V_b (d^{-1}) Single cell ave.
1	10.5	33.5	18.1 ± 0.6	1.4 ± 0.03	21.2 ± 0.6	0.57	1,450	0.9	1.2	0.86	0.96
2	12.2	32.3	0.88 ± 0.1	0.4 ± 0.01	3.8 ± 0.1	0.31	243	0.7	0.38	0.44	0.84
3	10.6	33.4	13.6 ± 1.5	1.2 ± 0.1	16.0 ± 1.4	0.48	347	0.8	0.43	0.43	1.07
4	10.9	33.0	9.6 ± 0.3	0.9 ± 0.01	6.2 ± 0.4	0.38 ± 0.2	465	4.5	2.25	0.41	0.74
5	11.6	32.8	7.2 ± 0.3	0.7 ± 0.03	2.0 ± 0.6	0.23	1,030	5.2	1.2	0.21	0.70
7	13.9	32.5	3.7 ± 0.9	0.4 ± 0.004	3.6 ± 0.9	0.22	66.2	0.4	0.12	0.26	0.63

Southern Transect

St.	T (°C)	Salinity	$[NO_3^-]$	$[PO_4^{2-}]$	$[Si(OH)_4]$	[dFe]	Diatoms	$bSiO_2$	ρ	V_b	V_b Single cell ave.
1	10.7	33.8	6.9 ± 0.2	0.77 ± 0.01	16 ± 0.3	0.36	12,400	10.6	11.5	0.74	0.98
2	10.5	33.3	14 ± 0.3	1.4 ± 0.03	12.4 ± 0.7	0.31	922	1.7	NA	NA	1.48
3	11.4	33.7	11 ± 1	1.0 ± 0.02	11 ± 0.4	0.30	2,940	5.9	7.9	0.85	1.10
4	11.6	33.4	10 ± 0.1	0.96 ± 0.01	7.2 ± 0.3	0.29	2,270	4.2	3.8	0.64	0.92
5	13.8	33.0	4.5 ± 0.2	0.6 ± 0.02	2.7 ± 0.3	0.36	34	0.6	0.08	0.13	0.81
6	15.8	32.8	0.55 ± 0.08	0.34 ± 0.01	2.8 ± 0.07	0.31	NA	0.08	0.009	0.10	
7	15.9	32.8	0.09 ± 0.06	0.29 ± 0.01	2.6 ± 0.06	0.24	7.5	0.06	0.006	0.10	0.95

Specific silica production rates of co-occurring taxa were weighted according to

fraction of $bSiO_2$ content and averaged for each station to compare with silica production

rates measured with ^{32}Si. Specific silica production rates averaged from single-cell

production rates were 10-90% higher than the specific silica production rates measured with

^{32}Si (Fig. 4). Specific silica production rates measured with ^{32}Si are normalized to the

standing stock of $bSiO_2$ which includes both living, actively growing cells and inactive or

pieces of cells as detritus. The detritus will tend to cause an underestimate of the specific

silica production rate compared to that of the living cells. By comparing the two measures of

specific silica production rates we can estimate the fraction of $bSiO_2$ pool that is detrital.

This comparison assumes that, although there were more taxa present, the eleven taxa included in the single-cell measurements are representative of the entire community. The fraction of $bSiO_2$ in the living cells was highest near shore on the transects, 80-90%, and decreased away from shore. The farthest offshore station of the northern transect had 60% of the $bSiO_2$ in living cells and the farthest offshore station of the southern transect had only 10%.
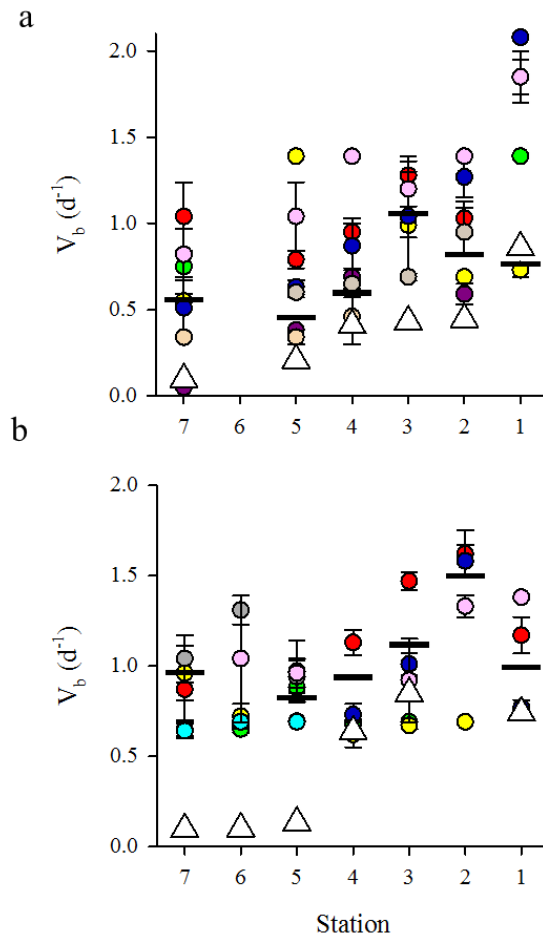
Figure 3-4: Average specific silica production rate for taxa along the a) northern and b) southern transect. Taxa colors match the key from Fig 3. White triangles are specific silica production measured with 32Si, solid, horizontal, lines are the weighted average of the taxa-resolved specific silica production rates.

Single-cell silica production

Single-cell silica production rates (pmol Si cell^{-1} d^{-1}) varied more between taxa than the silica production rates for the same taxon in different environments (Fig. 5a). Within taxonomic groups, silica production ranged one to three orders of magnitude while differences between diatom taxa spanned over three orders of magnitude. The small pennates, *F. pseudonana* and *N. americana,* had the lowest median silica production rate, 0.06 pmol Si cell^{-1} d^{-1}. The large centric, *P. alata* had the highest median silica production rate 5.6 pmol Si cell^{-1} d^{-1} (Fig. 5a, average taxa silica production rates by station in Supplemental data).
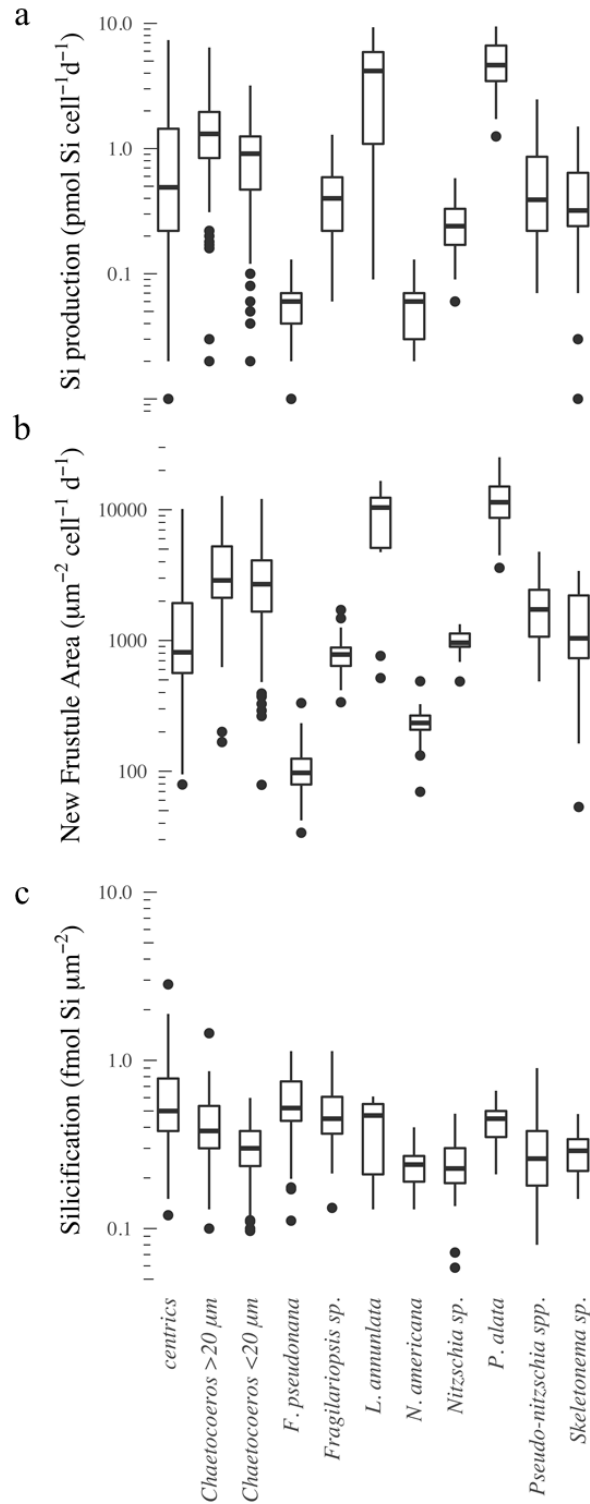
Figure 3-5: Si production (a), new frustule surface area (b), and silicification (c) combined across stations for all taxa examined in this study. The box represents the, 25th, median and 75th quartiles. The whiskers extend 1.5 times the distance between the first and third quartiles, dots denote data that extend beyond the end of the whiskers.

Two frustule attributes affect the amount of silica that a cell produces: the rate at which new frustule area is created (μm^2 cell^{-1} d^{-1}) and the degree of silicification of the new frustule (fmol Si μm^{-2}) with the cellular silica production rate (pmol Si cell^{-1} d^{-1}) being simply the product of the two. Within a taxonomic group, the new frustule surface area (SA) created during the 24 h incubation spanned two orders of magnitude; among different taxa it spanned three orders of magnitude (Fig. 5b). In contrast, silicification varied less than one order of magnitude both within a taxon and between taxa (Fig. 5c). Frustule SA and silicification have equal potential to alter the amount of silica a cell produces—for example doubling the SA of new frustule created or doubling silicification will result in a two-fold increase in silica production. Among the diatom communities examined here, new frustule SA accounted for most of the variability in silica production rates (Fig. 6a). The station and taxa averaged SA of new frustule created over a day explains 86% (p <0.001) of the variance in average cellular silica production rate while differences in average silicification explains only 7% (p = 0.02, Fig. 6b). When the regression is run with all data points instead of averages, the SA of new frustule accounts for 86% (p <0.001) and silicification is 17% (p <0.001), with the two regression coefficients summing to near unity as expected since the production rate is the product of the two variables.

58
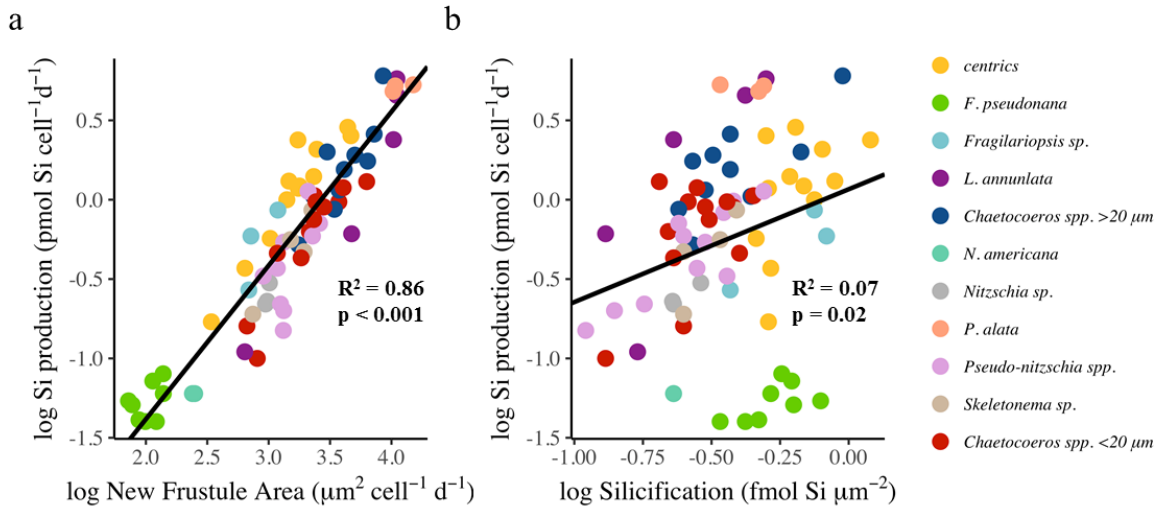
Figure 3-6: The relationship between silica production and new frustule area (a) or silicification (b). Each point represents the average value for a taxon at one station. The coefficient of determination is given for the standard least squares regression.

Given the importance of SA_{new} to silica production it is critical to understand what factors govern the extent of new frustule created. With the approximation that silicification across the frustule is uniform, SA_{new} is the product of two factors: cell size expressed as surface area (μm^2 cell^{-1}) and growth rate (d^{-1}). Between these factors, SA had the largest relative dynamic range from 46 μm^2 cell^{-1} for *F. pseudonana* to 25,000 μm^2 cell^{-1} for *P. alata*. The maximum growth rate realized by a diatom taxon ranged from 0.46 d^{-1} to 2.08 d^{-1} (Supplemental data Table 1). Considering all taxa together, the SA of taxa at the beginning of the incubation, SA_{int}, explained 75% ($p < 0.001$) of the variability in total community new surface area created while growth rate explained 1% ($p = 0.49$, Fig. 7). Closer inspection of Figure 7b shows that while the relationship overall is not significant between growth rate and new frustule SA, it is fairly strong for a number of individual taxa with new frustule SA increasing approximately linearly with growth rate over the short duration (24 h) of these experiments. *L. annulata* and *Chaetoceros* < 20 μm groups had the strongest relationship between growth rate and new frustule area. The slope for species *L. annulata* was 1.9

59

$(R^2=0.95, p=0.005)$ and *Chaetoceros* < 20 μm the slope was 0.44 $(R^2=0.43, p=0.01)$. No significant relationship was found between cell size and slope of the relationship between growth rate and SA_{new} likely due to the limited number of taxa examined.
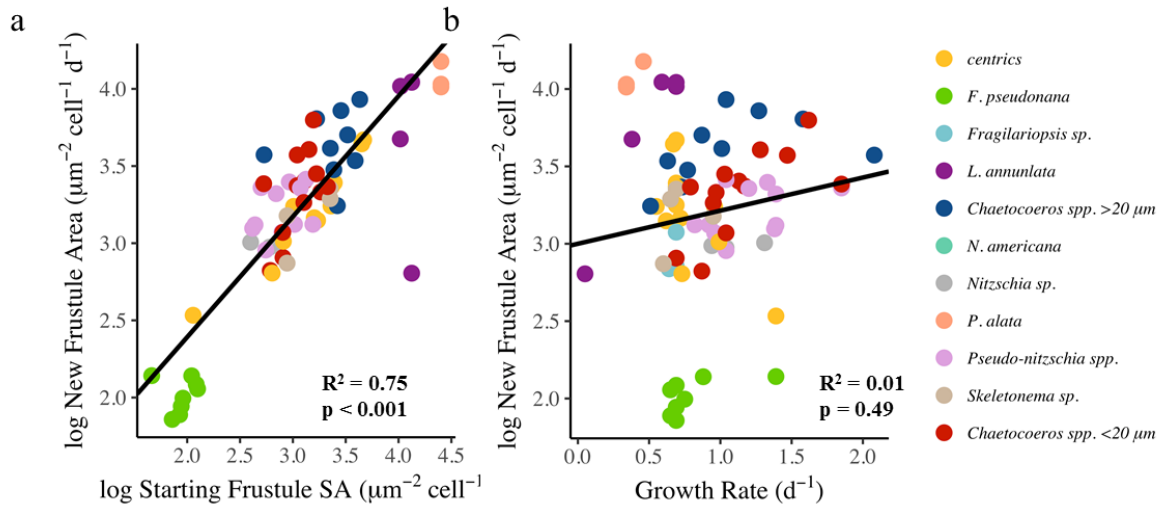
Figure 3-7: The relationship between new frustule surface area and cell size i.e. starting frustule surface area (a) or growth rate (b). Each point represents the average value for a taxon at one station. Standard least squares regression model.

The single-cell analysis allows for the first quantitative evaluation of how well cell abundance predicts silica production compared to surface area. Across taxa, the fractional contribution to total SA_{new} explained 92% $(p < 0.01)$ of the variability in the fractional contribution to silica production with a slope of 0.97 $(p < 0.01)$ (Fig. 8a). That is a much stronger relationship than that between relative population size (fraction of total cell abundance), which only explained 62% $(p < 0.01)$ of the variation in contribution to silica production. Fractional contribution to total cell surface area, SA_{int}, explained 89% $(p < 0.01)$ of the variability in the taxa's proportional contribution to Si production however the slope is slightly less, 0.93 $(p < 0.01)$, than the relation with fraction of SA_{new} (regression not shown).
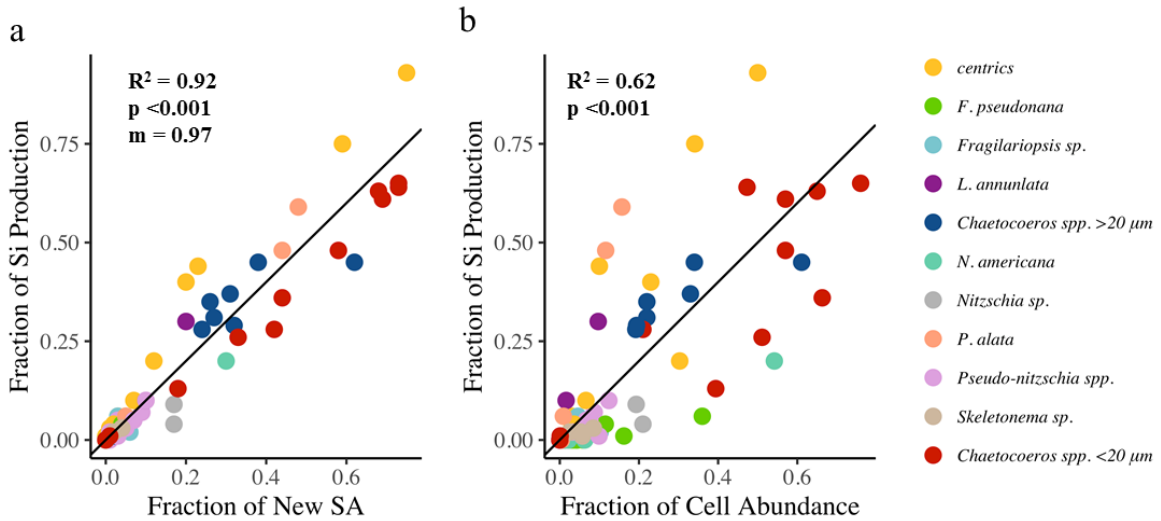
Figure 3-8: Relationship between fraction of silica production and fraction of new frustule SA (a) or fraction of cell abundance (b). Each point represents the average value for a taxon at one station. The line depicts the one to one ratio. Regression model is standard least squares.

The analysis above shows that a taxon's contribution to short-term (<1 d) silica production can be reasonably calculated from its fractional contribution to the new frustule SA produced, however, relative species abundances will shift over time because of differences in growth and loss rates among taxa. While we cannot evaluate loss terms (e.g. apoptosis, grazing mortality) there are two patterns of growth rate emerge among the taxa examined: 1) a persistence pattern where the taxon maintains a similar growth rate across transects even as the environment changes and 2) a dynamic response where the growth rate of the taxon changes with nutrient concentration (Fig. 9). Growth rate varies little within *F. pseudonana, P. alata, Skeletonema sp.,* and centrics, which show a more persistent pattern across transects. *Chaetoceros* show a more dynamic growth rate pattern, where growth rate peaks nearshore in higher nutrient water and declines away from shore. The growth rate of *Pseudo-nitzschia spp.* is not clearly dynamic or persistent; the noisy pattern likely arises from the grouping of multiple species within this classification as well as only a few cells being imaged at some of the stations.
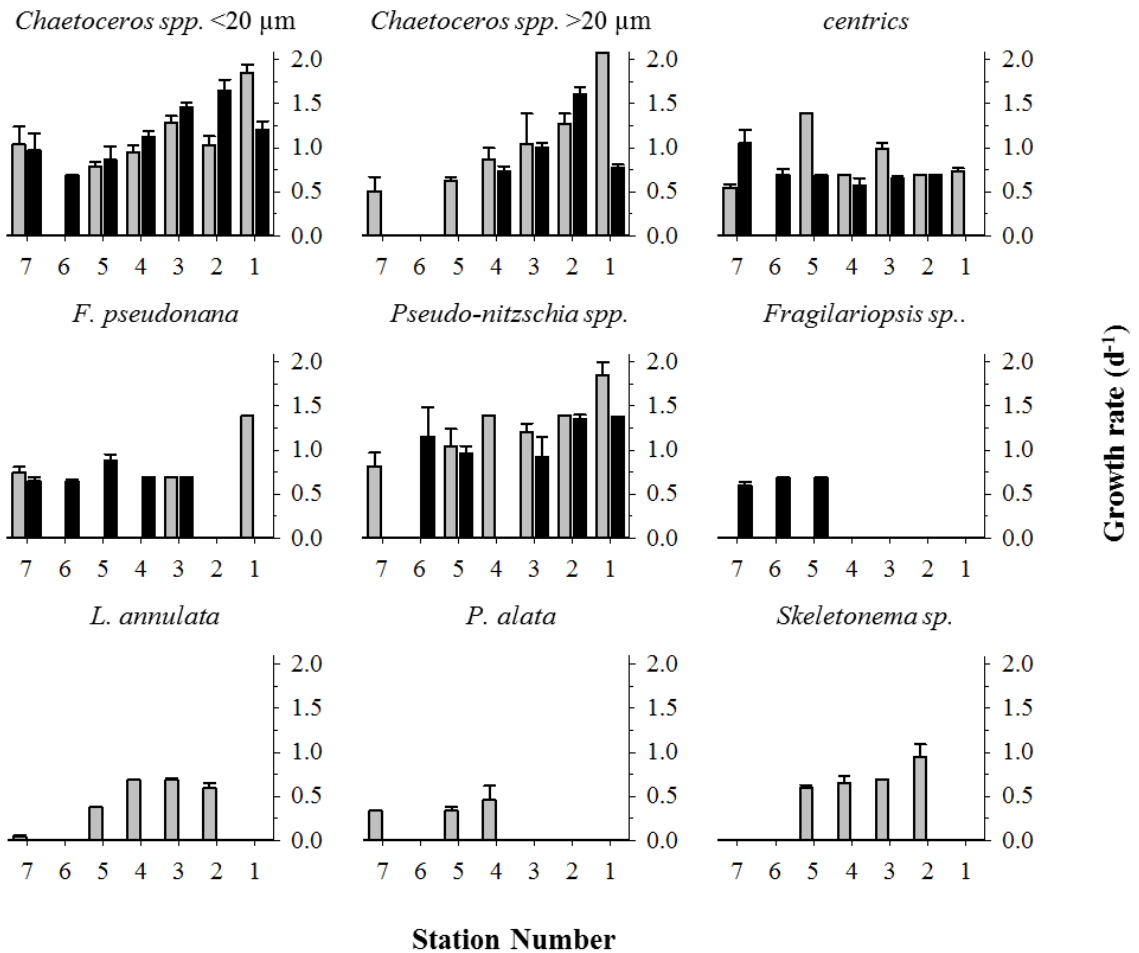
Figure 3-9: Taxa-specific growth rate across the northern (gray bars) and southern (black bars) transects. Error bars are standard error, where error bars are absent N=1. Station one is closest to shore and seven is farthest offshore.

Of all the taxa examined, growth rate was only significantly correlated with macronutrient concentrations for the two size classes of *Chaetoceros* and *Pseudo-nitzschia spp*. There was no significant effect of transect on the relationship between macronutrients and growth rate, thus data from both transects was combined for the linear regressions. The coefficient of determination (R^2) of growth rate of *Chaetoceros* >20 μm with relation to $[NO_3^-]$, $[PO_4]$, and $[Si(OH)_4]$ was 0.41 ($p = 0.05$), 0.46 ($p = 0.03$), and 0.47 ($p = 0.05$) respectively. The coefficient of determination (R^2) of growth rate of *Chaetoceros* <20 μm with relation to $[NO_3^-]$, $[PO_4]$, and $[Si(OH)_4]$ was 0.68 ($p <0.001$), 0.75 ($p <0.001$), and 0.76

(p <0.001) respectively. The growth rate of *Pseudo-nitzschia spp*. was significantly only correlated with [Si(OH)$_4$], R^2 = 0.46 (p = 0.02). There was not a significant relationship between growth rate and [dFe] for any of the taxa examined.

Discussion

The PDMPO method allowed quantification of the relative importance of different diatom taxa to total community silica production. The close agreement between the silicon content of cells measured with PDMPO and SXRF adds rigor to the measurements. Through the use of confocal microscopy we are able to evaluate how the interplay between three-dimensional cell surface area, silicification, and growth rate affect the contribution of an individual taxon to the total silica produced by the diatom community.

Diatom contributions to silica production

Only one to two of the eleven taxa measured at each station were responsible for the majority of community silica production (Fig. 3). The monopoly of silica production by two or three taxa only becomes apparent using single-cell analysis that can partition silica production between taxon in a community. Relatively large cell size and abundance are common attributes among taxa that dominate silica production. In this study, surface area was the best indicator of short-term silica production rate with silicification playing a relatively minor role (Fig. 6).

The minimal influence of silicification was a surprising result, as prior observations off the California coast have shown a strong positive effect of low dFe on diatom silicification (e.g. Hutchins and Bruland 1998). However, these previous experiments were conducted with the addition of 2.5-10 nM Fe over four days while our incubations were

shorter and were not amended with Fe and thus represented a short glimpse into the physiology of diatoms in different environmental conditions rather than the release from limitation. While we did see differences in silicification within individual taxa (Fig. 5c) the variation in new frustule area was much larger, making surface area the dominant factor accounting for variation in silica production among taxa.

Despite their relatively low abundance, large diatom species have been hypothesized to disproportionately contribute to silica production, with a number of studies pointing to large cells being important contributors to biogeochemical cycles (e.g. Villareal et al. 1996; Goldman and McGillicuddy 2003; Durkin et al. 2012). Our results further support the importance of large cells—when comparing single-cells of different diatom species, silica production rates were more influenced by cell size (Fig. 6a) than silicification (Fig. 6b). The most striking example of a disproportionately high contribution of large-rare-cells to community silica production can be seen at station 4 and 5 in the northern transect. *P. alata* is a large diatom cell (length 200-1000 µm, width 7-10 µm) whose abundance accounted for only 12% and 16%, respectively, of the total cells in the community analyzed, but it was responsible for 45% of the silica produced at station 4 and 56% the silica produced at station 5 (Fig. 3). The disproportionate contribution of large cells to silica production is also highlighted in Figure 8b where cells above the 1:1 line produce more silica than suggested by their numerical abundance.

The dissolution of detrital biogenic silica in surface waters supports regenerative diatom production (Nelson et al. 1995) and its presence causes biomass-normalized silica production rates to underestimate the activity of living cells (Krause et al. 2010). The comparison between community level specific silica production rates determined using ^{32}Si

and taxon specific rates using PDMPO provides insights into these processes as it enables

the pool of $bSiO_2$ to be divided between detritus and that associated with living cells. The

average specific silica production rate of taxa at a station were calculated from PDMPO data

by averaging the quotient of the silica production rate and the silica content of the cell across

all cells of each taxon. The Si content of the cells from PDMPO (Supplemental Table 1)

agrees well with other findings (Brzezinski 1985; Baines et al. 2010). The slope of the

relationship between cell SA and Si content calculated for this data: $\log(\text{Si content}) = (0.98$

$\pm 0.05)*\log(\text{SA}) - (3.4 \pm 0.15)$, $(R^2 = 0.86)$ falls slightly below the regression from

Brzezinski (1985) for laboratory clones: $\log(\text{Si content}) = (1.25 \pm 0.11)*\log(\text{SA}) - (3.8 \pm$

$0.35)$, $(R^2 = 0.84)$ and those from Baines et al. (2010) for the equatorial Pacific, $\log(\text{Si}$

$\text{content}) = (1.13 \pm 0.31)*\log(\text{SA}) - (3.4 \pm 0.76)$, $(R^2 = 0.59)$ and the Southern Ocean, $\log(\text{Si}$

$\text{content}) = (1.77 \pm 0.23)*\log(\text{SA}) - (4.3 \pm 0.59)$, $(R^2 = 0.89)$ (Supplemental data Fig. 1).

Consistent with previous findings that cell viability is usually highest under optimal

growth conditions (Znachor et al. 2015) detritus made up a small fraction, 10-20%, of the

$bSiO_2$ pool when silica production rates were high (Fig. 4). At the more oligotrophic stations

(5, 6, and 7 of the southern transect), detritus was 70-90% of the $bSiO_2$ pool (Fig. 4). This is

similar to estimates of $bSiO_2$ detritus in the equatorial Pacific which were estimated to

consistently be ~80% of the total $bSiO_2$ pool (Krause et al. 2010). The increasing proportion

of detritus away from shore is also in agreement with the idea that a larger fraction of silica

production is supported by recycled Si in oligotrophic regions and new Si in high Si

production environments (Brzezinski et al. 2003). This suggests that community level

measurements of biomass-normalized rates of silica production made with tracers in the

oligotrophic ocean are significantly underestimated.

65

Our data support the expectation that because diatom silica is predominantly associated with the cell wall, a taxon's contribution to community silica production, at any point in time, should be related to the fraction of total community surface area represented by a taxon. Additionally, over time scales shorter than a day silica production can be partitioned between co-occurring diatoms based upon a taxon's fractional contribution to new frustule surface area (Fig. 8a), but, for this data set, reasonable estimates can be made based on total cell surface area alone (Fig. 7a).

Community silica production rates of are often measured over relatively short (<1 d) ship-board incubations (e.g. Leblanc et al. 2002; Krause et al. 2011b) which, capture a snapshot of a dynamic system. Here, we have shown bulk ship-board silica production rates can be accurately partitioned among diatom species using cell SA similar to the Blain et al. (1997) approach for partitioning $bSiO_2$. Thus, future work that seeks to identify the most influential diatom taxa of a community need only add cell size estimates to taxonomic identification and abundance measurements with the caveat that the approach will underestimate the contribution of fast growing taxa because using SA ignores differences in growth rate. Because cells produce new frustule area as they grow, cell division exponentially increases a taxon's combined SA. This accentuates the role of growth rate in silica production on longer time scales by causing the relative contribution of specific taxa to shift as differences in growth rate alter the fractional contribution of taxa to total community surface area.

The relative importance of size (SA) and growth rate to silica production can be further explored by considering the amount of time needed for a smaller, faster-growing

taxon to create more surface area than a larger, slower-growing taxon. The surface area of each taxon through time increases exponentially:

$$SA_{total} = SA_{T0}e^{\mu t} \tag{3}$$

where SA_{total} is the combined surface area (μm^2) of all cells produced over time t (d), by a taxon growing at the average rate μ (d^{-1}) and SA_{T0} is the total surface area of all the cells in the taxon at time zero. This equation can be used to compare diatom taxa or single diatom cells. When comparing taxa the SA is the combined SA of all cells from a taxon and μ is the average growth rate of the species. Defining equation 3 for two different taxa, setting the equations equal to each other, and solving for t gives the amount of time needed for the smaller SA cells with a faster growth rate ($SA_{1.T0}$, μ_1) to create the same amount of surface area and thus produce approximately the same amount of silica as the larger, slower-growing, cells ($SA_{2.T0}$, μ_2) (Equation 4); for t to have a non-zero, real solution the $SA_2 > SA_1$ and $\mu_1 > \mu_2$.

$$t = \frac{\ln(SA_{2.T0}) - \ln(SA_{1.T0})}{\mu_1 - \mu_2} \tag{4}$$

Equation 4 can infer the temporal period required for a species successional shift to produce a biogeochemical shift during a bloom sequence. The time required for a small fast-growing taxon to create the same total surface area as a slower growing but larger taxon depends only on the difference in their growth rates and the difference between their SAs and not on the absolute values of either SA or growth rate. For example, consider two comparisons among four hypothetical taxa where the difference in SA ($\Delta\ln(SA)$) and difference in growth rate ($\Delta\mu$) are equal in each comparison, despite differences in SA and μ among taxa. In the first comparison, taxon one has a SA of 25,000 μm^2 and a growth rate of 0.69 d^{-1} and taxon two has a SA of 458 μm^2 and a growth rate of 1.49 d^{-1} (Fig. 10a). Through

67

time the smaller taxon produces new SA more quickly than the larger taxon so that by day five both taxa are equivalent in total surface area. The second comparison is between a taxon with a SA of 20 µm² and a growth rate of 1.8 d⁻¹ and a taxon with a SA of 1,097 µm² and a growth rate of 1.0 d⁻¹. Because the $\Delta\mu$ (0.8 d⁻¹) and Δln(SA) (4) are the same as in the first example, the two taxa in the second comparison are also equivalent in cumulative SA after five days despite having different absolute SA and growth rates (Fig. 10a).
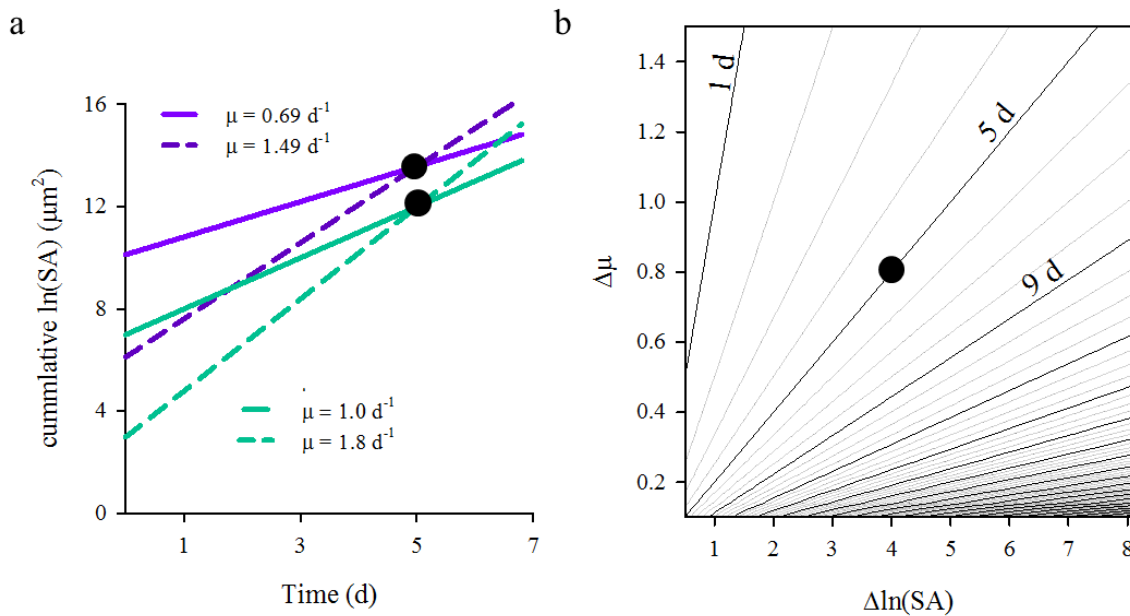
Figure 3-10: (a) Each line depicts a hypothetical taxon's cumulative, SA through time. A comparison is shown for two different sets of taxa—one pair is green and one pair is purple—with the same Δln(SA) and $\Delta\mu$ to illustrate how absolute values of SA and µ do not affect the time that passes before two taxa create the same amount of SA. The point in time where both species have created an equal amount of surface area is denoted with a black dot in a and b. (b) Shading within the plot denotes the length of time (d) for two taxa to create the same SA which is dependent upon the difference in growth rate as well as the difference in SA.

The length of time for the smaller taxa to dominate silica production depends on how much more SA the larger taxon has, Δln(SA$_{T0}$), and how much faster the smaller cell divides, $\Delta\mu$ (Fig. 10b). Up to the time plotted in Figure 10b, the larger, slower growing taxon, comprises a larger fraction of the total frustule SA and thus has produced a majority of the bSiO₂. Up to this time, size as manifest through SA is the dominant factor in relative

silica production between the two taxa. After the time plotted, the smaller, faster growing cell, overtakes its larger counterpart and comprises the majority of the SA and contributes the most to silica production. Thus, over the timescale of a diatom bloom the influence of rapid growth will increase in importance while the influence of large size will wane given the general trend of larger cells growing more slowly than smaller taxa. The most influential cells over the course of a multi-day bloom are those with high growth rate and high surface area.

Changes in the difference between the growth rate ($\Delta\mu$) of two taxa generally affects the amount of time for the taxa to create the same amount of SA ($bSiO_2$) more than differences in cell size $\Delta\ln(SA)$. Within the transect stations, the largest $\Delta\ln(SA)$ for co-occurring taxa was 7.3 and the largest $\Delta\mu$ was 1.1. The large difference in SA of the taxa corroborate the finding that, over the one day incubation, silica production was driven by initial cell SA rather than growth rate. However, given a few more days, the cells with the fastest growth rates would become the dominant contributor to $bSiO_2$ production. It should be noted that this shift from the importance of cell size to growth rate complicates the comparison of the overall results of different length incubations because the identity of the diatoms driving the biogeochemical dynamics will likely shift over longer incubations.

While differences in silicification minimally influenced silica production rates in the diatom communities studied here, there are instances where silicification could become an important factor such as when large cells have much thicker frustules than their smaller counterparts. Equation 4 can be modified to include the silicification (Z) of each species.

$$t = \frac{\ln(SA_{2.T0}*Z_2) - \ln(SA_{1.T0}*Z_1)}{\mu_1 - \mu_2} \tag{5}$$

In cases where the larger taxon is also more silicified, the smaller taxon will require more time to dominate silica production. The additional time needed for the smaller, less silicified taxon to dominate silica production is equivalent to the sum of the time shown in Figure 10b and $\ln(\frac{Z_2/Z_1}{\mu_1-\mu_2})$.

Finite resources and top-down control mechanisms will determine the duration of a bloom and set a time limit for shifts in relative silica production among taxa. A taxon's contribution to the $bSiO_2$ produced over the life of a bloom can be estimated using data collected through single-cell measurements and equation 4. Within the nearshore stations of the southern transect, *Chaetoceros spp.* <20 μm dominates the diatom assemblages, both numerically and in SA and thus was responsible for the vast majority of silica production at the four stations closest to shore (Fig. 3). The diatom assemblages at stations 1 through 4 have 1.2-4.7 days of growth remaining before the currently available $[Si(OH)_4]$ becomes depleted (calculated using V_b and $[Si(OH)_4]$ from Table 1 assuming no nutrient re-supply). For any other taxon to create as much silica as *Chaetoceros spp.* <20 μm in two days, it would need to grow at a rate that is 1.2 d^{-1} faster than *Chaetoceros* spp. <20 μm (Fig. 10). The growth rate estimates for other taxa did not approach this value nor is it likely that any would show such a large increase especially as nutrients are depleted. As the nearshore assemblages continue to grow *Chaetoceros spp.* <20 μm is thus predicted to continue to dominate silica production (unless it is preferentially lost) until $Si(OH)_4$ has been depleted.

The dominant silica producing taxa in the northern transect stations 4 and 5 could shift from *P. alata* to *Chaetoceros spp*. At these stations, silica production was dominated by large, slower-growing cells of *P. alata* but the *Chaetoceros* taxa were abundant and growing at least 0.2 d^{-1} faster than *P. alata.* Thus given enough time, resources, and lack of

70

disproportionate mortality loss, *Chaetoceros* would dominate silica production. If the growth rate remains the same for both taxa, it would take the *Chaetoceros spp.* <20 µm at station 4, 4.5 d and the *Chaetoceros spp.* >20 µm at station 5, 1.5 d to create as much surface area and $bSiO_2$ as *P. alata*. With the measured community silica production rates, $Si(OH)_4$ at station 4 and 5 will be depleted in 2.1 d and 1.6 d, respectively. The time needed for *Chaetoceros spp.* >20 µm to create as much SA as *P. alata* is greater at station 4 than nutrients can support. However, station 5 will likely have equal contributions to silica production from the *Chaetoceros spp.* <20 µm and *P. alata.*

The role of nutrient availability in silica production

The examples above highlight the importance of nutrient availability in setting a limit on the time diatom taxa have to compete and produce $bSiO_2$. The maximum $[Si(OH)_4]$ of 21.6 µM, and the average specific silica production rate of 0.43 d^{-1} observed in this study are consistent with others (Brzezinski et al. 1997) and suggest that silicic acid is available for ~10 days post upwelling along the California coast.

Not only do nutrient concentrations limit the duration of a bloom, but they can also affect cell physiology and alter growth rate. We observed that co-occurring diatoms growing in the same environment had a wide range of growth rates and taxa were differentially sensitive to changes in nutrient availability (Fig. 9). Even small changes in growth rate can have a substantial effect on the $bSiO_2$ created by a taxon over the course of a bloom—an increase in 0.1 d^{-1} results in twice as much new surface area created over seven days. Changes in growth rate driven by nutrient availability can potentially shape the community and the relative contributions of diatom taxa to silica production. The influence of nutrient

availability can be seen in the shifting growth rate of *Chaetoceros spp.* <20 µm, which was a prominent taxon across both transects.

The shifting importance of Chaetoceros

Diatom blooms dominated by *Chaetoceros* are common along the California coast (Dugdale and Wilkerson 1989; Hutchins and Bruland 1998; Venrick 1998) and other high nutrient regions like the subarctic Pacific (Durkin et al. 2013) and Southern Ocean (Assmy et al. 2013). Recent geographic assessments place *Chaetoceros* as the most abundant diatom in the global ocean (Malviya et al. 2016). Its cosmopolitan presence and often high abundance make the growth dynamics and silica production of *Chaetoceros* particularly salient.

The importance of *Chaetoceros* to silica production diminishes across the transects as nutrients decline. *Chaetoceros* had the most dynamic growth across transects (Fig. 9), ranging from 2.08 d^{-1} in the high-nutrient, near shore environment to 0.69 d^{-1} in the more oligotrophic stations (Supplemental Data). Nearshore, where nutrients are abundant, the combination of high growth rate and intermediate cell size made *Chaetoceros* the largest contributor to community silica production. In the more oligotrophic water, the high growth rate of *Chaetoceros* declined and silica production becomes dominated by large taxa, like *P.alata* or small cells that are able to persist in more oligotrophic water. The shifting importance of *Chaetoceros* exemplifies how environmental conditions differentially affect diatom taxa and reroute the transfer of nutrients through the ecosystem.

Conclusion

This paper presents the first direct, quantitative, measurements of cell-specific silica production and growth rates in mixed, diatom assemblages using PDMPO labelling. This single-cell analysis, though labor intensive, reveals the contribution of different taxa to community silica production and allows evaluation of those cell attributes that play a dominant role in the observed silica production rates in diatom communities. This analysis also eliminates the artifact of detritus, which artificially decreases community level specific silica production rates made using conventional tracers. The data reveal a wide range of silica production and growth rates among co-occurring diatom taxa that are experiencing the same environmental conditions as well as spatial variation within a taxon. These patterns offer clues as to how different taxa perceive and respond to their environment and the consequences for species succession and biogeochemistry.

Cell abundance has long been suspected as a poor predictor of the contribution of different diatom taxa to community silica production. However, given methodological constraints, direct and quantitative measurements of silica production by co-occurring diatom taxa were previously unavailable. Here, we have shown that the contribution of taxa to instantaneous silica production in a coastal upwelling zone is predominantly a function of the surface area of new frustule that they produce rather than their degree of silicification, a finding that would not be observable except through single-cell techniques. On timescales of days, the influence of a taxon's surface area diminishes and growth rate becomes more dominant in determining contribution to silica production. Taxa like *Chaetoceros* have an optimal combination of intermediate size and rapid growth fostering significant contribution to instantaneous silica production via high population surface area and to long-term

production via rapid growth rate consistent with the global numeric prominence of

Chaetoceros among diatoms (Malviya et al., 2016). The ability to quantify both the

contribution of individual taxa to silica production and the attributes that determine

contribution to silica production on daily and bloom-event timescales will aid efforts to

understand the controls on diatom and silica dynamics in the ocean and they will inform the

new generation of trait-based models linking community structure and biogeochemistry (e.g.

Follows et al. 2007).

Transect	Station	Taxon	N	Si prod. rate (pmol Si cell⁻¹ d⁻¹)	Silicification (fmol Si μm⁻²)	Growth rate (d⁻¹)	Cell SA (μm²)	Si content (pmol Si cell⁻¹)	New SA created (μm² d⁻¹)	Cell abundance (cell L⁻¹ ×10³)
Northern	1	centrics	36	0.37 ± 0.07	0.52 ± 0.07	0.73 ± 0.04	637 ± 59	0.4 ± 0.1	640 ± 59	351.6
	2		12	2.53 ± 0.65	0.50 ± 0.04	0.69 ± 0.00	4675 ± 1001	2.5 ± 0.6	4675 ± 1001	11.7
	3		26	0.57 ± 0.20	0.46 ± 0.05	0.99 ± 0.07	813 ± 305	0.5 ± 0.2	1029 ± 295	74.8
	4		1	1.40	0.61	0.69	2328	1.4	2328	15.6
	5		1	0.17	0.51	1.39	114	0.1	341	20.3
	7		17	1.18 ± 0.45	0.51 ± 0.07	0.55 ± 0.04	2293 ± 549	1.7 ± 0.4	1742 ± 542	10.1
Southern	1									66.3
	2		1	1.22	0.69	0.69	1778	1.2	1778	26.8
	3		8	2.86 ± 0.70	0.64 ± 0.07	0.67 ± 0.02	4481 ± 1005	2.9 ± 0.7	4402 ± 1038	73.1
	4		5	1.00 ± 0.27	0.75 ± 0.17	0.62 ± 0.07	1714 ± 435	1.4 ± 0.6	1406 ± 379	14.0
	5		7	2.08 ± 0.66	0.80 ± 0.12	0.69 ± 0.00	2468 ± 811	2.1 ± 0.7	2468 ± 811	2.9
	6		12	1.31 ± 0.25	0.89 ± 0.06	0.72 ± 0.07	1594 ± 396	1.3 ± 0.3	1461 ± 238	
	7		7	2.38 ± 0.81	1.20 ± 0.17	0.96 ± 0.15	1017 ± 326	1.5 ± 0.7	1731 ± 540	3.5
Northern	1	*Chaetoceros* <20μm	18	0.97 ± 0.17	0.36 ± 0.03	1.85 ± 0.10	530 ± 105	0.2 ± 0.0	2429 ± 355	1.5
	2		19	0.90 ± 0.14	0.30 ± 0.03	1.03 ± 0.10	1673 ± 189	0.5 ± 0.1	2818 ± 310	90.4
	3		41	1.19 ± 0.12	0.28 ± 0.01	1.28 ± 0.08	1420 ± 89	0.4 ± 0.0	4048 ± 384	116.9
	4		19	0.43 ± 0.04	0.23 ± 0.01	0.95 ± 0.08	1271 ± 131	0.3 ± 0.0	1836 ± 142	169.7
	5		22	0.75 ± 0.11	0.31 ± 0.03	0.79 ± 0.05	2127 ± 251	0.7 ± 0.1	2326 ± 231	640.9
	7		4	0.46 ± 0.07	0.40 ± 0.07	1.04 ± 0.20	802 ± 251	0.3 ± 0.0	1175 ± 51	26.9
Southern	1		22	1.06 ± 0.14	0.45 ± 0.03	1.17 ± 0.10	1096 ± 147	0.5 ± 0.1	2357 ± 319	9201.8
	2		19	1.30 ± 0.17	0.20 ± 0.01	1.62 ± 0.13	1564 ± 171	0.3 ± 0.0	6286 ± 699	487.8
	3		40	0.97 ± 0.08	0.26 ± 0.01	1.47 ± 0.05	1099 ± 68	0.3 ± 0.0	3731 ± 271	1608.0
	4		58	0.90 ± 0.05	0.38 ± 0.02	1.13 ± 0.07	1296 ± 97	0.5 ± 0.0	2541 ± 186	1526.0
	5		5	0.63 ± 0.38	0.22 ± 0.06	0.97 ± 0.17	1836 ± 782	0.6 ± 0.4	2146 ± 651	6.1
	6		5	0.10 ± 0.01	0.13 ± 0.01	0.69 ± 0.00	807 ± 124	0.1 ± 0.0	807 ± 124	
	7		4	0.16 ± 0.04	0.25 ± 0.05	0.87 ± 0.17	611 ± 178	0.1 ± 0.1	666 ± 127	
Northern	1	*Chaetoceros* >20μm	2	1.15 ± 0.31	0.30 ± 0.06	2.08 ± 0.00	534 ± 41	0.2 ± 0.0	3740 ± 28	34.3
	2		6	2.59 ± 0.33	0.37 ± 0.04	1.27 ± 0.12	2853 ± 304	1.0 ± 0.1	7228 ± 888	0.0
	3		2	6.03 ± 0.28	0.95 ± 0.51	1.04 ± 0.35	4296 ± 47	4.1 ± 2.2	8544 ± 4202	82.6
	4		16	1.91 ± 0.44	0.32 ± 0.03	0.87 ± 0.13	3298 ± 422	1.1 ± 0.2	5034 ± 1058	17.2
	5		11	0.87 ± 0.17	0.24 ± 0.02	0.63 ± 0.04	3889 ± 451	1.0 ± 0.2	3427 ± 499	26.9
	7		8	0.52 ± 0.19	0.27 ± 0.04	0.51 ± 0.16	2635 ± 356	0.8 ± 0.2	1751 ± 597	
Southern	1		37	2.00 ± 0.31	0.67 ± 0.03	0.77 ± 0.04	2443 ± 168	1.7 ± 0.1	2992 ± 443	2612.0
	2		22	1.75 ± 0.18	0.27 ± 0.02	1.58 ± 0.09	1677 ± 155	0.5 ± 0.1	6401 ± 519	184.9

Region	Species	#							
		3	70	1.55 ± 0.14	0.37 ± 0.01	1.01 ± 0.06	2263 ± 112	0.9 ± 0.1	4122 ± 362	956.8
Northern		4	46	1.05 ± 0.14	0.44 ± 0.03	0.73 ± 0.06	2175 ± 218	1.0 ± 0.1	2324 ± 260	770.3
	F. pseudonana	1	10	0.06 ± 0.01	0.52 ± 0.06	1.39 ± 0.00	46 ± 8	0.02 ± 0.0	139 ± 24	113.0
		2								5.5
		3	1	0.04	0.34	0.69	122	0.04	122	10.1
		4								19.0
		7	12	0.04 ± 0.003	0.42 ± 0.01	0.75 ± 0.06	91 ± 6	0.04 ± 0.0	99 ± 7	1.2
Southern		1	4	0.05 ± 0.002	0.79 ± 0.14	0.69 ± 0	72 ± 20	0.05 ± 0.0	72 ± 20	35.1
		2	2	0.04 ± 0.00	0.47 ± 0.00	0.69 ± 0.00	88 ± 3	0.04 ± 0.0	88 ± 3	49.9
		3	22	0.07 ± 0.01	0.57 ± 0.03	0.88 ± 0.07	110 ± 12	0.06 ± 0.0	138 ± 11	102.3
		4	24	0.05 ± 0.01	0.63 ± 0.05	0.65 ± 0.02	85 ± 2	0.05 ± 0.0	77 ± 4	10.4
		5	9	0.07 ± 0.01	0.62 ± 0.10	0.65 ± 0.04	125 ± 7	0.07 ± 0.0	114 ± 7	1.1
		6								7.3
		7								14.6
Southern	*Fragilariposis sp.*	2	1	0.59	0.83	0.69	717	0.6	717	
		3	5	0.86 ± 0.17	0.75 ± 0.14	0.69 ± 0.00	1188 ± 198	0.9 ± 0.2	1188 ± 197	1.3
		4	11	0.27 ± 0.05	0.37 ± 0.05	0.64 ± 0.04	762 ± 29	0.3 ± 0.0	689 ± 55	0.7
		5								
		6								
		7								
Northern	*L. annulata*	2	8	5.78 ± 0.96	0.50 ± 0.04	0.59 ± 0.06	13317	6.7 ± 0.6	11075 ± 1541	17.2
		3	3	4.55 ± 0.70	0.42 ± 0.08	0.69 ± 0.02	13317	5.9 ± 1.0	11028 ± 589	3.9
		4	1	2.39	0.23	0.69	10456	2.4	10390	5.5
		5	1	0.61	0.13	0.38	10390	1.3	4736	6.2
		7	2	0.11 ± 0.02	0.17 ± 0.01	0.05 ± 0.01	13317	2.3 ± 0.1	639 ± 123	
Northern	*N. americana*	1	30	0.06 ± 0.01	0.23 ± 0.01				240 ± 14	534.1
		2	2	0.06 ± 0.01	0.23 ± 0.01				250 ± 16	2.3
		3								15.6
		4								9.4
		5								13.3
Southern	*Nitzschia sp.*	1	14	0.23 ± 0.03	0.23 ± 0.02	0.94 ± 0.09	703 ± 82	0.2 ± 0.0	972 ± 57	46.8
		2	9	0.30 ± 0.04	0.29 ± 0.03	1.31 ± 0.08	398 ± 53	0.1 ± 0.0	1015 ± 42	36.5
		5								5.6
		6								1.5
		7								
Northern	*P. alata*	2	8	0.22 ± 0.04	0.23 ± 0.04	1.04 ± 0.13	604 ± 105	0.2 ± 0.1	943 ± 50	0.8

Region	Species	Station	n							
		3								0.8
		4	9	5.30 ± 0.96	0.34 ± 0.04	0.46 ± 0.16	25217 ±	8.6 ± 2.8	15047 ± 2193	49.9
		5	11	5.21 ± 0.82	0.49 ± 0.03	0.34 ± 0.04	25217 ±	12.3 ± 0.7	10727 ± 1599	151.3
		7	2	4.82 ± 0.39	0.47 ± 0.03	0.34 ± 0.00	25217 ±	11.8 ± 0.8	10290 ± 115	0.4
Northern	*Pseudo-nitzschia spp.*	1	6	0.83 ± 0.17	0.35 ± 0.05	1.85 ± 0.15	501 ± 132	0.2 ± 0.1	2293 ± 178	1.5
		2	3	1.13 ± 0.52	0.49 ± 0.13	1.39 ± 0.00	695 ± 160	0.4 ± 0.2	2094 ± 481	5.5
		3	11	0.59 ± 0.10	0.25 ± 0.03	1.20 ± 0.10	1178 ± 231	0.3 ± 0.1	2275 ± 213	18.7
		4	3	0.15 ± 0.06	0.11 ± 0.03	1.39 ± 0.00	438 ± 91	0.1 ± 0.0	1316 ± 274	42.9
		5	4	0.71 ± 0.33	0.24 ± 0.04	1.04 ± 0.20	1332 ± 169	0.3 ± 0.1	2597 ± 805	61.6
		7	8	0.54 ± 0.33	0.30 ± 0.10	0.82 ± 0.15	1547 ± 862	0.9 ± 0.9	1325 ± 316	3.1
Southern		1	1	0.22	0.18 ± 0.00	1.38 ± 0.00	416 ± 0	0.1 ± 0.0	1249 ± 0	132.5
		2	12	0.98 ± 0.15	0.38 ± 0.04	1.33 ± 0.06	926 ± 91	0.4 ± 0.1	2494 ± 155	57.3
		3	3	0.20 ± 0.06	0.14 ± 0.02	0.92 ± 0.23	1037 ± 400	0.2 ± 0.1	1324 ± 262	58.5
		4								42.1
		5	4	0.37 ± 0.08	0.28 ± 0.03	0.96 ± 0.08	787 ± 97	0.2 ± 0.0	1176 ± 131	2.5
		6	2	0.33 ± 0.05	0.36 ± 0.00	1.04 ± 0.35	554 ± 205	0.2 ± 0.1	903 ± 144	
		7								0.2
Northern	*Skeletonema sp.*	2	14	0.56 ± 0.12	0.34 ± 0.03	0.95 ± 0.14	883 ± 67	0.2 ± 0.0	1506 ± 284	9.4
		3	4	0.86 ± 0.06	0.39 ± 0.02	0.69 ± 0.00	2252 ± 221	0.9 ± 0.1	2252 ± 221	6.2
		4	13	0.47 ± 0.05	0.25 ± 0.01	0.65 ± 0.08	2254 ± 146	0.6 ± 0.1	1943 ± 187	36.6
		5	15	0.19 ± 0.02	0.25 ± 0.01	0.60 ± 0.03	882 ± 39	0.2 ± 0.0	743 ± 66	55.4

Sup. Figure 1: Comparison between data from this study, Brzezinski 1985, and Baines et al. 2010 of the relationship between surface area and silica content

Chapter 4 The hierarchical progression of silicon limitation on taxon-specific diatom silicification and growth in the California upwelling zone

Abstract

Silicon limitation impacts diatom silica production and potentially growth episodically or chronically across ocean environments. Interspecific differences in the capacity to cope with silicon limitation potentially alters the contribution of individual species to overall silica production and community structure. Laboratory experiments indicate that diatoms respond to silicon limitation first by decreasing their demand for silicon thereby delaying a reduction in growth rate. Once a cell's ability to lower cellular silica content is exceeded, the sufficiently severe silicon limitation will affect growth rate. These effects are examined for the first time in natural diatom assembles in the upwelling environment of Coastal California. Taxon-specific silica production rates, silicification, new frustule surface area, and growth rate were quantified using the fluorescent tracer, PDMPO, in paired incubations of water samples (ambient and $+19\ \mu M$ silicic acid ($Si(OH)_4$)) along two transects spanning the upwelling zone where ambient $[Si(OH)_4]$ ranged between $2.0 - 21.2\ \mu M$. Community-level measures of Si stress remained nearly constant across gradients in $[Si(OH)_4]$, while taxon-specific assessments revealed increasing variability in stress among taxa with decreasing $Si(OH)_4$. Cell silicification responded to increasing silicon limitation at a rate twice that for frustule surface area, but growth rate remained relatively unaltered—consistent with seminal culture studies. Surprisingly, additions of $Si(OH)_4$ did not alter the short-term relative contribution of individual taxa to community silica

production or the relative abundance of taxa. These results therefor suggest that primary

effect of the observed silicon limitation was diminished silicification.

Introduction

Elegant opal shells encase the microscopic cells of one of the most productive

primary producers in the world. Diatoms, create these structures by taking-up silicic acid

$(Si(OH)_4)$ from the water and polymerizing it into amorphous silica. Diatoms have an

obligate requirement for $Si(OH)_4$—growth halts in its absence (e.g. Darley and Volcani

1969). $Si(OH)_4$ availability can affect diatom silica production rates as well as growth rates.

Thus the concentration of $Si(OH)_4$ in the sunlit, surface, ocean can potentially limit the

abundance, distribution, and biogeochemical importance of diatoms across ocean regions

(Egge and Aksnes 1992; Dugdale et al. 1995; Rocha et al. 2002). The $[Si(OH)_4]$ in the

surface of the ocean has been shown to limit the rate of diatom silica production episodically

or chronically in all ocean provinces examined to date including the open ocean (Brzezinski

and Nelson 1996; Leynaert et al. 2001; Krause et al. 2012), coastal regions (Nelson and

Dortch 1996), and polar regions (Nelson and Tréguer 1992; Nelson et al. 2001). Despite the

overwhelming evidence for limitation of silica production rates, assessing whether diatom

growth is limited by low $[Si(OH)_4]$, as observed in culture (e.g. Paasche 1973a), has eluded

the field due to a lack of direct methodology to assess *in situ* growth rates of diatoms in

natural assemblages.

The rate of silica production and growth are related to $[Si(OH)_4]$ by the Michaelis-

Menten (eq. 1) and Monod (eq. 2) equations respectively:

$$V = \frac{V_m * [Si(OH)_4]}{K_s + [Si(OH)_4]} \tag{1}$$

$$\mu = \frac{\mu_m * [Si(OH)_4]}{K_\mu + [Si(OH)_4]} \tag{2}$$

Silicon uptake and production are tightly coupled in diatoms, while the Michaelis-Menten equation traditionally is applied to uptake rates, here we use it to describe silica production. The specific silica production rate (V) is a function of the concentration of $Si(OH)_4$, the maximum production rate (V_m) and the half-saturation constant (K_s), which is the $[Si(OH)_4]$ where V is half of V_m. Both specific silica production rate (V), which is the cellular silica production rate ρ (Si cell^{-1} d^{-1}) normalized to the silica content of a cell (Si cell^{-1}), and growth rate (μ) are hyperbolic functions of $[Si(OH)_4]$. Similarly, growth rate (μ) is related to $[Si(OH)_4]$ through the maximum growth rate (μ_m) and the half-saturation constant K_μ (i.e. concentration where μ is half of μ_m).

Laboratory culture experiments with a variety of diatom species show the median value of K_s to be 2.2 µM; K_μ is generally lower with a median value of 1.0 µM (Martin-Jézéquel et al. 2000 and references therein), meaning as $[Si(OH)_4]$ decreases the rate of silica production will decrease before growth rate is affected. In these culture experiments, doubling times are maintained even as uptake rates drop because cells reduce frustule silicon content. Diatoms can decrease cellular silica content three to four fold under severe silicon limitation (e.g. Guillard et al. 1973; Paasche 1975; Brzezinski et al. 1990), but as the severity of silicon limitation increases the capacity to decrease silicification is exceeded and both uptake and growth begin to diminish. The plasticity in silicification as a response to silicon limitation (Paasche 1973c; Brzezinski et al. 1990) has yet to be quantified in natural assemblages, but has been observed in a pennate diatom during a ship-based multi-day grow-out experiment on a natural community from the equatorial Pacific (Brzezinski et al. 2011a).

Half-saturation constants (K_s and K_μ), maximum production rate (V_m), and maximum

growth rate (μ_m), vary widely among diatom species (Martin-Jézéquel et al. 2000). This

interspecific variability suggests that within a natural diatom community, where taxa have

variable physiological capabilities, individual taxa could experience a unique level of silicon

limitation. Thus, silicon stress of a diatom community at any [$Si(OH)_4$] is a reflection of the

combined abundance and composition of taxa and their unique kinetic parameters. While

knowledge of the physiological nutrient capabilities of taxa have been extrapolated to

diatom population dynamics in the field (e.g. Tilman 1977) methodological limitations have

restricted direct measures of the response of taxa *in situ*.

The degree of silicon limitation has different implications for biogeochemical

cycling and for food web processes. Both [$Si(OH)_4$] and the combined physiologic

capabilities of the community will determine the degree of silicon limitation. Mild silicon

limitation, that stunts silica production rates and decreases silicification but does not alter

growth rate, could affect the fate of diatom biomass but bottom-up pressure of $Si(OH)_4$ on

phytoplankton community structure would not occur during mild silicon limitation.

However, mild silicon limitation could indirectly influence community structure through

top-down pressure because more lightly silicified cells are more susceptible to predation

(Assmy et al. 2013; Liu et al. 2016; Zhang et al. 2017a). Decreased silicification would

reduce cell density and decrease sinking velocity of cells and thus, could also have

biogeochemical implications. Less silicified cells would be more likely to remineralize and

dissolve at shallow depth compared to a more heavily silicified cell (Passow et al. 2011).

When the severity of silicon limitation is sufficient to limit diatom growth, species

succession within a diatom community (Tilman 1977b; Kilham and Tilman 1979) and

succession among phytoplankton groups (Egge and Aksnes 1992) can occur in addition to physiological changes, favoring those groups able to maintain higher growth rate in low [Si(OH)$_4$] environments.

Here, we used recently developed taxon-specific methods to measure the relative change in silicification and growth rate of co-occurring diatom taxa in relation to the degree of silicon limitation within the California upwelling zone. We describe taxon-specific changes in physiology between paired incubations of water samples that were either unaltered or spiked with a saturating addition of Si(OH)$_4$ to improve understanding of how silicon limitation affects the physiology of co-occurring diatom taxa and in-turn, how those physiological responses to silicon limitation may alter diatom community dynamics.

Methods

Sample collection

Data for this study was collected during the IrnBru (MV1405) cruise aboard the *R/V Melville* in July, 2014 along two transects off the California coast. The northern transect extended ~100 km southwest from Cape Blanco, Oregon (USA) and the southern transect extended ~200 km west from Point Arena, California (USA). Macronutrient and biogenic silica (bSiO$_2$) samples were collected along both transects as described in McNair et al. (in press).

At each station along the transects, silica production rates, growth rates, and silicification were measured in incubations of paired 'ambient' and '+Si' treatments to characterize the degree of silicon limitation. On each transect water for the incubations was collected at roughly two-hour intervals while the ship was underway (Fig. 1a) using the

surface-towed, trace metal clean, water pump, (i.e. the GeoFish, (Bruland et al. 2005)).

Water from the GeoFish was pooled into a trace-metal-clean carboy in a clean 'bubble' in

the ship's laboratory and then split into 250 mL polycarbonate bottles that had been cleaned

following trace metal protocols (Cuttler et al. 2014). The fluorescent tracer, PDMPO [2-(4-

pyridyl)-5-((4-(2-dimethylaminoethylamino-carbamoyl)methoxy)phenyl)oxazole] was

added to two bottles at a final concentration of 0.158 μM. The ambient treatment was not

altered further. The +Si treatment was spiked with a Chelex-cleaned sodium metasilicate

stock solution such that the final concentration was 19 μM greater than the ambient of

[$Si(OH)_4$]. To measure the silica production rates of the total diatom community at each

station, an additional pair of ambient and +Si bottles were spiked with the radioisotope ^{32}Si

(15,567 Bq μg^{-1}). 261 Bq of ^{32}Si was added to samples from the northern transect and 293

Bq of ^{32}Si was added to samples from the southern transect.

All the bottles were incubated for 24 h in deck-board, flow-through incubators and

processed as in McNair et al. (in press). Briefly, samples that had been incubated with

PDMPO were centrifuged, aspirated, preserved with methanol, and refrigerated until being

made into slides for confocal microscopy (McNair et al. 2015). Microscopy slides were

made using the concentration method described in McNair et al. (in press). PDMPO

fluorescence was quantified using the Olympus Fluoview confocal microscope in the

Neuroscience Research Institute at the University of California, Santa Barbara. Raw

PDMPO fluorescence was calculated using the image analysis software, Imaris 8.0.2. Raw

fluorescence emitted from the frustule-incorporated PDMPO was converted to moles of

SiO_2 using a fluorescent diatom standard (McNair et al. 2015). Fluorescence measures were

used to estimate cell-specific silica production rates, growth rates and silicification as

described in McNair et al. (in press). ^{32}Si incorporation rates were measured using low-level beta detection after aging samples into secular equilibrium between the ^{32}Si and its short-lived daughter isotope, ^{32}P (Krause et al. 2011a).

Metrics of Si limitation

The relative degree of silicon limitation for each taxon was characterized by comparing the rate of silica production in the +Si treatment to the rate of silica production in the ambient treatment (ρ_{+Si}/ρ_{amb}). Dividing the silica production rate (ρ) by the amount of silica in a cell produces the specific silica production rate V. Assuming the silica content of cells within a taxon was constant at the start of the incubation, the ratio of ρ_{+Si}/ρ_{amb} is the same as V_{+Si}/V_{amb} because the constant cellular silica content cancels from the numerator and denominator. The denotation, V_{+Si}/V_{amb} is more intuitive in relation to silicon kinetics and is thus used from this point forward. The addition of $Si(OH)_4$ is assumed to relieve cells from any silicon limitation that may be occurring in the ambient conditions and thus V_{+Si}/V_{amb} approximates V_m/V (eq. 1). A larger V_{+Si}/V_{amb} indicates more severe silicon limitation for the taxon under the ambient condition.

Similarly, to better understand the physiological changes that occur with silicon limitation, changes in silicification (Z), new frustule SA production rate (SA$_{new}$), and growth rate (μ) were characterized by dividing the metric in the +Si treatment by the paired measurement from the ambient treatment. These ratios are useful for characterizing and comparing silicon limitation across physiologically diverse taxa whose silica production rates can span three orders of magnitude (McNair et al. in press).

Data quality control

The taxon-specific data for silica production, growth rate, and silicification rate are inherently variable. Time and resources limit the number of images that can be imaged on the confocal microscope for each sample. This contrins the number of cells included in the averages for each taxon and results in a large standard error (S.E.) for the mean response of a taxon when only a few individuals are imaged. Silica production rates can vary widely within a genus or taxonomic group and taxa are often resolved only to the genus level. Variation also arises from intraspecific variability among cells. For instance, *Fragilariopsis pseudonana* had silica production rates that spanned an order of magnitude within a station from 0.01-0.04 pmol Si cell^{-1} d^{-1} to 0.10-0.14 pmol Si cell^{-1} d^{-1}. This variation is consistent with the findings of Durkin et al. (2012), who reported an order of magnitude range in PDMPO fluorescence in *Fragilariopsis sp.* (5 μm) from the subarctic Pacific when quantifying with a flow cytometer, which analyzes significantly more individuals. The necessary grouping of multiple species into the taxonomic groups reported here such as "centrics" and "*Pseudo-nitzschia spp.*" compounds apparent intraspecific differences. On average, the S.E. across measurements for different taxa was 36% of the mean for V_{+Si}/V_{amb}, 19% for Z_{+Si}/Z_{amb}, 26% $SA_{new+Si}/SA_{new-amb}$ and 12% for μ_{+Si}/μ_{amb}.

To reduce the influence of highly variable data points in our analyses, we filtered the data using two objective criteria: the number of cells included in the average needed to be greater than four in both treatments and the magnitude of the S.E. of V_{+Si}/V_{amb} had to be less than 70% of the average. This removed 23 out of 61 data points across the thirteen stations. After data filtration, the average S.E. relative to the mean decreased to 30% for V_{+Si}/V_{amb}, 16% of for Z_{+Si}/Z_{amb}, 23% for $SA_{new+Si}/SA_{new-amb}$, and increased to 13% for μ_{+Si}/μ_{amb}.

Statistics

All statistics were performed using JMP 12 software. Simple linear regressions were used to relate changes in growth rate, silicification, and the rate of new frustule surface area (SA) production to changes in silica production rate. An analysis of covariance (ANCOVA) was used to test for differences in the regressions between the transects. A reduced major axis regression (Bohonak 2004) was used to compare the relative contribution across taxa to community silica production in the ambient and +Si treatment.

The regressions between our silicon limitation metric based on specific silica production rate (V_{+Si}/V_{amb}) and the physiologic metrics based on silicification (Z_{+Si}/Z_{amb}), new frustule SA ($SA_{new+Si}/SA_{new-amb}$), and growth rate (μ_{+Si}/μ_{amb}) should converge at x, y = 1, 1 under the assumption that the Si addition raised each metric to the maximum specific rate. If $[Si(OH)_4]$ saturates silica production (i.e. $V_{+Si}/V_{amb} = 1$) then silicification, SA_{new} and growth rate, should also all be at maximum values with +Si/amb ratios of unity. The linear regressions were forced through (1, 1) by subtracting each limitation metric from a value of one, e.g. $1-V_{+Si}/V_{amb}$ and $1-Z_{+Si}/Z_{amb}$, which transposed the point (1, 1) to (0, 0). The least squares linear regression was then forced through 0 and the resulting equation translated back to the original parameter space giving a final equation for the line in the form:

$$V_{amb}/V_{+Si} = m* Z_{amb}/Z_{+Si} + (1-m) \tag{3}$$

Where m is the slope of the line from the linear regression that was forced through 0.

Results

Environmental setting

Stations within the two transects were generally confined to plumes of freshly upwelled water that extended perpendicularly away from the coast (Fig. 1a) with the exception of station 2 in the northern transect and the transition to more oligotrophic water in station 5-7 along the southern transect. Nearshore, the most recently upwelled water was cold with a high concentration of macronutrients. As the water moved offshore it warmed and nutrient concentrations decreased. A more thorough description of the environmental conditions can be found in McNair et al. (in press). The concentration of $Si(OH)_4$ was highly correlated with that of NO_3^- (R = 0.84, p < 0.001) and PO_4^{3-} (R = 0.96, p < 0.001) with all three nutrients decreasing in concentration away from shore (McNair et al. in press). Along the northern transect $[Si(OH)_4]$ ranged from 21.2 µM near shore to 2.0 µM offshore, along the southern transect $[Si(OH)_4]$ ranged from 15.4 µM to 2.3 µM near shore to offshore, respectively (Fig. 1b).
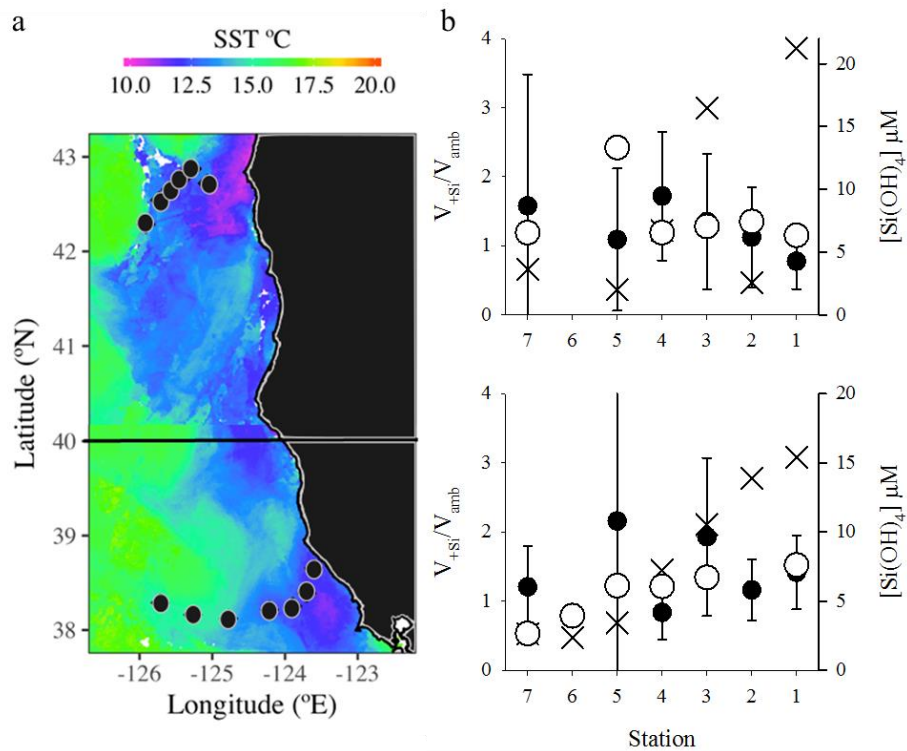
Figure 4-1: Figure 1: (a) MODIS 8 day composite of sea surface temperature (SST) for the northern and southern transect with stations denoted as circles, station 1 was closest to shore and 7 was farthest offshore. The black line at 40° latitude breaks the 8 day composite centered on July 20, 2014 for the northern transect from the composite centered on July 7, 2014 for the southern transect. Map adapted from McNair et al. (in press). (b) Relative increase in community silica production (V_{+Si}/V_{amb}) in the northern transect (top panel) and on the southern transect (bottom panel) as measured by ^{32}Si (white circles) and the community average weighted by production measured with PDMPO (black circles) with error bars representing standard error. Silicic acid concentration (x) in μM. ^{32}Si samples were omitted from: station 2 along the southern transect because the filter was compromised when the sample was drying, and from station 6 along the northern transect because a short kinetic experiment was conducted here rather than the 24 h incubations that were performed at all other stations. Station 6 is lacking a weighted taxon-specific average because of an issue with the sample for cell identification and enumeration.

Community changes in silica production

Despite the large range of [Si(OH)$_4$] across both transects, diatom community-level

silicon limitation was relatively constant (Fig. 1b). The correlation between [Si(OH)$_4$] and

(V_{+Si}/V_{amb}) was low and not significant for ^{32}Si data ($R^2 < 0.001$, p = 0.95). On average,

along the northern transect community silica production rates increased by $43 \pm 20\%$ (S.E.)

with the addition of 19 μM Si(OH)$_4$ (Fig. 1b). Along the southern transect community silica

production rates were similar in both treatments and only increased by $10 \pm 15\%$ (S.E.) on

89

average. Although the production-weighted averages of taxon-specific silica production

rates at each station included fewer taxa than were present in the entire community, they

generally agreed with the ^{32}Si measurements (Fig. 1b). However, the average effect of +Si

across stations using the taxon-weighted community measurement was lower than for ^{32}Si

along the northern transect with a $27 \pm 250\%$ increase on average in the +Si treatment. In the

southern transect, the taxon-weighted community measurement was higher than the ^{32}Si,

increasing $45 \pm 224\%$ on average across the stations (Fig. 1b). As with the ^{32}Si data, the

community production rates from the taxon-specific average silica production rates were not

correlated with $[Si(OH)_4]$ ($R^2 = 0.07$, $p = 0.40$).
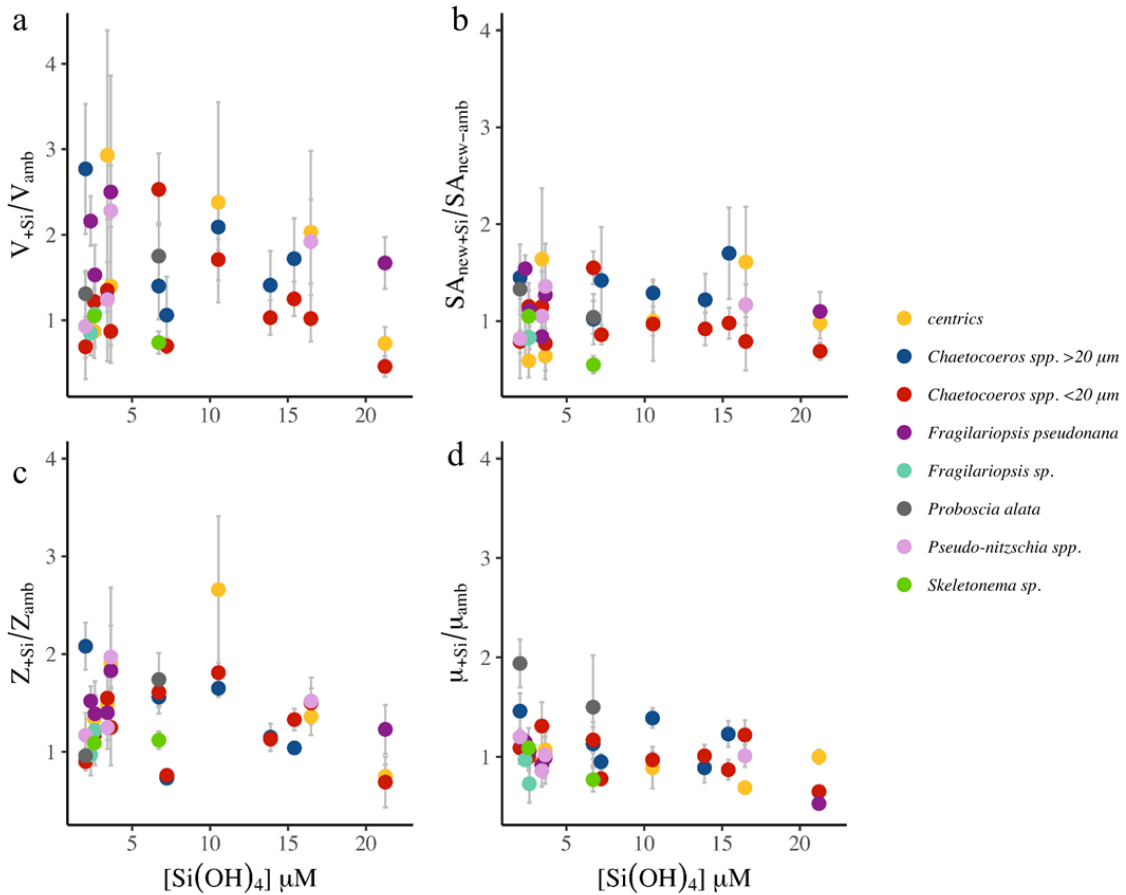
Figure 4-2: (a) The relative increase in silica production rate (b) the relative increase in new frustule SA, (c) the relative increase in silicification and (d) the relative change in growth rate between the ambient and enhanced treatments for taxa relative to the concentration of silicic acid in µM in the ambient condition.

While the total diatom community ratio of silica production in the +Si and ambient treatments was relatively constant there was a wide range in the relative change of silica production among taxa. Within a station taxonomic differences in V_{+Si}/V_{amb} spanned from <1 to ~3 (Fig. 2a). The variability of V_{+Si}/V_{amb} among taxa generally increased as $[Si(OH)_4]$ decreased. V_{+Si}/V_{amb} within a taxon varied as well (Table 1). Some taxa, such as *Skeletonema* sp. and *Chaetoceros spp.* <20 µm appeared Si-replete with V_{+Si}/V_{amb} generally close to 1 across the gradient in $[Si(OH)_4]$ (Fig. 2a, Table 1). Silica production rates for other taxa, such as the centrics and *Chaetoceros spp.* >20 µm were more silicon limited and

91

showed a large response to increased $Si(OH)_4$ with a 3-fold increase in silica production at some stations (Fig. 2a). The sensitivity of taxa to silicon limitation was examined by dividing the number of instances where V_{+Si}/V_{amb} was greater than 1.3 (30% was the average S.E. across taxa of V_{+Si}/V_{amb}) for a given taxon by the number of stations for which we had data for that taxon (Fig. 3). By this metric, *Fragilariopsis sp., Skeletonema sp.,* and *Chaetoceros spp.* <20 µm were the taxa least often silicon limited while *Proboscia alata, Chaetocoers spp.* >20 µm and *F. pseudonana* were the taxa most often silicon limited.
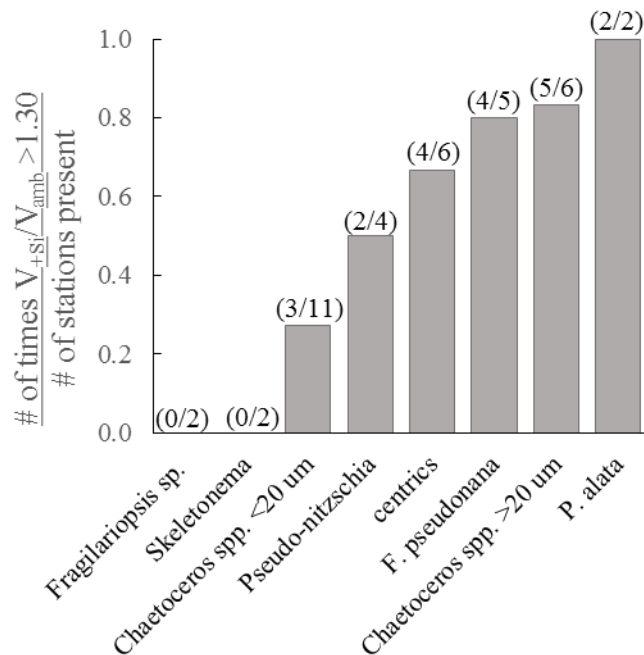
Figure 4-3: Relative stress of taxa across all stations. For each taxa the bars depict the quotient of the number of occurrences of V_{+Si}/V_{amb} greater than 1.3 divided to the number of stations in which that taxon was present, counts are given over each bar in parentheses.

The amount of silica that a cell produces over a given time is the product of the SA of the new frustule created (µm^2) and the silicification (Si µm^{-2}) of the new frustule. On average SA_{new+Si} was 8% more than $SA_{new-amb}$ but was more variable within a taxon at a given station (Fig. 2b). Silicification (Z) increased with in the +Si treatment by an average of 36% across taxa and stations (Fig. 2c). Similar to the pattern observed in V_{+Si}/V_{amb}, the

variability in Z_{+Si}/Z_{amb} generally increased among taxa with decreasing $Si(OH)_4$. However, the range of Z_{+Si}/Z_{amb} was narrower than V_{+Si}/V_{amb} with the largest increase in silicification being ~2, except for the high value for centric diatoms at the lowest concentration of $Si(OH)_4$ (Fig. 2c).

Taxon-specific growth rate only slightly increased with the addition of Si, 4% across stations and taxa (Fig. 2d). Growth rate was estimates by the pattern of partially, half, and fully labeled PDMPO cells as in McNair et al. (in press). Growth rate generally ranged from one to three divisions per day across taxa (McNair et al. in press). While growth rate on average was unaltered with additional Si, there were a few taxa, *P. alata* and *Chaetoceros spp.* <20 µm, that showed a 0.5 to 2-fold increase in growth rate when ambient $Si(OH)_4$ was less than 10 µM (Fig. 2c).

The relationship between V, Z, new frustule SA and µ

The coordination of physiological responses (i.e. silicification (Z), new surface area produced (SA_{new}), growth rate (µ)) as a function of silicon stress (V_{+Si}/V_{amb}) were examined among all taxa (Fig. 4). As described in the methods, all regressions were forced through the point (1, 1). All three least squares linear regressions were positively correlated with V_{+Si}/V_{amb} and resulted in the relationships:

Silicification: $Z_{+Si}/Z_{amb} = 0.58 \pm 0.06$ x (V_{+Si}/V_{amb}) + 0.42 (p <0.001)

New surface area: $SA_{new+Si}/SA_{new-amb} = 0.29 \pm 0.04$ x (V_{+Si}/V_{amb}) + 0.71 (p <0.001)

Growth: $\mu_{+Si}/\mu_{amb} = 0.08 \pm 0.05$ x (V_{+Si}/V_{amb}) + 0.92 (p = 0.12)

The slopes of the regressions indicate the relative change in each of the parameters as the degree of limitation of the production of silica (V_{+Si}/V_{amb}) increases. Data were pooled

across transect as there was no significant difference of slopes between the transects (ANCOVA, p >0.05).
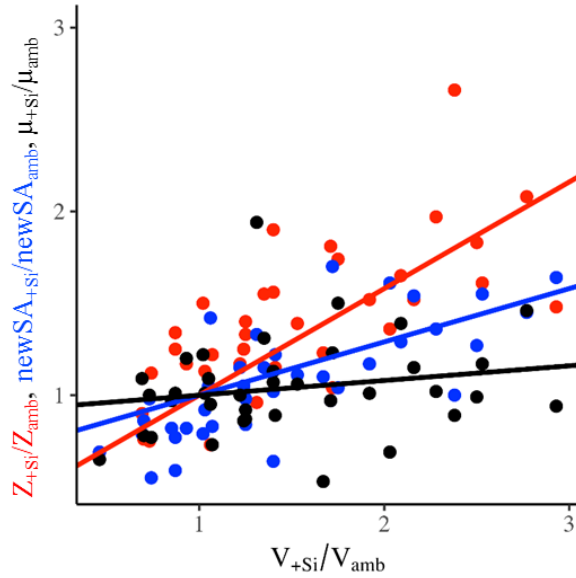
Figure 4-4: Relationships between changes in silicification (Z), new frustule SA (SA$_{new}$) and growth rate (μ) with increased silicon limitation (V$_{+Si}$/V$_{amb}$). All least squares linear regressions were forced through (x, y) = (1, 1).

Silicification and the SA of new frustule equally contribute to the rate of silica production such that the degree of silicon limitation (V$_{+Si}$/V$_{amb}$) can be related to differences in silicification and SA$_{new}$ by:

$$V_{+Si}/V_{amb} = (SA_{new+Si} / SA_{new-amb}) \text{ x } (Z_{+Si}/Z_{amb}) \tag{4}$$

Equation 4 holds for the regression lines in Figure 4 such that the product of Z$_{+Si}$/Z$_{amb}$ and SA$_{new+Si}$ /SA$_{new-amb}$ generally predicts the measured V$_{+Si}$/V$_{amb}$ to better than 5% (not shown).

Across the range of observed silicon limitation, the most pronounced physiological change between the ambient and +Si treatments was silicification. The difference between treatments in new frustule SA was roughly half of the change in silicification. Growth rate did not significantly change with silicon limitation.

94

Fraction of community silica production and abundance

To better understand the role of [Si(OH)$_4$] in community silica production and community composition, the fractional contribution of each taxon to total silica production and to total cell abundance were compared in the ambient and +Si treatments (Fig. 5). Despite two to three-fold differences in silica production rate between treatments across taxa (Fig. 5a) the slope of the reduced major axis regression between a taxon's contribution to silica production under ambient [Si(OH)$_4$] and after Si augmentation was close to unity, 1.03 $\pm$ 0.06 (S.E.) ($R^2 = 0.91$) signifying a taxon's contribution to community silica production was essentially unaltered with the addition of Si(OH)$_4$. Similarly, the fractional abundance of taxa at the end of the incubation, which was calculated using growth rate and initial cell abundance, was not different between the ambient and +Si treatment (Fig. 5b). The slope of the reduced major axis regression for the abundance measures was 0.99 $\pm$ 0.04 (S.E.) ($R^2 = 0.96$).
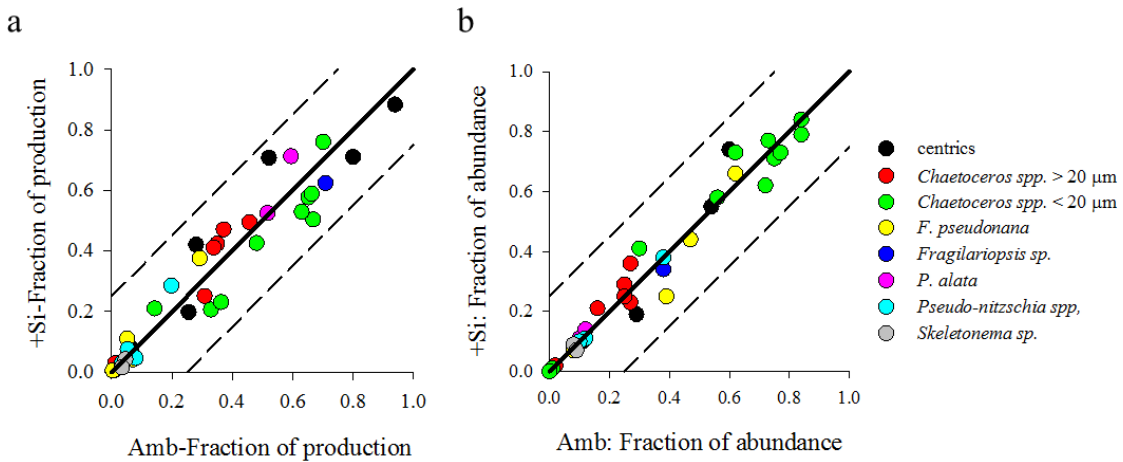
Figure 4-5: (a) The fractional contribution of taxa to community silica production in the ambient and +Si treatments. (b) The fractional abundance of taxa in the ambient and +Si treatment. In both plots the 1:1 line is depicted as a solid black line. The dashed black lines represent the 95% prediction interval.

Discussion

Limitation of total diatom community silica production by suboptimal [Si(OH)$_4$] has been observed in every oceanic region examined to date (Nelson and Tréguer 1992; Brzezinski and Nelson 1996; Nelson and Dortch 1996; Leynaert et al. 2001; Nelson et al. 2001; Krause et al. 2012). Here we present the first field-based, taxonomically resolved, assessments of silicon limitation data on cellular Si uptake as well as the first observations on the response of growth rate and its relation to variations in silica production as driven by [Si(OH)$_4$]. These single-cell measurements resolve taxon-specific responses that can then be related back to the observed community level response and changes in diatom community composition. We have shown that changes in [Si(OH)$_4$] result in a wide range of silicon limitation among co-occurring diatom taxa. Yet, despite the range in the sensitivity among taxa to changes in [Si(OH)$_4$] the data indicated a collective trend where silicon limitation caused cells to alter silicification more than the extent of new frustule SA created with minimal effects on growth rate. The lack of a growth-rate response in our data set is expected based on culture data. In culture diatoms are capable of thinning their frustules by a factor of 3-4 in response to low [Si(OH)$_4$] (e.g. Guillard et al. 1973; Paasche 1975; Brzezinski et al. 1990) which agrees with our observations (Fig 4). Thus, growth rate would be predicted to remain largely unaltered until cells exceeded the limit to frustule thinning. In our field observations, where the lowest [Si(OH)$_4$] was 2.0 μM, thinning was generally ≤ 2 (Fig. 4) and thus above the thinning threshold such that little impact on growth rate is expected and none was observed.

We have also shown that silicon limitation minimally affected the distribution of silica production among taxa and their relative abundance. While taxon-specific rates of

silica production significantly increased with the addition of $Si(OH)_4$, the fractional

contribution of each taxa to total community silica production remained unaltered.

Additionally, silicon limitation did not significantly alter a taxon's fractional abundance

within the community. These results suggest the primary manifestation of silicon limitation

in the upwelling system of the California current at the time of our study was the creation of

more lightly silicified diatom cells.

Community silicon limitation

The degree of silicon limitation recorded in this study was less severe than observed

in other ocean regions. The concentration of $Si(OH)_4$ in surface waters across the transects

only marginally limited diatom community silica production. The increase in silica

production in the +Si treatment suggests that the diatom communities at each station were

operation at roughly 77% of maximum rates (i.e. $1 \div V_{+Si}/V_{amb}$) on average (Fig. 1b). In the

equatorial upwelling region of the Pacific, silica production on average was 59% of

maximum (Brzezinski et al. 2008). In more oligotrophic environments silica production was

limited to 42% - 50% of maximum in the North Pacific subtropical gyre (Brzezinski et al.

1998; Krause et al. 2012) and 12-16% of maximum in the Sargasso Sea (Brzezinski and

Nelson 1996).

The modest degree of silicon limitation recorded in this study is similar to that

recorded during an upwelling event Monterey Bay, CA (Brzezinski et al. 1997). Within the

upwelling plume in Monterey Bay, ambient $[Si(OH)_4]$ between 25-10 µM supported nearly

maximum silica production rates. The onset of silicon limitation was observed as $[Si(OH)_4]$

decreased below 10 µM to the point where silica production was 63% of maximum rate

when $[Si(OH)_4]$ was 5 µM. While we did not observe a similar trend of increasing silicon

limitation with decreasing [Si(OH)$_4$], the range of silicon limitation observed in the diatom communities along the transects falls within that of Brzezinski et al. (1997). The degree of silicon limitation observed here suggests that the taxon-specific responses to silicon limitation are representative of this system.

Taxon-specific silicon limitation

While silicon limitation was similar across [Si(OH)$_4$] at the community level, taxon-specific silicon limitation reflected a range of affinity for Si among taxa for silica production. Taxa with low K$_s$ constants (Equation 1) are able to maintain high production rates as [Si(OH)$_4$] decreases resulting in V$_{+Si}$/V$_{amb}$ close to one. Conversely, taxa with high K$_s$ constants become silicon limited at higher concentrations of [Si(OH)$_4$] which is reflected in a higher V$_{+Si}$/V$_{amb}$. While the low coverage of taxon across stations limits our ability to predict taxon-specific K$_s$, a taxon's relative sensitivity to silicon limitation was diagnoses by normalizing the number of times a taxon exhibited silicon stress to the number of stations at which the taxon was observed (Fig. 3). *P. alata, F. pseduonana* and the large *Chaetoceros spp.* >20 µm were silicon limited in most of the stations in which they were observed. While the small *Chaetoceros spp.* >20 µm were silicon limited only 25% of the time. The range in sensitivity to silicon limitation among taxa can also be seen in the increased variability of V$_{+Si}$/V$_{amb}$ as the concentration of Si(OH)$_4$ decreased (Fig 2a). At high Si(OH)$_4$ concentration, differences in K$_s$ minimally influence V$_{+Si}$/V$_{amb}$ because all taxa are producing silica at close to maximal rate, which collapses V$_{+Si}$/V$_{amb}$ to ~1. As Si(OH)$_4$ concentration decreases, V$_{+Si}$/V$_{amb}$ between taxon diverge due to taxon-specific differences in K$_s$ creating the pattern of increased variability with decreasing [Si(OH)$_4$] observed in Figure 2a.

Diatom taxa exhibited a diverse range of silicon limitation through changes in silica production rates, however, the physiological manifestation of that limitation was generally conserved among taxa. As mentioned above, the rate of silica production is the product of SA_{new} and silicification (Eq. 4). Decreasing silicification was the primary manifestation of silicon limitation across the observed taxa (Fig. 4). The more lightly silicified cells in the ambient treatment suggest that, as cells became silicon-limited, they decreased their cellular Si quota and with the addition of $Si(OH)_4$ they were released from silicon limitation and were able to restore optimal silicification. The extent of new frustule SA (SA_{new}) was less affected than silicification by silicon limitation as seen by the slope of the regression line in Figure 4 which is half that for silicification. The smaller changes in SA_{new} translated into minimal difference in growth rate with increasing silicon limitation (Fig. 4).

Changes in SA_{new} and growth rate are linked because the pattern of fluorescent labeling of the frustule was used to calculate growth rate. However, changes in new frustule SA between the ambient and +Si treatments do not necessarily translate to large differences in growth rate. Growth rate is calculated as the natural logarithm of the original frustule surface area and the newly created frustule SA.

$$\mu = \ln\left(\frac{SA + SA_{new}}{SA}\right) \tag{5}$$

Making μ_{+Si}/μ_{amb} always smaller than $SA_{new+Si}/SA_{new-amb}$.

The resulting rank-order of physiologic response from a strong response of silicification to a more modest response of new frustule SA and finally to no significant influence on growth rate, suggests that the main adaptation to silicon limitation in these natural communities was to reduce silicification to maximize growth rate. While this response has been observed in laboratory studies (Paasche 1973c; Brzezinski et al. 1990) it

99

has never before been directly quantified in the field. Our work provides the first direct field evidence that diatoms are adapted to maximize growth rate at the expense of other aspects of cell physiology. Such a response is consistent with the r-strategy of diatom adaptation whereby they are adapted to respond quickly to inputs of nutrients (e.g. Sommer 1983) and thus thrive high turbulence environments (e.g. Margalef 1978). By prioritizing growth rate cells produce the maximum number of individuals for a given pulse of $Si(OH)_4$.

Silicon limitation resulted in a greater response in silicification compared to growth, indicating that K_μ occurs at a much lower $Si(OH)_4$ concentrations than K_s such that cells will first decrease silica production rates then growth rate under silicon limitation. The relationship between K_s and K_μ can be evaluated by solving the Michaelis-Menten (eq. 1) and Monod (eq. 2) for $[Si(OH)_4]$, and then setting them equal to each other and solving for μ_m/μ:

$$\frac{\mu_m}{\mu} = \frac{V_m}{V}\left(\frac{K_\mu}{K_s}\right) - \left(\frac{K_\mu}{K_s} - 1\right) \tag{6}$$

Where μ_m and μ are approximated by the measured μ_{+Si} and μ_{amb}, respectively and V_m and V are approximated by V_{+Si} and V_{amb}, respectively. This equation is in the same form as the regressions from Figure 4 ($\mu_{+Si}/\mu_{amb} = 0.08 \pm 0.05$ x $(V_{+Si}/V_{amb}) + 0.92$ (p = 0.12)) such that the slope of V_{+Si}/V_{amb} versus μ_{+Si}/μ_{amb} is the ratio of K_μ to K_s. While the slope of the regression was not significant it suggests that K_μ is on the order of ten times less than K_s.

Biogeochemcial implications of silicon limitation

Under the conditions sampled, silicon availability was not a dominant force in shaping diatom community composition. The insensitivity of growth rate was achieved by adjusting cellular Si content, such a shift potentially altered taxon-specific contributions to total community silica production. However, within the environmental conditions observed,

neither community composition nor fractional production rates were significantly altered by the end of the incubation with the addition of $Si(OH)_4$ (Fig. 5). Any changes in growth rate attributable to silicon limitation were too small to overcome the large difference in initial cell abundance between taxa in one day. The effect of growth rate compounds over time and thus any difference in growth rate between the ambient and +Si treatments will be more pronounced on longer timescales (see McNair et al. in press). Although unrealistic to assume that relative growth rates would remain the same as the bloom progresses, it is informative to examine how much time would have to pass for a noticeable community shift to occur between the ambient and +Si conditions. The 95% prediction interval of the fractional abundance relationship (Fig. 5b) suggests that a notable shift would occur when the difference in fractional abundance between the ambient and +Si treatments (Δ fractional abundance) was >0.25 (Fig. 5). Using the growth rates measured in the incubation and the initial cell abundance, Δ fractional abundance was calculated over the course of 6 days (Fig. 6a), which is a relevant timescale for diatom bloom formation in the California upwelling zone (Largier et al. 2006). There are only three instances across the stations and taxa where the fractional abundance of a taxon is 0.25 times more in the +Si condition compared to the ambient condition after six days (Fig. 6a). This result suggests that even given multiple days, the small differences in μ from silicon limitation has minimal impact on community structure in the observed conditions. In environments where the ambient $[Si(OH)_4]$ is low enough to severely limit diatom growth, e.g. <0.5 µM observations in the California Current, (Krause et al. 2015) or Mississippi River Plume (Nelson and Dortch 1996)), $[Si(OH)_4]$ could affect community structure.
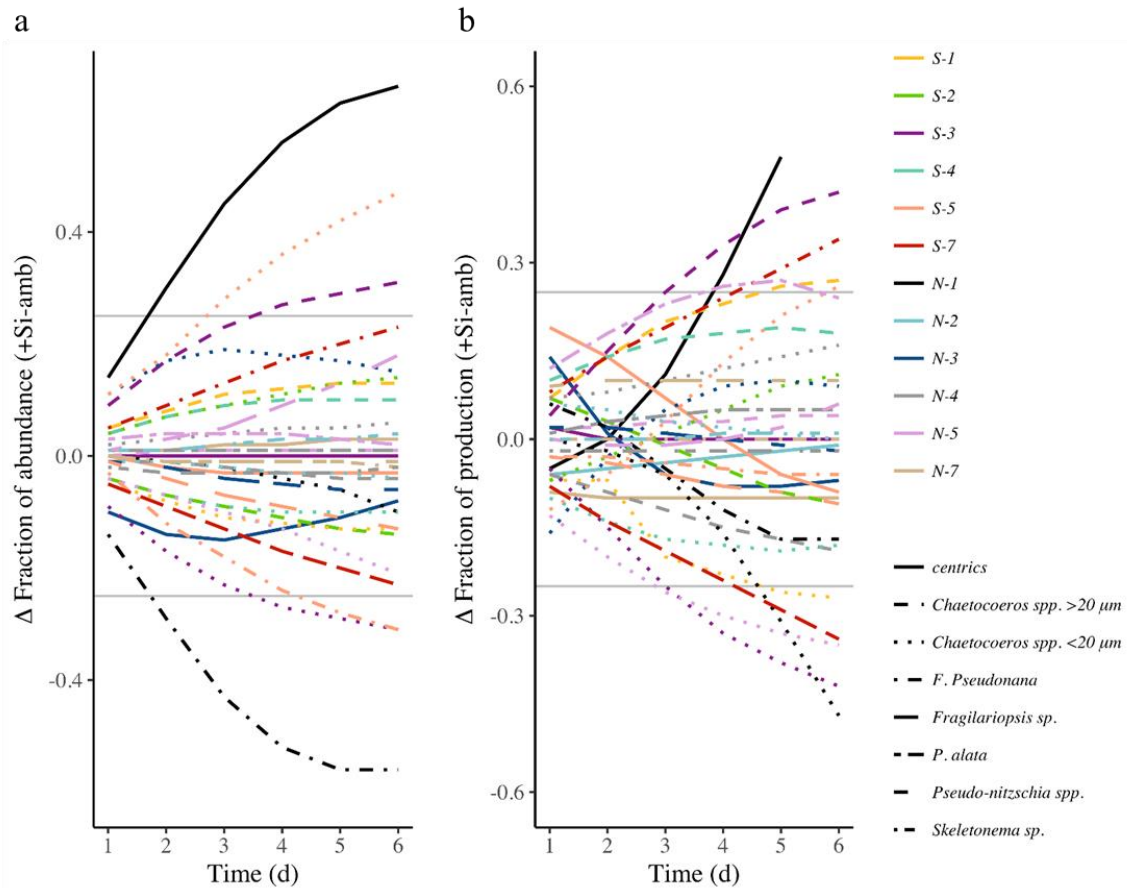
Figure 4-6: (a) The predicted difference in a taxon's fractional abundance between the ambient and +Si treatment through time (b) The predicted difference in a taxon's fractional production between the ambient and +Si treatment through time. Taxon are denoted by lines of the same type while stations are denoted by lines of the same color. Legend denotes the transect by north (N) or south (S) and station number. The gray lines at 0.25, represent the limit for the fractional production and abundance to fall outside the 95% prediction interval in Figure 5.

A diatom taxon's contribution to community silica production is directly related to the total amount of frustule surface area represented by all cells of a taxon, which is a function of cell size and cell abundance (McNair et al in press). Similar to community composition, changes in silica production rate that occurred with increased $Si(OH)_4$ were too small to overcome the large initial differences in fractional contributions to silica production (Fig 5a). Projecting the differences in fractional production between the ambient and +Si conditions (Δ fractional production) over six days shows that four taxa exceed the 0.25 limit (Fig. 6b). In the upwelling environment of the California current, where phytoplankton have

roughly 5-7 days of growth between upwelling events (Largier et al. 2006), diatom

community composition and fractional production is likely determined primarily by the

production of the vast majority of cells at or near maximum growth rate under nutrient

replete conditions rather than the growth rates that evolve with decreasing nutrient

concentrations and the ensuing substrate limitation.

Silicon limitation has been observed to play a similar role of minimally impacting

community structure in other systems. In the equatorial Pacific ambient [Si(OH)$_4$], which

was similar to the lowest concentrations observed on our transects, reduced silica production

rates to 63% of maximum (Brzezinski et al. 2011a). In this region, the addition of Si(OH)$_4$

increased cellular silica but did not alter consumption of macronutrients or diatom

community composition (Brzezinski et al. 2011a). This suggests that the diatom

communities in the equatorial Pacific also have K_μ<<K_s. In regions where silicon limitation

of silicon production is more severe [Si(OH)$_4$] could also influence growth rate and directly

contribute to the structuring of phytoplankton communities as suggested by Egge and

Aksnes (1992) or diatom community succession as suggested by Nelson and Dortch (1996).

Future work will need to resolve both the change in silica production rate and diatom growth

rate across diatom taxa to illuminate this fundamental question about the strength of silicon

as a bottom-up factor in structuring phytoplankton communities.

While silicon limitation did not play a fundamental role in structuring community

composition or community silica production in this study, its effect on silicification could

have implications for the for the fate of diatom biomass and the biogeochemical cycling of

nutrients in the region. The coordinated decrease in silicification as Si(OH)$_4$ concentrations

decline could increase the probability of diatom biomass being recycled within the surface

ocean (Passow et al. 2011) rather than sinking and removing those nutrients from the surface ocean where they are in highest demand. Salter et al. (2007) found the highest fraction of surface production was exported to depth in the Southern Ocean when the community was dominated by heavily silicified diatoms. Additionally decreasing silicification could increase diatom susceptibly to grazing (Assmy et al. 2013; Liu et al. 2016; Zhang et al. 2017) and thus fortify the transfer of energy from primary producer to consumer.

Chapter 5 Conclusion and Outlook

Table 4-1: The relative change in silica production rate (V), silicification (Z), new frustule surface area (SA_{new}), and growth rate (μ), for taxa along the northern and southern transect. Data was filtered using two objective criteria: the number of cells included in the average needed to be greater than four in both treatments and the magnitude of the S.E. of V_{+Si}/V_{amb} had to be less than 70% of the average

Transect	Taxon	Station	N	V_{+Si}/V_{amb}	Z_{+Si}/Z_{amb}	$SA_{new+Si}/SA_{new-amb}$	μ_{+Si}/μ_{amb}	$[Si(OH)_4]$ μM
Southern	centrics	3	8	2.4 ± 1.2	2.7 ± 0.8	1.0 ± 0.4	0.9 ± 0.2	10.5
		5	7	2.9 ± 1.5	1.5 ± 0.3	1.6 ± 0.7	0.9 ± 0.0	3.4
Northern		1	36	0.7 ± 0.2	0.8 ± 0.1	1.0 ± 0.2	1.0 ± 0.1	21.2
		2	12	0.9 ± 0.3	1.3 ± 0.2	0.6 ± 0.2	1.0 ± 0.1	3.8
		3	27	2.0 ± 1.0	1.4 ± 0.2	1.6 ± 0.6	0.7 ± 0.1	16.0
		7	17	1.4 ± 0.7	1.9 ± 0.4	0.6 ± 0.2	1.1 ± 0.1	3.6
Southern	*Chaetoceros spp.* >20 μm	1	37	1.7 ± 0.5	1.0 ± 0.1	1.7 ± 0.5	1.2 ± 0.1	15.4
		2	22	1.4 ± 0.4	1.2 ± 0.1	1.2 ± 0.3	0.9 ± 0.2	13.9
		3	70	2.1 ± 0.3	1.7 ± 0.1	1.3 ± 0.1	1.4 ± 0.1	10.5
		4	46	1.1 ± 0.5	0.7 ± 0.1	1.4 ± 0.6	1.0 ± 0.1	7.2
Northern		4	16	1.4 ± 0.4	1.6 ± 0.2	1.0 ± 0.3	1.1 ± 0.2	6.7
		5	11	2.8 ± 0.8	2.1 ± 0.2	1.5 ± 0.3	1.5 ± 0.2	2.0
Southern	*Chaetoceros spp.* <20 μm	1	22	1.3 ± 0.2	1.3 ± 0.1	1.0 ± 0.2	0.9 ± 0.1	15.4
		2	19	1.0 ± 0.2	1.1 ± 0.1	0.9 ± 0.2	1.0 ± 0.1	13.9
		3	40	1.7 ± 0.2	1.8 ± 0.1	1.0 ± 0.1	1.0 ± 0.1	10.5
		4	58	0.7 ± 0.1	0.8 ± 0.1	0.9 ± 0.1	0.8 ± 0.1	7.2
		5	5	1.4 ± 0.8	1.6 ± 0.4	1.2 ± 0.4	1.3 ± 0.2	3.4
Northern		1	17	0.5 ± 0.1	0.7 ± 0.3	0.7 ± 0.1	0.7 ± 0.1	21.2
		2	19	1.2 ± 0.3	1.2 ± 0.2	1.2 ± 0.2	1.0 ± 0.1	3.8
		3	41	1.0 ± 0.3	1.5 ± 0.2	0.8 ± 0.3	1.2 ± 0.2	16.0
		4	19	2.5 ± 0.4	1.6 ± 0.2	1.6 ± 0.2	1.2 ± 0.1	6.7
		5	22	0.7 ± 0.1	0.9 ± 0.1	0.8 ± 0.1	1.1 ± 0.1	2.0
		7	4	0.9 ± 0.4	1.3 ± 0.4	0.8 ± 0.3	1.0 ± 0.3	3.6
Southern	*F. pseudonana*	5	22	1.3 ± 0.2	1.4 ± 0.1	0.8 ± 0.1	0.9 ± 0.1	3.4
		6	24	2.2 ± 0.3	1.5 ± 0.2	1.5 ± 0.1	1.2 ± 0.1	2.3
		7	9	1.5 ± 0.4	1.4 ± 0.3	1.1 ± 0.1	1.1 ± 0.1	2.6

Northern	1	10	1.7 ± 0.3	1.2 ± 0.3	1.1 ± 0.2	0.5 ± 0.0	21.2
	7	12	2.5 ± 0.3	1.8 ± 0.2	1.3 ± 0.1	1.0 ± 0.1	3.6
Southern *Fragilariopsis sp.*	6	5	0.9 ± 0.3	1.0 ± 0.2	0.8 ± 0.2	1.0 ± 0.0	2.3
	7	11	1.1 ± 0.4	1.2 ± 0.4	0.8 ± 0.1	0.7 ± 0.2	2.6
Northern *P. alata*	4	9	1.8 ± 0.4	1.7 ± 0.3	1.0 ± 0.2	1.5 ± 0.5	6.7
	5	11	1.3 ± 0.3	1.0 ± 0.1	1.3 ± 0.3	1.9 ± 0.2	2.0
Southern *Pseudo-nitzschia spp.*	5	4	1.2 ± 0.4	1.3 ± 0.2	1.1 ± 0.2	0.9 ± 0.2	3.4
Northern	3	11	1.9 ± 0.5	1.5 ± 0.2	1.2 ± 0.2	1.0 ± 0.1	16.0
	5	4	0.9 ± 0.6	1.2 ± 0.2	0.8 ± 0.4	1.2 ± 0.3	2.0
	7	8	2.3 ± 1.6	2.0 ± 0.7	1.4 ± 0.4	1.0 ± 0.2	3.6
Northern *Skeletonema sp.*	2	14	1.1 ± 0.3	1.1 ± 0.1	1.1 ± 0.3	1.1 ± 0.2	3.8
	4	13	0.7 ± 0.1	1.1 ± 0.1	0.6 ± 0.1	0.8 ± 0.1	6.7

Chapter 6 Conclusions and future directions

The role of diatoms in biogeochemical cycles has been envisioned as a box within a larger system. Inputs of silicic acid are fed into the box, converted to biogenic silica and then leave the box through loss terms such as sinking, dissolution or grazing (e.g. Moore et al. 2002; Parekh et al. 2006). There was an understanding that the rate that silicic acid was converted to silica depended upon essential nutrients but regional changes in community composition was an unknown variable.

Results from this dissertation suggest that the rate of silica production and temporal evolution of silicic acid depletion is influenced by the diatom community composition. A community composed of relatively large cells would be expected to produce more silica in a day and thus decrease silicic acid concentration more than a community of smaller cells. Thus, not only does the composition of the diatom community likely affect the fate of biologic nutrients through differences in sinking rates (e.g. Passow et al. 2011) and preferential grazing (e.g. Assmy et al. 2013), but also has consequences for 'downstream' silica production.

Decreasing silicic acid concentration, within the environment studied here, coincided with a wide range of silicon limitation among diatom taxa. Differences in silicon limitation did not affect community composition or the fractional contribution of cells to silica production but did affect the silica content of cells. This suggests that frustules of silicon limited diatoms would have reduced mineral ballast relative to nutrient replete conditions, decreasing their export potential and contribution to removal of nutrients from the surface ocean.

The primary findings of the work detail diatom dynamics that were only observable with methodical techniques that enabled the resolution of single-cell production rates and growth rates from a mixed assemblage. Streamlining and expansion and adaptation of this method to will help advance our understating of diatom ecology and the role of diatoms in global biogeochemical cycles.

Future directions

In this study we found that community composition was an important part of the silicon cycle and that silicon limitation did not affect diatom growth rate and thus was not an important factor in shaping the community. The range of silicic acid observed across these transects was likely not low enough to induce severe enough silicon limitation to limit growth. Thus it is possible that diatom growth could be limited by silicon concentration in other regions of the world. Future work would use PDMPO to look at diatom dynamics in more chronically silicon limitation systems to see if silicon plays an essential role in diatom community composition or phytoplankton community composition.

The importance of community composition in regulating downstream nutrient concentrations begs the question, what determines community composition? In a dynamic system such as the California coast, community composition is probably more related to maximum growth rates rather than the ability of cells to cope with nutrient stress. Fundamental differences in physiology among species seems to play a central role. With the surge of molecular techniques there is an exciting outlook for future work to look at the cellular mechanics that result in differences in growth rate.

The mechanism of top-down control on community composition will also be an illuminating future research direction. The results presented in chapter three stipulate an

assumption of 'no preferential loss due to grazing'. Future work that can examine specific grazing pressure and link that to community composition and biogeochemistry will be essential in broadening our general understanding of the ocean.

References

Alexander, H., B. D. Jenkins, T. a. Rynearson, and S. T. Dyhrman. 2015. Metatranscriptome analyses indicate resource partitioning between diatoms in the field. Proc. Natl. Acad. Sci. **112**: E2182–E2190.

Alldredge, A. L., and M. W. Silver. 1988. Characteristics, dynamics and significance of marine snow. Prog. Oceanogr. **20**: 41–82.

Alvarado, N. D. 2012. A modified protocol for monitoring silicic acid uptake in natural phytoplankton assemblages. University of California Santa Cruz.

Annenkov, V. V, E. N. Danilovtseva, S. N. Zelinskiy, T. N. Basharina, T. A. Safonova, E. S. Korneva, Y. V Likhoshway, and M. A. Grachev. 2010. Novel fluorescent dyes based on oligopropylamines for the in vivo staining of eukaryotic unicellular algae. Anal. Biochem. **407**: 44–51.

Armstrong, R. A., C. Lee, J. I. Hedges, S. Honjo, and S. G. Wakeham. 2001. A new, mechanistic model for organic carbon fluxes in the ocean based on the quantitative association of POC with ballast minerals. Deep Sea Res. Part II Top. Stud. Oceanogr. **49**: 219–236.

Assmy, P., V. Smetacek, M. Montresor, C. Klaas, J. Henjes, V. H. Strass, J. M. Arrieta, U. Bathmann, G. M. Berg, E. Breitbarth, B. Cisewski, L. Friedrichs, N. Fuchs, G. J. Herndl, S. Jansen, S. Kragefsky, M. Latasa, I. Peeken, R. Rottgers, R. Scharek, S. E. Schuller, S. Steigenberger, A. Webb, and D. Wolf-Gladrow. 2013. Thick-shelled, grazer-protected diatoms decouple ocean carbon and silicon cycles in the iron-limited Antarctic Circumpolar Current. Proc. Natl. Acad. Sci. **110**: 20633–20638.

Baines, S. B., B. S. Twining, M. A. Brzezinski, D. M. Nelson, and N. S. Fisher. 2010.

Causes and biogeochemical implications of regional differences in silicification of marine diatoms. Global Biogeochem. Cycles **24**: GB4031.

Biller, D. V., and K. W. Bruland. 2012. Analysis of Mn, Fe, Co, Ni, Cu, Zn, Cd, and Pb in seawater using the Nobias-chelate PA1 resin and magnetic sector inductively coupled plasma mass spectrometry (ICP-MS). Mar. Chem. **130**–**131**: 12–20.

Biller, D. V., T. H. Coale, R. C. Till, G. J. Smith, and K. W. Bruland. 2013. Coastal iron and nitrate distributions during the spring and summer upwelling season in the central California Current upwelling regime. Cont. Shelf Res. **66**: 58–72.

Blain, S., A. Leynaert, P. Treguer, M.-J. Chretiennot-Dinet, and M. Rodier. 1997. Biomass, growth rates and limitation of Equatorial Pacific diatoms. Deep. Res. I **44**: 1255–1275.

Bohonak, A. 2004. RMA Software for Reduced Major Axis Regression.

Broecker, W. S., and T.-H. Peng. 1982. Tracers in the Sea, Lamont-Doherty Geological Observatory.

Bruland, K. W., E. L. Rue, G. J. Smith, and G. R. DiTullio. 2005. Iron, macronutrients and diatom blooms in the Peru upwelling regime: brown and blue waters of Peru. Mar. Chem. **93**: 81–103.

Brzezinski, M. A. 1985. The Si:C:N ratio of marine diatoms: Interspecific variability and the effect of some environmental variables. J. Phycol. **21**: 347–357.

Brzezinski, M. A. 1992. Cell-Cycle effects on the kinetics of silicic acid uptake and resource competition among diatoms. J. Plankton Res. **14**: 1511–1539.

Brzezinski, M. A., S. B. Baines, W. M. Balch, C. P. Beucher, F. Chai, R. C. Dugdale, J. W. Krause, M. R. Landry, A. Marchi, C. I. Measures, D. M. Nelson, A. E. Parker, A. J. Poulton, K. E. Selph, P. G. Strutton, A. G. Taylor, and B. S. Twining. 2011a. Co-

limitation of diatoms by iron and silicic acid in the equatorial Pacific. Deep Sea Res.
Part II Top. Stud. Oceanogr. **58**: 493–511.

Brzezinski, M. A., and D. J. Conley. 1994. Silicon deposition during the cell cycle of
Thalassiosira weissflogii (Bacillariophyceae) determeined using dual Rhodamine 123
and Propidium Iodide Staining. J. Phycol. **30**: 45–55.

Brzezinski, M. A., C. Dummousseaud, J. W. Krause, C. I. Mesasures, D. M. Nelson, C.
Dumousseaud, C. I. Measures, J. W. Krause, C. I. Measures, and D. M. Nelson. 2008.
Iron and silicic acid concentrations together regulate Si uptake in the equatorial Pacific
Ocean. Limnol. Oceanogr. **53**: 875–889.

Brzezinski, M. A., J. L. Jones, K. Bidle, and F. Azam. 2003. The balance between silica
production and silica dissolution in the sea. Insights from Monterey Bay, California
applied to the global data set. Limnol. Oceanogr. **48**: 1846–1854.

Brzezinski, M. A., J. W. Krause, M. J. Church, D. M. Karl, B. Li, J. L. Jones, and B.
Updyke. 2011b. The annual silica cycle of the North Pacific subtropical gyre. Deep Sea
Res. I **58**: 988–1001.

Brzezinski, M. A., and D. M. Nelson. 1989. Seasonal changes in the silicon cycle within a
Gulf Stream warm-core ring. Deep. Res. **36**: 1009–1030.

Brzezinski, M. A., and D. M. Nelson. 1995. The annual silica cycle in the Sargasso Sea near
Bermuda. Deep. Res. I **42**: 1215–1237.

Brzezinski, M. A., and D. M. Nelson. 1996. Chronic substrate limitation of silicic acid
uptake rates in the western Sargasso Sea. Deep. Res. II **43**: 437–453.

Brzezinski, M. A., D. M. Nelson, V. M. Franck, and D. E. Sigmon. 2001. Silicon dynamics
within an intense open-ocean diatom bloom in the Pacific sector of the Southern Ocean.

Deep. Res. II **48**: 3997–4018.

Brzezinski, M. A., R. J. Olson, and S. W. Chisholm. 1990. Silicon availability and cell-cycle progression in marine diatoms. Mar. Ecol. Prog. Ser. **67**: 83–96.

Brzezinski, M. A., D. R. Phillips, F. P. Chavez, G. E. Friederich, and R. C. Dugdale. 1997. Silica production in the Monterey, California upwelling system. Limnol. Oceanogr. **42**: 1694–1705.

Brzezinski, M. A., C. J. Pride, V. M. Franck, D. M. Sigman, J. L. Sarmiento, K. Matsumoto, N. Gruber, G. H. Rau, and K. H. Coale. 2002. A switch from $Si(OH)_4$ to NO_3^- depletion in the glacial Southern Ocean. Geophys. Res. Lett. **29**: 10.1029/2001GL014349.

Brzezinski, M. A., T. A. Villareal, and F. Lipschultz. 1998. Silica production and the contribution of diatoms to new and primary production in the central North Pacific. Mar. Ecol. Prog. Ser. **167**: 89–104.

Buesseler, K. O. 1998. The decoupling of production and particle export in the surface ocean. Global Biogeochem. Cycles **12**: 297–310.

Claquin, P., V. Martin-Jézéquel, J. C. Kromkamp, M. J. W. Veldhuis, and G. W. Kraay. 2002. Uncoupling of silicon compared with carbon and nitrogen metabolisms and the role of the cell cycle in continuous cultures of *Thalassiosira pseudonana* (Bacillariophyceae) under light, nitrogen, and phosphorus control. J. Phycol. **38**: 922–930.

Conley, D. J., S. S. Kilham, and E. Theriot. 1989. Differences in silica content between marine and freshwater diatoms. Limnol. Oceanogr. **34**: 205–213.

Cuttler, G., P. Andersson, L. Codispoti, P. Croot, R. Francois, M. Lohan, H. Obata, and M. R. van der Loeff. 2014. Sampling and sample-handling protocols for GEOTRACES

cruises, version 2.0. 1–238.

Darley, W. M., and B. E. Volcani. 1969. Role of silicon in diatom metabolism. A silicon
    requirement for deoxyribonucleic acid synthesis in the diatom Cylindrotheca
    fusiformis Reimann and Lewin. Exp. Cell Res. **58**: 334–342.

Diwu, Z., C.-S. Chen, C. Zhang, D. H. Klaubert, and R. P. Haugland. 1999. A novel
    acidotropic pH indicator and its potential application in labeling acidic organelles of
    live cells. Chem. Biol. **6**: 411–418.

Dortch, Q., N. N. Rabalais, E. R. Turner, and N. A. Qureshi. 2001. Impacts of Changing
    Si/N Ratios and Phytoplankton Species Composition, p. 37–48. *In* N.N. Rabalais and
    R.E. Turner [eds.], Coastal Hypoxia: Consequences for Living Resources and
    Ecosystems. American Geophysical Union.

Dugdale, R. C., and F. P. Wilkerson. 1989. New production in the upwelling center at Point
    Conception, California: temporal and spatial patterns. Deep Sea Res. **36**: 985–1007.

Dugdale, R. C., F. P. Wilkerson, and H. J. Minas. 1995. The role of a silicate pump in
    driving new production. Deep Sea Res. **42**: 697–719.

Durkin, C. a., S. J. Bender, K. Yu Karen Chan, K. Gaessner, D. Grünbaum, and E. Virginia
    Armbrust. 2013. Silicic acid supplied to coastal diatom communities influences cellular
    silicification and the potential export of carbon. Limnol. Oceanogr. **58**: 1707–1726.

Durkin, C. a., A. Marchetti, S. J. Bender, T. Truong, R. Morales, T. Mock, and E. Virginia
    Armbrust. 2012. Frustule-related gene transcription and the influence of diatom
    community composition on silica precipitation in an iron-limited environment. Limnol.
    Oceanogr. **57**: 1619–1633.

Egge, J. K., and D. L. Aksnes. 1992. Silicate as regulating nutrient in phytoplankton

competition. Mar. Ecol. Prog. Ser. **83**: 281–289.

Field, C. B., M. J. Behrenfeld, J. T. Randerson, P. Falkowski, and J. T. Randerson. 1998.
Primary production of the biosphere: Integrating terrestrial and oceanic components.
Science (80-.). **281**: 237–240.

Finlay, B. J. 2002. Global dispersal of free-living microbial eukaryote species. Science **296**:
1061–1063.

Finney, B. P., I. Gregory-Eaves, M. S. V. Douglas, and J. P. Smol. 2002. Fisheries
productivity in the northeastern Pacific Ocean over the past 2,200 years. Nature **416**:
729–733.

Flynn, K. J., and V. Martin-Jezequel. 2000. Modelling Si-N-limited growth of diatoms. J.
Plankton Res. **22**: 447–472.

Follows, M. J., S. Dutkiewicz, S. Grant, and S. W. Chisholm. 2007. Emergent Biogeography
of Microbial Communities in a Model Ocean. Science (80-.). **315**: 1843–1846.

Franck, V. 2002. Iron and zinc effects on silicon and nitrate uptake in high-nutrient, low-
chlorophyll regions off central California, the Southern Ocean and the eastern tropical
Pacific. University of California, Santa Barbara.

Friedrichs, M. A. M., J. A. Dusenberry, L. A. Anderson, R. A. Armstrong, F. Chai, J. R.
Christian, S. C. Doney, J. Dunne, M. Fujii, R. Hood, D. J. McGillicuddy, J. K. Moore,
M. Schartau, Y. H. Spitz, and J. D. Wiggert. 2007. Assessment of skill and portability
in regional marine biogeochemical models: Role of multiple planktonic groups. J.
Geophys. Res. Ocean. **112**: 1–22.

Goering, J. J., D. M. Nelson, and J. A. Carter. 1973. Silicic acid uptake by natural
populations of marine phytoplankton. Deep. Res. **20**: 777–789.

Goldman, J. C. 1993. Potential role of large oceanic diatoms in new primary production. Deep Sea Res. Part I Oceanogr. Res. Pap. **40**: 159–168.

Goldman, J. C., and D. J. McGillicuddy. 2003. Effect of large marine diatoms growing at low light on episodic new production. Limnol. Oceanogr. **48**: 1176–1182.

Guillard, R. R. L., P. Kilham, T. A. Jackson, and G. R. R. L. K. P. and T. A. Jackson. 1973. Kinetics of silicon-limited growth in the marine diatom Thalassiosira pseudonana Hasle and Heimdal (= Cyclotella nana Hustedt). J. Phycol. **9**: 233–237.

Harrison, K. G. 2000. Role of increased marine silica input on paleo- pCO_2 levels. Paleoceanography **15**: 292–298.

Holland, H. D. 1984. The Chemical Evolution of the Atmosphere and Oceans, Princeton University Press.

Hoppenrath, M., M. Elbrächter, and G. Drebes. 2007. Marine Phytoplankton. Selected microphytoplankton species from the North Sea around Helgoland and Sylt,.

Hutchins, D. A., and K. W. Bruland. 1998. Iron-limited diatom growth and Si:N uptake ratios in a coastal upwelling regime. Nature **393**: 561–564.

Hutchins, D. A., G. R. DiTullio, Y. Zhang, and K. W. Bruland. 1998. An iron limitation mosaic in the California upwelling regime. Limnol. Oceanogr. **43**: 1037–1054.

Hutchins and K. W. Bruland, D. A. 1995. Fe, Zn, Mn and N transfer between size classes in a coastal phytoplankton community: trace metal and major nutrient cycling compared. J. Mar. Res. **53**: 297–313.

Ingall, E. D., J. M. Diaz, A. F. Longo, M. Oakes, L. Finney, S. Vogt, B. Lai, P. L. Yager, B. S. Twining, and J. a Brandes. 2013. Role of biogenic silica in the removal of iron from the Antarctic seas. Nat. Commun. **4**: 1981.

Jin, X., N. Gruber, J. P. Dunne, J. L. Sarmiento, and R. A. Armstrong. 2006. Diagnosing the contribution of phytoplankton functional groups to the production and export of particulate organic carbon, $CaCO_3$, and opal from global nutrient and alkalinity distributions. Global Biogeochem. Cycles **20**: GB2015.

Kerkhoff, A. J., and B. J. Enquist. 2009. Multiplicative by nature: Why logarithmic transformation is necessary in allometry. J. Theor. Biol. **257**: 519–521.

Kilham, P., and D. Tilman. 1979. The importance of resource competition and nutrient gradients for phytoplankton ecology. Arch. Hydrobiol. (Beih): Ergebn. Limnol. **13**: 110–119.

Kooistra, W. H. C. F., R. Gersonde, L. K. Medlin, and D. G. Mann. 2007. The Origin and Evolution of the Diatoms: Their Adaptation to a Planktonic Existence, p. 207–249. *In* Evolution of Primary Producers in the Sea. Elsevier.

Krause, J. W., M. A. Brzeinski, and J. L. Jones. 2011a. Application of low-level beta counting of ^{32}Si for the measurement of silica production rates in aquatic environments. Mar. Chem. **127**: 40–47.

Krause, J. W., M. A. Brzezinski, R. Goericke, M. R. Landry, M. D. Ohman, M. R. Stukel, and A. G. Taylor. 2015. Variability in diatom contributions to biomass, organic matter, production and export across a frontal gradient in the California Current Ecosystem. Jounral Geophys. Res. Ocean. **120**: 1–16.

Krause, J. W., M. A. Brzezinski, M. R. Landry, S. B. Baines, D. M. Nelson, K. E. Selph, A. G. Taylor, and B. S. Twining. 2010. The effects of biogenic silica detritus, zooplankton grazing, and diatom size structure on silicon cycling in the euphotic zone of the eastern equatorial Pacific. Limnol. Oceanogr. **55**: 2608–2622.

Krause, J. W., M. A. Brzezinski, T. A. Villareal, and C. Wilson. 2012. Increased kinetic efficiency for silicic acid uptake as a driver of summer diatom blooms in the North Pacific subtropical gyre. Limnol. Oceanogr. **57**: 1084–1098.

Krause, J. W., D. M. Nelson, and M. A. Brzezinski. 2011b. Biogenic silica production and the diatom contribution to primary production and nitrate uptake in the eastern equatorial Pacific Ocean. Deep Sea Res. Part II Top. Stud. Oceanogr. **58**: 434–448.

Krause, J. W., D. M. Nelson, and M. W. Lomas. 2009. Biogeochemical responses to late-winter storms in the Sargasso Sea, II: Increased rates of biogenic silica production and export. Deep. Res. Part I Oceanogr. Res. Pap. **56**: 861–874.

Largier, J. L., C. A. Lawrence, M. Roughan, D. M. Kaplan, E. P. Dever, C. E. Dorman, R. M. Kudela, S. M. Bollens, F. P. Wilkerson, R. C. Dugdale, L. W. Botsford, N. Garfield, B. Kuebel Cervantes, and D. Kora??in. 2006. WEST: A northern California study of the role of wind-driven transport in the productivity of coastal plankton communities. Deep. Res. Part II Top. Stud. Oceanogr. **53**: 2833–2849.

LeBlanc, K., and D. A. Hutchins. 2005. New applications of a biogenic silica deposition fluoro phore in the study of oceanic diatoms. Limnol. Oceanogr. Methods **3**: 462–476.

Leblanc, K., B. Quéguiner, M. Fiala, S. Blain, J. Morvan, and R. Corvaisier. 2002. Particulate biogenic silica and carbon production rates and particulate matter distribution in the Indian sector of the Subantarctic Ocean. Deep. Res. II **49**: 3189–3206.

Leynaert, A., P. Tréguer, C. Lancelot, and M. Rodier. 2001. Silicon limitation of biogenic silica production in the equatorial Pacific. Deep. Res. I **48**: 639–660.

Liu, H., M. Chen, F. Zhu, and P. J. Harrison. 2016. Effect of Diatom Silica Content on

Copepod Grazing, Growth and Reproduction. Front. Mar. Sci. **3**: 89.

Lohan, M. C., A. M. Aguilar-Islas, and K. W. Bruland. 2006. Direct determination of iron in acidified (pH 1.7) seawater samples by flow injection analysis with catalytic spectrophotometric detection: Application and intercomparison. Limnol. Oceanogr. Methods **4**: 164–171.

Malviya, S., E. Scalco, S. Audic, F. Vincent, A. Veluchamy, L. Bittner, J. Poulain, P. Wincker, D. Iudicone, C. de Vargas, A. Zingone, and C. Bowler. 2016. Insights into global diatom distribution and diversity in the world's ocean. Proc. Natl. Acad. Sci. **113**: E1516–E1525.

Mann, K. 1993. Physical oceanography, food chains, and fish stocks: a review. ICES J. Mar. Sci. **50**: 105–119.

Marchetti, A., and N. Cassar. 2009. Diatom elemental and morphological changes in response to iron limitation: A brief review with potential paleoceanographic applications. Geobiology **7**: 419–431.

Marchetti, A., and P. J. Harrison. 2007. Coupled changes in the cell morphology and the elemental (C, N and Si) composition of the pennate diatom *Pseudo-nitzschia* due to iron deficiency. Limnol. Oceanogr. **52**: 2270–2284.

Margalef, R. 1978. Life-forms of phytoplankton as survival alternatives in an unstable environment. Ocean. Acta **1**: 493–509.

Martin-Jézéquel, V., M. Hildebrand, M. A. Brzezinski, V. Martin-Jezequel, M. Hildebrand, M. A. Brzezinski, and V. Martin-Jézéquel. 2000. Silicon metabolism in diatoms: implications for growth. J. Phycol. **36**: 821–840.

Martin, J. H., R. M. Gordon, and S. E. Fitzwater. 1991. The case for iron.

Matsumoto, K., J. L. Sarmiento, and M. A. Brzezinski. 2002. Silicic acid "leakage" from the
Southern Ocean as a possible mechanism for explaining glacial atmospheric pCO_2.
Global Biogeochem. Cycles **16**: doi:10.1029/2001GB001442.

McNair, H. M., M. A. Brzezinski, and J. W. Krause. 2015. Quantifying diatom silicification
with the fluorescent dye, PDMPO. Limnol. Oceanogr. Methods **13**: 587–599.

Menden-Deuer, S., and E. J. Lessard. 2000. Carbon to volume relationships for
dinoflagellates, diatoms, and other protist plankton. Limnol. Oceanogr. **45**: 569–579.

Meyerink, S. W., M. J. Ellwood, W. A. Maher, G. Dean Price, and R. F. Strzepek. 2017.
Effects of iron limitation on silicon uptake kinetics and elemental stoichiometry in two
Southern Ocean diatoms, *Eucampia antarctica* and *Proboscia inermis*, and the
temperate diatom *Thalassiosira pseudonana*. Limnol. Oceanogr. ,
doi:10.1002/lno.10578

Moore, J. K., S. C. Doney, J. A. Kleypas, D. M. Glover, and I. Y. Fung. 2002. An
intermediate complexity marine ecosystem model for the global domain. Deep. Res.
Part II Top. Stud. Oceanogr. **49**: 403–462.

Myklestad, S. 1977. Production of carbohydrates by marine planktonic diatoms. II.
Influence of the N/P ratio in the growth medium on the assimilation ratio, growth rate,
and production of cellular and extracellular carbohydrates by Chaetoceros affinis var.
willei Hust. J. Exp. Mar. Bio. Ecol. **29**: 161–179.

Nelson, D. M., and M. A. Brzezinski. 1990. Kinetics of silicic acid uptake by natural diatom
assemblages in two Gulf Stream warm-core rings. Mar. Ecol. Prog. Ser. **62**: 283–292.

Nelson, D. M., M. A. Brzezinski, D. E. Sigmon, and V. M. Franck. 2001. A seasonal
progression of Si limitation in the Pacific sector of the Southern Ocean. Deep. Res. II

48: 3973–3995.

Nelson, D. M., and Q. Dortch. 1996. Silicic acid depletion and silicon limitation in the plume of the Mississippi River: evidence from kinetic studies in spring and summer. Mar. Ecol. Prog. Ser. **136**: 163–178.

Nelson, D. M., S. S. Goering, S. S. Kilham, and R. R. L. Guillard. 1976. Kinetics of silicic acid uptake and rates of silica dissolution in the marine diatom Thalassiosira pseudonana. J. Phycol. **12**: 246–252.

Nelson, D. M., and P. Tréguer. 1992. Role of silicon as a limiting nutrient to Antarctic diatoms: evidence from kinetic studies in the Ross Sea ice-edge zone. Mar. Ecol. Prog. Ser. **80**: 255–264.

Nelson, D. M., P. Treguer, M. A. Brzezinski, A. Leynaert, and B. Queguiner. 1995. Production and dissolution of biogenic silica in the ocean : Revised global estimates, comparison with regional data and relationship to biogenic sedimentation. Global Biogeochem. Cycles **9**: 359–372.

Paasche, E. 1973a. Silicon and the ecology of marine planktonic diatoms: I. *Thalassiosira psuedonana* (Cyclotella nana) grown in chemostats with silicate as the limiting nutrient. Mar. Biol. **19**: 117–126.

Paasche, E. 1973b. Silicon and the Ecology of Marine Plankton Diatoms . II . Silicate-Uptake Kinetics in Five Diatom Species. Mar. Biol. **19**: 262–269.

Paasche, E. 1973c. Silicon and the Ecology of Marine Plankton Diatoms . I . *Thalassiosira pseudonana* (Cyclotella nana) Grown in a Chemostat with Silicate as Limiting Nutrient. Mar. Biol. **19**: 117–126.

Paasche, E. 1975. Growth of the plankton diatom Thalassiosiranordenskioeldii Cleve at low

silicate concentrations. J. Exp. Mar. Bio. Ecol. **18**: 173–183.

Paasche, E. 1980. Silicon content of five marine plankton diatom species measured with a

    rapid filter method. Limnol. Oceanogr. **25**: 474–480.

Parekh, P., M. J. Follows, S. Dutkiewicz, and T. Ito. 2006. Physical and biological

    regulation of the soft tissue carbon pump. Paleoceanography **21**.

Parker, C. E., M. T. Brown, and K. W. Bruland. 2016. Scandium in the open ocean: A

    comparison with other group 3 trivalent metals. Geophys. Res. Lett. **43**: 2758–2764.

Parsons, T., Y. Maita, and C. Lalli. 1984. A Manual of Chemical and Biological Methods

    for Seawater Analysis, Pergamon Press Ltd.

Passow, U., M. A. French, and M. Robert. 2011. Biological controls on dissolution of

    diatom frustules during their descent to the deep ocean: Lessons learned from

    controlled laboratory experiments. Deep Sea Res. Part I Oceanogr. Res. Pap. **58**: 1147–

    1157.

Pokras, E. M., and A. C. Mix. 1985. Eolian Evidence for Spatial Variability of Late

    Quaternary in Tropical Africa '. Quat. Res. **24**: 137–149.

Pomeroy, L. R. 1974. The Ocean's Food Web, A Changing Paradigm. Bioscience **24**: 499–

    504.

Pondaven, P., O. Ragueneau, P. Tréguer, A. Hauvespre, L. Dezileau, and J. L. Reysss. 2000.

    Resolving the "opal paradox" in the Southern Ocean. Nature **405**: 168–172.

Rocha, C., H. Galvao, and A. Barbosa. 2002. Role of transient silicon limitation in the

    development of cyanobacteria blooms in the Guadiana estuary, south-western Iberia.

    Mar. Ecol. Prog. Ser. **228**: 35–45.

Salter, I., R. S. Lampitt, R. Sanders, A. J. Poulton, A. E. S. Kemp, B. Boorman, K. Saw, and

R. Pearce. 2007. Estimating carbon, silica and diatom export from a naturally fertilised phytoplankton bloom in the Southern Ocean using PELAGRA: A novel drifting sediment trap. Deep Sea Res. Part II Top. Stud. Oceanogr. **54**: 2233–2259.

Saxton, M. A., N. A. D'Souza, R. A. Bourbonniere, R. M. L. McKay, and S. W. Wilhelm. 2012. Seasonal Si:C ratios in Lake Erie diatoms — Evidence of an active winter diatom community. J. Great Lakes Res. **38**: 206–211.

Shimizu, K., Y. Del Amo, M. A. Brzezinski, G. D. Stucky, and D. E. Morse. 2001. A novel fuorescent silica tracer for biological silicication studies. Chem. Biol. **8**: 1051–1060.

Shipe, R. F., and M. A. Brzezinski. 1999. A study of Si deposition synchrony in *Rhizosolenia* (Bacillariophyceae) mats using a novel ^{32}Si autoradiographic method. J. Phycol. **35**: 995.

Shipe, R. F., M. A. Brzezinski, C. Pilskaln, and T. A. Villareal. 1999. *Rhizosolenia* mats: An overlooked source of silica production in the open sea. Limnol. Oceanogr. **44**: 1282–1292.

Smetacek, V. 1999. Diatoms and the Ocean Carbon Cycle. Protist **150**: 25–32.

Smith, C. J., K. S. Baker, and P. Dustan. 1981. Fluorometric techniques for the measurement of oceanic chlorophyll in the support of remote sensing. Scripps Institution of Oceanography, Reference 81-17.

Smith, R. J. 2009. Use and misuse of the reduced major axis for line-fitting. Am. J. Phys. Anthropol. **140**: 476–486.

Sommer, U. 1983. Nutrient competition between phytoplankton species in multispecies chemostat experiment. Arch. Hydrobiol. **96**: 399–416.

Takeda, S. 1998. Influence of iron availability on nutrient consumption ratio of diatoms in

oceanic waters. Nature **393**: 774–777.

Tantanasarit, C., A. J. Englande, and S. Babel. 2013. Nitrogen, phosphorus and silicon uptake kinetics by marine diatom Chaetoceros calcitrans under high nutrient concentrations. J. Exp. Mar. Bio. Ecol. **446**: 67–75.

Tilman, D. 1977a. Resource competition between plankton algae: an experimental and theoretical approach. Ecology **58**: 338–348.

Tilman, D. 1977b. Resource competition between planktonic algae: an experimental and theoretical approach. Ecology **58**: 338–348.

Tilman, D. 1982. Resource Competition and Community Structure, Princeton University Press.

Timmermans, K. R., B. Van der Wagt, and H. J. W. de Baar. 2004. Growth rates, half-saturation constants, and silicate, nitrate, and phosphate depletion in relation to iron availability of four large, open-ocean diatoms from the Southern Ocean. Limnol. Oceanogr. **49**: 2141–2151.

Tréguer, P. J., and C. L. De La Rocha. 2013. The world ocean silica cycle. Ann. Rev. Mar. Sci. **5**: 477–501.

Tréguer, P., D. M. Nelson, A. J. Van Bennekom, D. J. Demaster, P. Treguer, A. Leynaert, and B. Queguiner. 1995. The Silica in the Balance World Ocean : A Reestimate. Science (80-.). **268**: 375–379.

Twining, B. S., S. B. Baines, J. B. Bozard, S. Vogt, E. a. Walker, and D. M. Nelson. 2011. Metal quotas of plankton in the equatorial Pacific Ocean. Deep. Res. Part II **58**: 325–341.

Utermohl, H. 1958. Zur Vervollkommnung der quantitativen Phytoplankton-Methodik,

Schweizerbart.

La Vars, S. M., M. R. Johnston, J. Hayles, J. R. Gascooke, M. H. Brown, S. C. Leterme, and A. V. Ellis. 2013. $^{29}Si\{^1H\}$ CP-MAS NMR comparison and ATR-FTIR spectroscopic analysis of the diatoms *Chaetoceros muelleri* and *Thalassiosira pseudonana* grown at different salinities. Anal. Bioanal. Chem. **405**: 3359–3365.

Venrick, E. 1998. Spring in the California Current: the distribution of phytoplankton species, April 1993 and April 1995. Mar. Ecol. Prog. Ser. 73–88.

Venrick, E. L. 1974. The distribution and significance of Richelia intracellularis Schmidt in the North Pacific Central Gyre. Limnol. Oceanogr. **19**: 437–445.

Villareal, T. A., M. A. Altabet, and K. Culver-Rymsza. 1993. Nitrogen transport by vertically migrating diatom mats in the North Pacific Ocean. Nature **363**: 709–712.

Villareal, T. A., S. Woods, J. K. Moore, and K. Culver-Rymsza. 1996. Vertical migration of *Rhizosolenia* mats and their significance to NO_3^- fluxes in the central North Pacific gyre. J. Plankton Res. **18**: 1103–1121.

Wilken, S., B. Hoffmann, N. Hersch, N. Kirchgessner, S. Dieluweit, W. Rubner, L. J. Hoffmann, R. Merkel, and I. Peeken. 2011. Diatom frustules show increased mechanical strength and altered valve morphology under iron limitation. Limnol. Oceanogr. **56**: 1399–1410.

Zhang, S., H. Liu, Y. Ke, and B. Li. 2017a. Effect of the Silica Content of Diatoms on Protozoan Grazing. Front. Mar. Sci. **4**, doi:10.3389/fmars.2017.00202

Zhang, S., H. Liu, Y. Ke, and B. Li. 2017b. Effect of the Silica Content of Diatoms on Protozoan Grazing. Front. Mar. Sci. **4**, doi:10.3389/fmars.2017.00202

Zimmerman, R. C., J. N. Kremer, and R. C. Dugdale. 1987. Acceleration of nutrient uptake

by phytoplankton in a coastal upwelling ecosystem: A modeling analysis. Limnol. Oceanogr. **32**: 359–367.

Znachor, P., and J. Nedoma. 2008. Application of the PDMPO Technique in Studying Silica Deposition in Natural Populations of *Fragilaria Crotonensis* (Bacillariophyceae) At Different Depths in a Eutrophic Reservoir. J. Phycol. **44**: 518–525.

Znachor, P., P. Rychtecký, J. Nedoma, and V. Visocká. 2015. Factors affecting growth and viability of natural diatom populations in the meso-eutrophic Římov Reservoir (Czech Republic). Hydrobiologia , doi:10.1007/s10750-015-2417-8

Znachor, P., V. Visocká, J. Nedoma, and P. Rychtecký. 2013. Spatial heterogeneity of diatom silicification and growth in a eutrophic reservoir. Freshw. Biol. **58**: 1889–1902.